



University of Stuttgart
Germany

Faculty 6: Aerospace Engineering and Geodesy

Geodesy & Geoinformatics

Annual Report 2019



editing and layout:

volker walter, markus antoni, martin metzner, aloysius wehr

Dear friends and colleagues,

It is our great pleasure to present to you this annual report on the 2019 activities and academic highlights of the Department of Geodesy and Geoinformatics of the University of Stuttgart. The Department consists of the four institutes:

- Institute of Geodesy (GIS),
- Institute for Photogrammetry (ifp),
- Institute of Navigation (INS),
- Institute of Engineering Geodesy (IIGS),

and is part of the Faculty of Aerospace Engineering and Geodesy.

Research

This annual report documents our research contributions in many diverse fields of Geodesy and Geoinformatics: from satellite and physical geodesy through navigation, remote sensing, engineering surveying and telematics to photogrammetry, geographical information systems and location based services. Detailed information on projects and research output can be found in the following individual institutes' sections.

Teaching

We were able to welcome 32 new BSc students in winter term 2018/2019 (initially 42 students enrolled). For the first semester of the MSc program for Geodesy and Geoinformatics 19 students enrolled and we welcomed 15. Please visit our website www.geodaesie.uni-stuttgart.de for additional information on the programs.

Our successful international MSc program Geomatics Engineering (GeoEngine) exists already 14 years. Probably due establishment of tuition fees for non-EU students in 2018, we saw a decline of new students, this time 37 enrolled and we welcomed 19.

Awards and Scholarships

We want to express our gratitude to our friends and sponsors, most notably:

- Verein Freunde des Studienganges Geodäsie und Geoinformatik an der Universität Stuttgart e.V. (F2GeoS),
- Ingenieur-Gesellschaft für Interfaces mbH (IGI),
- DVW Landesverein Baden-Württemberg,

who support our programs and our students with scholarships, awards and travel support. Below is the list of the recipients of the 2019 awards and scholarships. The criterion for all prizes is academic performance; for some prizes GPA-based, for other prizes based on thesis work. Congratulations to all recipients!

Uwe Sörgel, Associate Dean (Academic)

Uwe.soergel@ifp.uni-stuttgart.de

Award	Recipient	Sponsor	Programme
Karl-Ramsayer Preis	Mr. Michael Kölle	Department of Geodesy & Geoinformatics	Geodesy & Geoinformatics
BSc Thesis Award	Mr. David Collmar	F2GeoS	Geodesy & Geoinformatics
MSCThesis Award	Mrs. Laura Balangé	F2GeoS	Geodesy & Geoinformatics

Institute of Engineering Geodesy



Geschwister-Scholl-Str. 24 D

70174 Stuttgart

Germany

Tel.: +49 711 685 84041

Fax: +49 711 685 84044

sekretariat@iigs.uni-stuttgart.de or

firstname.secondname@iigs.uni-stuttgart.de

<http://https://www.iigs.uni-stuttgart.de/>

Head of Institute

Prof. Dr.-Ing. habil. Volker Schwieger

Secretary

Elke Rawe

Ute Schinzel (until 31.07.2019)

Desiré Schreib (since 01.10.2019)

Scientific Staff

M.Sc. Laura Balangé

M.Sc. Urs Basalla

M.Sc. Aiham Hassan

M.Sc. Gabriel Kerekes

Dr.-Ing. Otto Lerke

M.Sc. Philipp Luz

Dr.-Ing. Martin Metzner

M.Sc. Annette Schmitt (until 31.03.2019)

M.Sc. Martin Wachsmuth

M.Sc. Jinyue Wang

Dr.-Ing. Li Zhang

Quality Modeling

Terrestrial Laser Scanning

Monitoring

Terrestrial Laser Scanning

Machine Guidance

Digital Map

Engineering Geodesy

Multi-Sensor-Systems

Kinematic Positioning

Map Matching

Monitoring

Technical Staff

Andreas Kanzler

Martin Knihs

Lars Plate

External Teaching Staff

Dipl.-Ing. Jürgen Eisenmann	Geschäftsbereichsleiter Landratsamt Ostalbkreis, Geoinformation und Landentwicklung
Dipl.-Ing. Christian Helfert	Fachdienstleiter Flurneueordnung im Landkreis Biberach
Dipl.-Math. Ulrich Völter	Geschäftsführer der Fa. Intermetric
Dr.-Ing. Thomas Wiltshko	Daimler AG, Mercedes-Benz Cars; Research and Development

PhD-Students

M.Sc. Julia Aichinger	Terrestrial Laser Scanning
M.Sc. Alexandra Avram	GNSS
M.Sc. Marko Gasparac	GNSS and Digital Map
Dipl.-Ing. Patric Hindenberger	Location Referencing
M.Sc. Yu Li	Digital Map
M.Sc. Dung Trung Pham	Kinematic Positioning
Dipl.-Ing. Annette Scheider	Multi-Sensor-Systems
M.Sc. Tobias Schröder	Automation of Production Process
M.Sc. Yihui Yang	Multi-Sensor-Systems
M.Sc. Christian Bader	Kinematic Laser Scanning

General View

The Institute of Engineering Geodesy (IIGS) is directed by Prof. Dr.-Ing. habil. Dr. h.c. Volker Schwieger. It is part of Faculty 6 "Aerospace Engineering and Geodesy" within the University of Stuttgart. Prof. Schwieger holds the chair in "Engineering Geodesy and Geodetic Measurements". Since 2017, he is the Dean of Faculty 6.

In addition to being a member of Faculty 6, Prof. Schwieger is co-opted to Faculty 2 "Civil and Environmental Engineering". Furthermore, the IIGS is involved in the Center for Transportation Research of the University of Stuttgart (FOVUS). Thus, the IIGS actively continues the close collaboration with all institutes in the field of transportation, especially with those belonging to Faculty 2.

Since 2011, Prof. Schwieger is a full member of the German Geodetic Commission (Deutsche Geodätische Kommission - DGK). Furthermore, he is a member of the section „Engineering Geodesy“ within the DGK.

On October 31, 2019, Prof. Schwieger was awarded an honorary doctorate (Doctor Honoris Causa, Dr. h.c.) in a ceremony at the Technical University of Civil Engineering Bucharest, Romania. The award was made by the Rector Prof. Dr. Radu Sorin Vacareanu and the President of the Senate Prof. Dr. Iohan Neuner. The honorary doctorate was awarded to Prof. Schwieger

as a sign of the high recognition of his remarkable contributions to the development and promotion of engineering geodesy, both in teaching and research, but also in appreciation of his important role at international level. Moreover, of course it is for his undoubted merits in developing and consolidating the cooperation and friendship with the Technical University of Civil Engineering Bucharest, during a quarter of a century. Last but not least, in deep gratitude for his way of positively highlighting Romania's culture, history and monuments on numerous occasions at international level.

The institute's main tasks in education focus on geodetic and industrial measurement techniques, kinematic positioning and multi-sensor systems, statistics and error theory, engineering geodesy and monitoring, GIS-based data acquisition, and transport telematics. Here, IIGS is responsible for the above-mentioned fields within the curricula of "Geodesy and Geoinformatics" (Master and Bachelor in German) and for "GEOENGINE" (Master for Geomatics Engineering in English). In addition, the IIGS provides several courses in German for the curricula of "Aerospace Engineering" (Bachelor and Master), "Civil Engineering" (Bachelor and Master), "Transport Engineering" (Bachelor and Master) and "Technique and Economy of Real Estate" (Bachelor). Furthermore, lectures are given in English to students within the Master course "Infrastructure Planning". Finally, eLearning modules are applied in different curricula.

In 2018 the Cluster "Integrative Computational Design and Construction for Architecture" (IntCDC), for which the University of Stuttgart has submitted an application for funding as part of the excellence strategy to strengthen top-level research in Germany, has been awarded funding for the next seven years. The cluster IntCDC aims to harness the full potential of digital technologies in order to rethink design and construction, and enable groundbreaking innovations for the building sector through a systematic, holistic and integrative computational approach. As a member of the cluster (IntCDC), the IIGS's research in the field of new construction methods is intensified in cooperation with architects, civil engineers, computer scientists, production engineers, and other scientists from various research institutions from inside and outside the University of Stuttgart.

The current research and project work of the institute is expressed in the course contents, thus always presenting the actual state-of-the-art to the students. As a benefit of this, student research projects and theses are often implemented in close cooperation with the industry and external research partners. The main research focuses on kinematic and static positioning, analysis of engineering surveying processes and construction processes, machine guidance, monitoring, transport and aviation telematics, process and quality modeling. The daily work is characterized by intensive co-operation with other engineering disciplines, especially with traffic engineering, civil engineering, architecture, and aerospace engineering.

At this year's GAERO-Fest Laura Balangé received the award from the association "Freunde des Studiengang Geodäsie und Geoinformatik an der Universität Stuttgart e.V. (F2GeoS)" for the best master thesis 2018. The prize was presented by Matthias Wengert (member of the board). On 22th July 2019, Ms. Balangé also received the prize for the best Master's thesis 2018 within the Faculty 6 from the Association of Friends of the University of Stuttgart.

The Title of the thesis is "Implementation of the Sea Level Equation" and her MSc thesis at the Geodetic Institute was supervised by PD Dr.-Ing. habil. Johannes Engels. Furthermore her work was awarded on the DVW CAMPUS GEOINNOVATION at the Intergeo 2019.

Research and Development

Precise Seamless 6-DoF Positioning for Georeferenced Assembly Control

The presented contribution is nested within the research project 16 "Robotic Assembler" which is part of the overarching research network II "Longspan Buildings" belonging to the cluster of excellence "Integrative Computational Design and Construction for Architecture (IntCDC)" funded by the Deutsche Forschungsgemeinschaft (DFG).



The goal of the project is the 6-DoF pose determination, consisting of positions and attitudes for the guidance process of the robotic assembly platform. Therefore the setup of a network of robotic total stations (RTS) (Figure 1) is planned. Beside the 6-DoF pose determination the research area considers the optimization of the geometric network configuration under aspects of accuracy and reliability as well as the ability to propose suggestions regarding the on-site arrangement of RTS for performance improvements of seamless positioning. Further research aspects are the steering of different RTSs within the network and the fusion of their data using data fusion algorithms like extended Kalman filter, unscented Kalman filter or particle Filter.

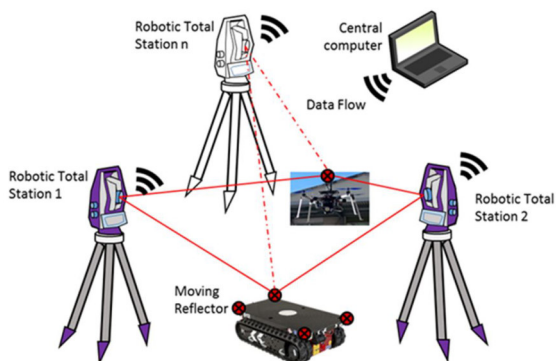


Figure 1: Principle sketch of RTS network.

Supported by the Deutsche Forschungsgemeinschaft (DFG, German Research Foundation) under Germany's Excellence Strategy - EXC 2120/1 - 390831618.

Holistic Quality Model for IntCDC Building Systems

During the framework of the Cluster of Excellence for Integrative Computational Design and Construction for Architecture, a Holistic Quality Model is to be developed. This model includes social, environmental and technical components. Thus, this project is a cooperation between the Institute for Social Sciences (SOWI), the Institute for Acoustic and Building Physics (IABP) and the Institute for Engineering Geodesy (IIGS). Each of the partners provides an column of the overall quality model. These columns are shown with exemplary quality characteristics in Figure 2.

Gefördert durch
DFG Deutsche
 Forschungsgemeinschaft

IntCDC
 CLUSTER OF EXCELLENCE

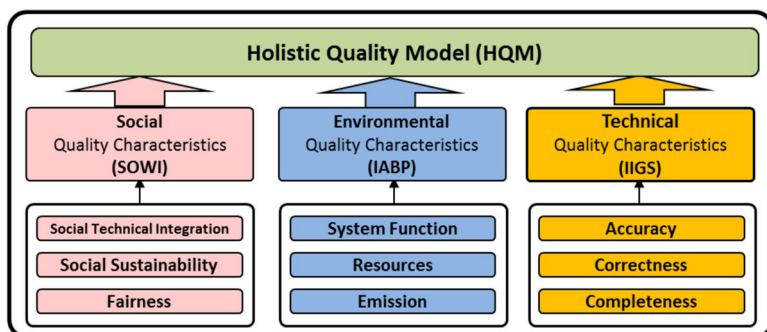


Figure 2: Holistic Quality Model.

In a first step, the general understanding of the terms of quality was identified between the three partners. After that, a survey starts to learn about the general requirements for the quality model from the different disciplines included in the cluster. The results of the survey, i.e. the characteristics which are considered as important, such as accuracy, completeness and timeliness, have now been extended with further characteristics from the norms and standards of all disciplines involved in IntCDC, for example architecture, civil engineering or mechanical engineering. Thus, the model was extended by the features load bearing capacity, fire protection and water permeability.

With these extended quality characteristics, the structure of characteristics, condensed parameters and primary parameters were introduced (Figure 3). The condensed parameters consist of several primary parameters. In addition, the values of the condensed parameters are based on the values of the primary parameters. A primary parameter is a parameter that can be measured.

Supported by the Deutsche Forschungsgemeinschaft (DFG, German Research Foundation) under Germany's Excellence Strategy - EXC 2120/1 - 390831618.

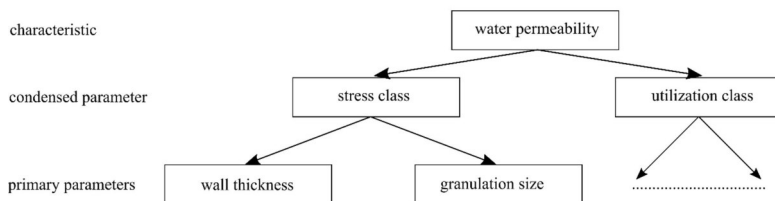


Figure 3: Structure of characteristics, condensed parameters and primary parameters.

Quality Assurance for Wooden Pavilions

The Institute for Computational Design and Construction (ICD) has planned a wooden pavilion for the Bundesgartenschau 2019 in Heilbronn. This pavilion consists of so-called cassettes made of glued spruce wood. It is planned for this pavilion to manufacture the cassettes with low tolerances, i.e. the cassettes are milled true to shape. It should be investigated how precisely the milling process of the cassettes is carried out. Laser tracker measurements were made along the edges that come into contact with other elements. These measured edges were compared with the CAD model of the corresponding cassette. The average deviation of the measurements from the theoretical CAD model is 0.35 mm, which is sufficient for the robotic production of the cassettes.

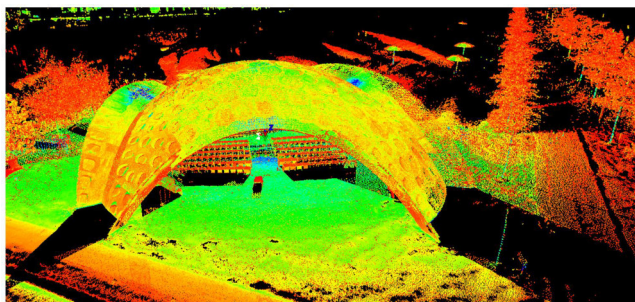


Figure 4: Two epoch comparison of recordings from April and August. Differences are in the range of a few millimetres.

Furthermore, the pavilion was scanned during construction and during its lifetime at the Bundesgartenschau at recurring intervals. Any changes should be detected here. No significant deformation of the structure was detected in the multi-epoch comparisons (Figure 4).

The ICD has planned a wooden tower also for the Remstal Gartenschau 2019 (Figure 5). Half of the wooden elements were built in Switzerland. These wooden elements were built with curved wooden bilayers. The approximately 30 curved panels of wooden bilayers were scanned at the "Blumer-Lehmann" workshop in Gossau (CH) to determine the radii along them. In a next step, the wooden bilayers were glued together to form two fifteen-meter-long

elements. These were also scanned in the factory. From these larger elements the finished components were milled out and scanned again. These scans are used for quality control and data storage. The tower was built near Urbach. The tower is scanned every 3 months to document the changes over its minimum 5 years lifetime. Furthermore, the humidity and temperature of the wood is measured in different parts of the tower.



Figure 5: Network measurement when measuring the fixed point network.

The aim here is to determine a possible correlation between moisture/temperature and the deformation of the wood. In order to georeference the individual epochs, a fixed point network was set up on site.

NURBS Modeling for Terrestrial Laser Scan Point Clouds in the Context of Deformation Analysis

For deformation analysis of complex surfaces, NURBS surfaces (non-uniform rational B-spline surfaces) are determined from real laser scan point clouds. The NURBS surfaces of the different epochs are to be brought to coincidence by means of parameter-dependent superposition. In the presented approach the control points required for the NURBS surfaces result directly from laser scan points and are not determined by means of estimation methods. For a shape-correct control grid formation an intensive examination of necessary conditions at the edges of the point clouds as well as a selection of control polygons from the point cloud are necessary. Since in this work tensor product surfaces are used for NURBS determination whose control grid is based on a rectangular grid structure, a uniform control grid structure must first be created before NURBS surfaces can be calculated. In order to achieve this goal, two knot insertion algorithms will be investigated to determine new knots and control points. However, a change of shape of the curve or surface has to be avoided. While Boehm's algorithm inserts one knot at a time, the Oslo Algorithm allows for the simultaneous insertion of several knots. Nevertheless, the repeated insertion of knots with low computational effort with Boehm's algorithm must be set in relation to the one-time computational step with high computational effort with the Oslo algorithm.

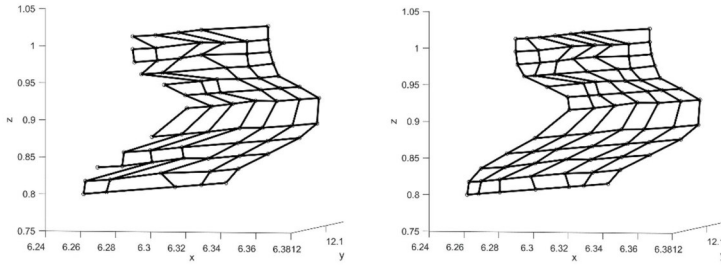


Figure 6: Control point grid consisting of control point polygons of different numbers (left). Control point grid consisting of control point polygons with the same number of points (right).

Figure 6 shows on the left side an exemplary control grid whose control polygons consist of different numbers of knot points. The right graph presents the result of the Boehm algorithm, whose knots insertion formed the basis for the formation of a tensor product NURBS surface. Figure 7 shows a third-degree NURBS surface. A stochastic investigation of the assumed non-shape changes is to be added to the previous analyses.

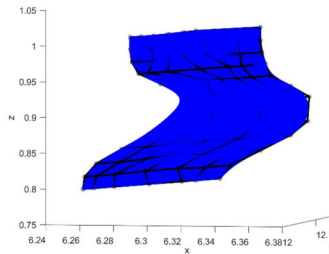


Figure 7: NURBS-surface of degree three.

Integrated Space-time Modeling Based on Correlated Measurements for the Determination of Survey Configurations and the Description of Deformation Processes (IMKAD II)

This project aims at bringing new contributions in analyzing deformation processes with high spatial resolution Terrestrial Laser Scanning (TLS). The IMKAD II project, foresees measurement campaigns for objects of different dimensions. This is necessary for studying the existing variances, covariances and correlations of TLS point clouds. The Elementary Error Model (EEM) is used to determine a synthetic variance-covariance matrix (VCM). In August 2019 the first measurement campaign

Gefördert durch
DFG Deutsche
 Forschungsgemeinschaft

at the Kops lake in Austria took place. The Kops water dam is a concrete storage dam built between 1962 and 1969, and administrated by the Vorarlberger Illwerke AG. It is considered a hybrid type made out of a gravity dam and an arch dam with artificial counterfort or abutment. The crown spans over 400 m, its height is 122 m from foundation to crest and it has a crest width of 6 m. Only measurements of the downstream (airside) arch dam are considered, since this can be interesting to model by means of B-Spline surfaces in the future. Results of the Leica HDS 7000 scans are further analysed after applying the EEM with solely instrumental error sources. Two instrumental error models are examined in parallel. In order to have an idea about the existing spatial correlations, different sections are selected on the dam airside (Figure 8) and correlations from one point to all other points in that section are calculated.

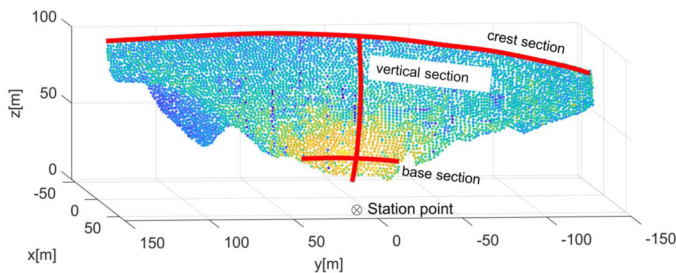


Figure 8: Sections used for spatial correlation analysis.

Results of the existing correlations for the crest section can be seen in Figure 9 for both studied instrumental error models. Additionally, the standard deviation along the same axis (Y) is represented. These are all intermediate steps needed for a fully populated VCM, indispensable in the deformation analysis. A second measurement campaign will be completed in 2020.

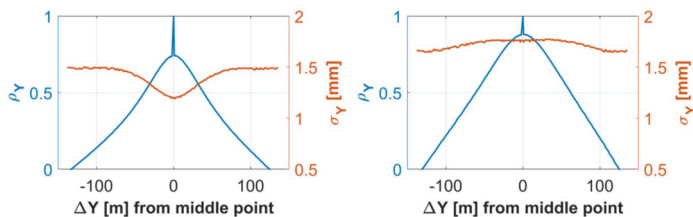


Figure 9: Spatial correlations and standard deviations along the crest section (model 1 on the left, model 2 on the right).

Automated Control for Car Door Adjustments Based on Neural Networks

The following research is the result of a partnership between IIGS and the Tec-Fabric at the Mercedes-Benz AG plant in Sindelfingen. The aim of this project is to realize an automated system providing the worker with a reference for car door adjustments. In the production

process of a modern car the doors are built-in in a highly automated procedure, where multiple sensors and robots jointly calculate the optimum position of the door in relation to the side wall of the car. The precision of the alignment is verified by a final measurement. Two cases are considered: 1) the results are within the given tolerance, 2) the result is outside the tolerance. In the second case, the door is manually adjusted by human workers in a so called post-processing station. The workers rely on their experience and on the measurement results. The process therefore is based on trial and error, which is not very cost-effective. The challenge of the project was to make this heuristic adjustment process more determined and technically supported. Doors are dimensionally stable. Consequently, the door hinge screws define the three-dimensional orientation without any additional deformation components. As a consequence, the measured gap and flush values of the final measurement depend on the condition of the door hinge screws. Correlation between an input (i.e. gap-profile and values of gap and flush) and output (screw and direction of turn) are solid indicators for the usability of neural networks. To investigate the impact of each screw as well as their turning direction, two cases are implemented (Figure 10). In the first case the model is only trained on the detection of the affected screw, the second case also considers the turning direction clockwise (+) or counter-clockwise (-). In the first case the three true classes (S1, S2, S3) represent the three screws of the door hinges. The second case includes six true classes; one for each screw and its turning direction.

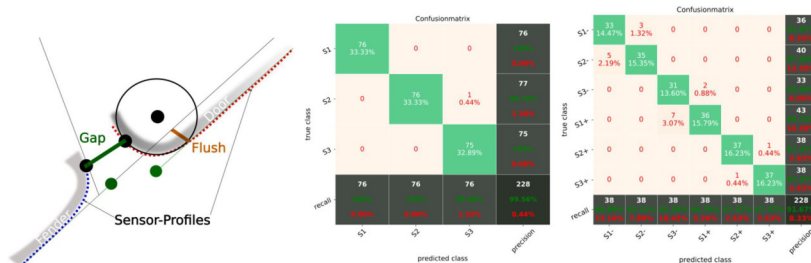


Figure 10: Input values with gap, flush and sensor-profiles (left), the resulting confusion matrix for the first (center) and the second case (right).

The first case has a 99.56 % precision, which is nearly perfect, considering that the training data with 234 measurements is rather small. The second case with its precision of 91.67 % is not as good as the first case, but still promising. The outcome encourages further investigations. Nowadays, the neural network is helping workers to adjust the doors in a field test. The results of the field test will give an impression about the applicability and will be discussed in later publications.

Non-Linearity of System and Observation Models

The non-linearity of a model is one of the most important characteristics in the estimation algorithms of kinematic positioning applications. Almost all estimation algorithms deal with

in the non-linear environment of both system and observation models. The non-linearity of a system model and an observation model measured by the multivariate association is compared here. The quantity of non-linearity of these models can provide the information to use suitable estimation algorithms.

The non-linearity of a model is an amount that is determined by the non-linear relationship between the input and output variables. Multivariate association (MVA) is employed as a measure of the linear relationship between two sets of variables. Hence, 1-MVA is used to measure the non-linearity of the model. If 1-MVA is close to 0, the model is nearly linear. Inversely, if 1-MVA is close to 1, the model is non-linear. The procedure for determination of non-linearity of a model is depicted in Figure 11. Measures of non-linearities of system and observation models are evaluated for the case of kinematic positioning application

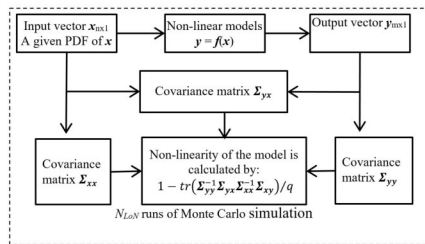


Figure 11: Determination of the non-linearity using 1-MVA.

Supposing that a moving object is tracked by two radars located at reference points. This object moves from the west to the east in the x-y plane with a constant velocity v and is observed during the period of 100 epochs with a data rate Δt of 1 s. Two radars can provide information about the bearing angle. Their measurement accuracies are σ_{α} . The standard deviations of process noise, including acceleration a_{ξ} and rotational rate φ_{ξ} , for modeling the moving object are small with $a_{\xi} = 0.04 \text{ m/s}^2$ and $\varphi_{\xi} = 0.04 \text{ rad/s}^2$.

The straight line model and the bearing angle model are applied for the system model and the observation model, respectively in this study. These models are non-linear models with respect to the state vector. In these evaluations, the non-linearity of these models is determined with variation of their influencing factors. The data rate Δt , velocity v , and orientation change $\Delta\varphi$ are considered as its influencing factors for the system model and the measurement uncertainty and the geometry are corresponding factors for the observation model. Note that the distance between radars and the moving object characterizes the geometry.

Figure 12 shows that the non-linearity of the system model is relatively small (< 0.06% or 6%), and it also changes with its influencing factors. The small quantity for the system model is due to the assumption of the standard deviation of process noise. In this case, the mathematical function of the system model is to describe the behaviour of a moving object that moves in a straight trajectory with constant velocity. In contrast, the non-linearity of the observation model is relatively high (nearly 0.5% or 50%) compared to that of the system

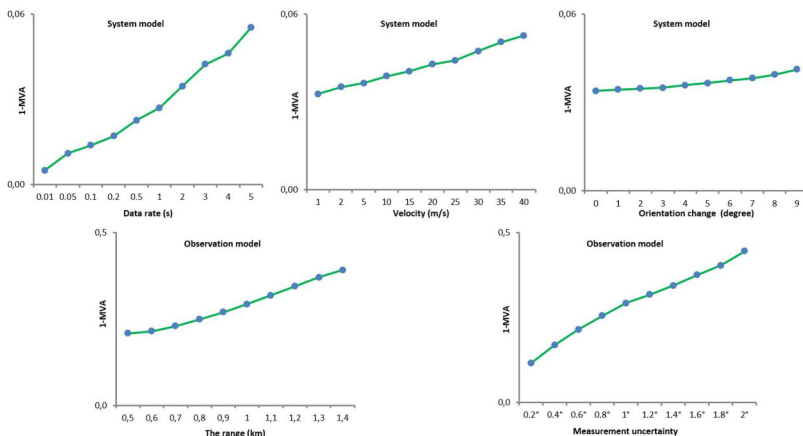


Figure 12: Non-linearity of the system and observation models due to varying of influencing factors.

model. Both observation geometry and measurement uncertainty considerably influence the non-linearity of this model. The change in the non-linearity of this model according to the two above influencing factors are 0.2 and 0.4 (20% and 40%), respectively. The high quantity in the non-linearity of the observation model is due to the mathematical functions of its model and influencing factors. In this case, the distance and bearing angle are non-linear models concerning the state vector and the measurement uncertainty is high. As a result, the non-linearity of the observation model is considerably higher than that of the system model according to the high uncertainty from low-cost sensors. The non-linearity of these models is a useful characteristic for applying suitable algorithms or hybrid algorithms in estimation.

Ghosthunter II - Telematics System against Ghost Drivers using GNSS

The Ghosthunter II project is carried out in cooperation with the Institute of Space Technology and Space Applications at the University of the Federal Armed Forces Munich and the company NavCert.

One of the most important topics of the project is investigating whether the time required to detect a wrong-way driver on motorway ramps can be reduced by using lane-precise maps. A wrong-way driver should be detected even if the lanes are not yet separated. However, this is only possible with lane-precise maps and a map matching algorithm adapted to this kind of maps. A map matching algorithm is utilized to allocate the measured vehicle position on the most probable road link or with the lane-precise map matching the most probable lane link. In this work, an algorithm is developed that performs map matching based exclusively on GNSS positions and a digital lane-precise map (shown in Figure 13). This is provided by 3D Mapping

Supported by:



on the basis of a decision
by the German Bundestag

Solutions GmbH. The algorithm is based on three factors: heading, distance and connectivity. In contrast to other algorithms the connectivity is calculated in real time from the map data.

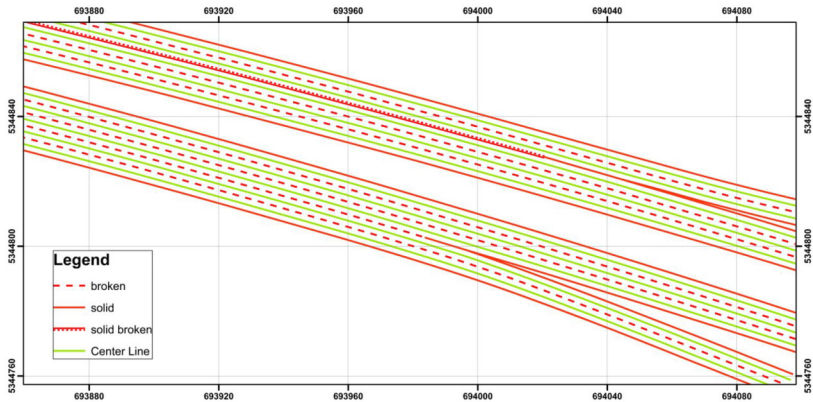


Figure 13: Detail of the lane-precise map.

The basis for this new map matching algorithm is the algorithm developed by the IIGS during the Ghosthunter I project. As mentioned above, the connectivity is no longer included in the lane-precise map. Thus, a new approach has to be found to take these into account. The connectivity is therefore calculated in real time from the existing lane markings.

Each crossing of a lane marker results in a penalty or reward. The connectivity of the segment results from the sum of these. The algorithm not only checks whether the lane change is possible, but also how well the driven distance matches the map distance required for the drive from the last segment to the test segment. The overall accuracy is then made up of these two sub-connectivity elements and then be used like directly calculated connectivity in the map matching algorithm.

With these modifications the algorithm identifies the correct lane with 100% for high accuracies ($\sigma=0.05$ m) and with 94% for medium accuracies ($\sigma=1.50$ m).

The research project Ghosthunter II, is granted by the German Federal Ministry of Economic Affairs and Energy (BMWi) and the German Aerospace Center (DLR) under grant number 50 NA 1802.

TransSec - Autonomous Emergency Manoeuvring and Movement Monitoring for Road Transport Security

The European Project TransSec (Autonomous emergency manoeuvring and movement monitoring for road transport security) is funded by the European Commission within the program Horizon H2020 for three years. This project was started in February 2018 and its goal is to design and implement a built-in intelligent safety system to prevent trucks and transport of goods to be misused for illegal purposes such as terror attacks. IIGS is one of the five partners involved in TransSec project.



One task of IIGS is to get the precise positioning of the trucks by integrating the data from GNSS and other additional sensors such as IMU. IIGS focuses on a Kalman-filter with strapdown algorithm in the positioning module.

The other task of the IIGS is to design and implement a map-aiding approach that considers on-road and particularly off-road scenarios for truck positions in order to detect potential risks. These two tasks will be described in the following text.

TransSec- Positioning Module

For the research project TransSec, the IIGS created a positioning module together with OHB Digital Solutions GmbH (formerly TeleConsult Austria), one of the project partners. Since the GNSS availability is decreased and even complete outages occur in urban city canyons and other obstructed areas like tunnels, we designed an integrated multi-sensor positioning system. The sensor data fusion uses GNSS and inertial measurement unit (IMU) inputs and is done using an error state Kalman filter. The filter estimates the position, velocity and attitude of the vehicle as well as the biases for the accelerometers and gyroscopes. The overall algorithm is divided into two parts. In the first part the IMU measurements and results of the previous filter update are used to predict the vehicles current state. This part is often called strapdown algorithm. Within the strapdown algorithm firstly the measurements of the gyroscopes are used to predict the new attitude of the vehicle. With the new attitude the measurements of the accelerometers, measured in the vehicles body frame, get transformed in the earth frame. With the accelerations in the earth frame it is possible to predict the vehicles velocity, which is also represented in the earth frame. Finally, the predicted new velocity is used to predict the vehicles new position. This strapdown algorithm is running with the frequency of the IMU measurements. Whenever a GNSS position is available, the second part of the overall algorithm which is the actual Kalman filter update, is done and a new state vector is estimated.

In Figure 14 the result of the current algorithm is shown. The situation shows a turning to the right at an intersection. The red crosses show the GNSS positions and the black dots are the predictions of the vehicle position using IMU measurements. Since the IMU measurement frequency was high with 100 Hz, the dots are so close to each other that they appear as lines

at this scale. The small jumps (see figure 14) at the new GNSS position are due to the high accuracy of RTK GNSS compared to IMU measurements. This leads to a higher weighting in the Kalman filter compared to the GNSS measurements and results in these small jumps.

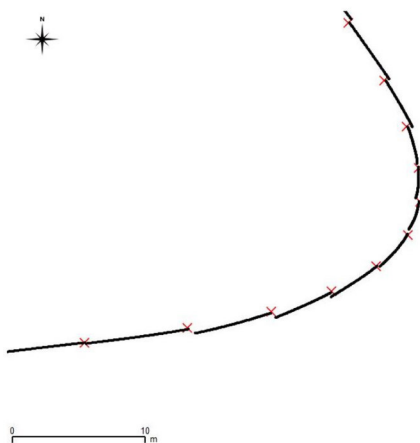


Figure 14: A turn to the right.

TransSec - Map-Aiding

Within this project, the Institute of Engineering Geodesy (IIGS) at the University of Stuttgart designed and implemented a map-aiding approach that considers on-road and particularly off-road scenarios for truck positions in order to detect potential risks. As a result, map-aiding provides the most probable road link, multiple candidate road links, the estimated off-road distance and additional information like total weight score/probability and perpendicular distance for each link to the TransSec risk estimation module. According to the test results, the map-aiding performs quite well even at complex road conditions such as road intersections, junctions, overpass and underpass.

The map-aiding approach can be regarded as a modified and improved algorithm based on map-matching. The most probable road link and other candidate road links in the defined buffer zone derived from map-matching are used as base information in the map-aiding. The functionalities lane identification and on/off-road estimation are based on the information of number of lanes extracted from the digital road map data and the assumption that the lane generally keeps an approximately constant width of 3.5 meters. If the truck is on-road, the algorithm estimates on which lane the truck is probably travelling. If the perpendicular distance from the truck position to the most probable road link exceeds the range of the road width, the truck position is identified as off-road and the off-road distance is estimated by subtracting half of the road width from the perpendicular distance.



Figure 15: An example of map-aiding result with off-road estimation .

As shown in Figure 15, the road on which the truck is travelling consists of two lanes. Even when the estimated deviation exceeds 3.5 meters slightly, the vehicle position (denoted with a small red circle) is identified as off-road. The estimated off-road distance is 0.73 meters for the current vehicle position. The perpendicular foot of the off-road vehicle position on the identified reference link is represented with a light red rectangle symbol.

Dynamic Location Referencing: Probability- and Fuzzy Logic-Based Decision Systems

Location Referencing is a well-known methodology to transfer geo-objects from one digital map to another and typically used to share traffic information. Here, especially the dynamic methods play a major role, as they are developed to transfer Location References (LR) between different maps in such cases where no common databases and/or common structures are available. Location Referencing Methods follow a one-dimensional three-step process of encoding the LR in the sender system, transferring and decoding the LR in the receiver system without any iterations (Figure 16).



Figure 16: Process of Location Referencing.

For dynamic Location Referencing Methods, the key issue is to find the correct geo-object in the target map which corresponds to the geo-object in the source map. So far, in nearly all methods a deterministic algorithm is implemented to perform this. Given the fact that geodata as well as the matching procedure for geodata have some uncertainty, it is obvious to research uncertainty-based algorithms.

As pointed out in the previous annual report, two different uncertainty-based approaches were picked up and investigated in detail. Firstly, a probability-based approach using a specifically formulated decision algorithm based on a predefined set of criteria (geometrical, topological, syntactical and semantical) and secondly a fuzzy-based approach implementing a fuzzy-based decision system based on the same set of criteria. Evaluating the performance in a QGIS-based module, the probability-based and fuzzy-based approaches show similar results with an average hit rate up to 90% and improve the results of a comparable deterministic approach (OpenLR) in average by 12 percentage points. The probability-based approach was presented on LBS Conference 2019 in Vienna and published in the corresponding conference volume.

Based on the results obtained so far and further discussions, additional research and working approaches were identified, which will be investigated in the course of the year.

Multipath Behavior under Static and Kinematic Conditions

The study of multipath delays and behavior is important to further understand how a GNSS receiver processes them and turns them into errors that are present on the pseudo ranges. Ray tracing techniques are known in the literature to realistically model multipath, considering all the complex changes of the GNSS signals in both time and frequency domain. Most of the ray tracing algorithms for predicting the radio signal strength, phase, and delay are based on the computation of the wave's reflection, diffraction, and scattering. Due to the high accuracy of the method, a ray-tracing software together with a GNSS signal generator were used to study the multipath behavior under static and kinematic conditions.

Figure 17 shows the environment which was used for the ray-tracing simulations. The vehicle is the carrier of the receiving antenna. This is simulated on the rooftop. The white lines represent line-of-sight signals and the blue ones show signal reflections. Signal diffraction is also computed and symbolized by the red lines. The multipath signals are generated by means of a GNSS simulator. GPS and Galileo signals are simulated and the first strongest multipath signals are taken into consideration. The hardware channel number, i.e. the number of GNSS signals which can be physically generated are limiting this method. Nevertheless, literature support the idea that two multipath rays per satellite provide realistic results. The rest of the multipath signals i.e. third, fourth reflection might anyway be too weak to be perceived by the receiver.

The right side of Figure 17 shows the simulation results for static and kinematic simulations using the same 3D scenario and satellite constellation. The delays produced through reflections from all visible satellites are plotted. As expected, the reflection pattern is different. In a static case, multipath reflections change slowly with the satellite movement. In kinematic

simulation, the reflections constantly change due to the rapidly changing environment. The results show high multipath delays more often in the static case. This is because due to kinematics, an unfavourable geometry (satellite-environment-receiver) which produces a certain delay occurs only shortly.

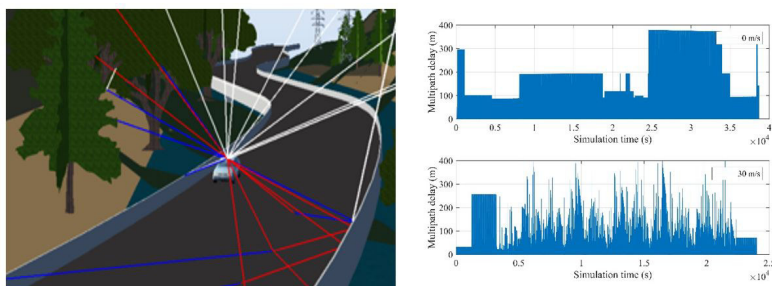


Figure 17: Ray tracing simulation of static and kinematic vehicle. Simulated multipath delays resulting from the simulation are plotted on the right side.

Automated Multi-Sensor Early Warning System on the Three Gorges Dam - DAAD PPP China

In order to realize an automated multi-sensor early warning system near the Three Gorges Dam in China, the project-based personal exchange between IIGS at the University of Stuttgart and the School of Geodesy and Geomatics (SGG) at the University of Wuhan, which started at the beginning of 2017, was extended for one more year (from 01.01. to 31.12.2019). The project is supported by the DAAD (German Academic Exchange Service) and the CSC (China Scholar Council).

During the extension period of the project (in September 2019) a new measurement campaign at the measurement site Lianziya rock fall (Figure 18) was performed. The instruments used in this campaign to investigate the deformation of the rock fall were similar to those used in the former campaign (performed in March 2018). These are (see Figure 19) a GB-SAR (Ground-based Synthetic Aperture Radar), a TLS (Terrestrial Laser Scanning) and GNSS (Global Navigation Satellite System). Besides these instruments, a total station has been used to define a local three dimensional geodetic network, in which the Ground Control Points (GCP) of GB-SAR and TLS and the measurement points of GNSS are measured. This facilitates the transformation of measurement data from the different systems mentioned above into the same local geodetic network and leads to future data fusion.

The first results of the deformation analysis were determined by comparing TLS point clouds from 2018 and 2019. This comparison showed no significant displacement in this period. The result was confirmed through analysis of GNSS data gathered in the same epochs.



Figure 18: Lianziya rock fall at the Yangtze River in China.



Figure 19: Instruments used for the deformation measurements. From left to right: GB-SAR, GNSS-receiver and TLS.

Quality Assurance of Geodetic Measuring and Evaluation Methods 2019, 180th DVW Seminar of DVW Working Group 3 "Measuring Methods and Systems" on 27th and 28th June 2019 in Stuttgart

The 180th DVW Seminar on Quality Assurance took place on 27th and 28th June in Stuttgart. Here, four sessions were offered. On 27th June the seminar started with the session on Fundamentals. The first session was followed by the session on quality for BIM, Geodata and TLS. On the second day, the third session on DVW Merkblätter continued at 8:30 am. With presentations on quality assurance in practice the 180th DVW seminar was concluded. In the rooms of the conference hotel "campus guest" both the lectures and the joint dinner took place. The seminar was well attended with 59 participants who came from all over Germany and Austria, with a majority from Baden-Württemberg. In an evaluation that took place at the end, the seminar was rated as a great success and another seminar of this kind was welcomed. All four sessions were rated as good, although in the first sessions (Fundamentals and Quality for BIM, Geodata and TLS) there was partly a lack of practical relevance discussed. In the course of the seminar organization a book on "Quality assurance of geodetic measurement and evaluation methods 2019" was prepared and published. This book includes the written versions of all presentations from all lecturers.

Publications

Refereed Publications

- Avram, A.; Schwieger, V.; El Gemayel, N.: Experimental results of multipath behavior for GPS L1-L2 and Galileo E1-E5b in static and kinematic scenarios. *Journal of Applied Geodesy*, Vol. 13, Issue 4, pp. 279-290, deGruyter, Berlin, 2019.
- Hassan, A.; Xu, J.; Xing, C.; Schwieger, V.: A contribution to variance analysis of 3D-displacement extracted from GB-SAR measurements. *Journal of Geodesy, Cartography and Cadastre - No 10 / 2019*, ISSN 1454-1408, Bucharest, Romania.
- Hindenberger, P.; Schwieger, V.: Dynamic Location Referencing: Probability-Based Decision System, *Adv. Cartogr. GIScience Int. Cartogr. Assoc.*, 2, 6, <https://doi.org/10.5194/ica-adv-2-6-2019>, 2019.
- Schwieger, V.; Menges, A.; Zhang, L.; Schwinn, T.: Engineering Geodesy for Integrative Computational Design and Construction. *ZfV, Heft 4/2019*.
- Wang, J.; Metzner, M.; Schwieger, V.: Potential Enhancement for Wrong-way Driver Detection using Precise Attribute Information. *Journal of Navigation*, 1-14. doi: 10.1017/S037346319000663
- Zhang, L.; Schwieger, V.: Reducing Multipath Effect of Low-Cost GNSS Receivers for Monitoring by Considering Temporal Correlations. 4th Joint International Symposium on Deformation Monitoring 2019, Athens, Greece.
- Zhang, L.; Wang, J.; Wachsmuth, M.; Gasparac, M.; Schwieger, V.: Die Rolle digitaler Karten für Sicherheitsfunktionen im Straßenverkehr. *ZfV, Heft 4/2019*.

Non-Refereed Publications

- Schwieger, V.; Lerke, O.; Kerekes, G.: Image-Based Target Detection and Tracking Using Image-Assisted Robotic Total Stations. *FIG Working Week 2019*, Hanoi, Vietnam.
- Schwieger, V.; Zhang, L.: Qualität in der Ingenieurgeodäsie - Begriff und Modellierung. 180. DVW-Seminar „Qualitätssicherung geodätischer Mess- und Auswerteverfahren 2019“, am 27. und 28. Juni 2019 in Stuttgart, Wißner-Verlag, Augsburg, 2019.
- Zhang, L.; Wang, J.; Wachsmuth, M.; Gasparac, M.; Trauter, R.; Schwieger, V.: Role of Digital Maps in Road Transport Security. *FIG Working Week 2019*, Hanoi, Vietnam.

Presentations

- Schwieger, V.: Smart Engineering Geodesy - Construction and Monitoring. Wuhan, China; September 11, 2019.

Schwieger, V.: Smart Engineering Geodesy - Construction and Monitoring. Bucharest, Romania; October 29, 2019.

Schwieger, V.: Engineering Geodetic Research Developments and the Romanian-German Story. Bucharest, Romania; October 31, 2019.

Zhang, L.: Automatisierte Prävention von Terrorattacken mit LKW. Intergeo 2019, 17.09.2019, Berlin.

Activities at the University and in National and International Organisations

Volker Schwieger

Dean of the Faculty of Aerospace Engineering and Geodesy, University of Stuttgart
Full member of the German Geodetic Commission (Deutsche Geodätische Kommission - DGK)

Member of the section „Engineering Geodesy“ within the German Geodetic Commission (DGK)

Chief Editor of Peer Review Processes for FIG Working Weeks and Congresses

Member of Editorial Board “Journal of Applied Geodesy”

Member of Editorial Board “Journal of Applied Engineering Science”

Member of Editorial Board “Journal of Geodesy and Geoinformation”

Martin Metzner

Member of the NA 005-03-01 AA “Geodäsie” at the DIN German Institute for Standardization

Coursedirector of the MSc Program GeoEngine at the University of Stuttgart

Li Zhang

Co-Chair of Working Group 5.6 „Cost Effective Positioning“ within FIG Commission 5 (Positioning and Measurement)

Chair of Working Group „Quality Assurance“ within Commission 3 „Measurement Methods and Systems“ of Deutscher Verein für Vermessungswesen (DVV)

Doctorates

Florian Zimmermann: Analysis and mitigation of site-dependent effects in static and kinematic GNSS applications. Universitäts- und Landesbibliothek Bonn, 2019. Hauptberichter: Prof. Dr.-Ing. Heiner Kuhlmann, Mitberichter: Prof. Dr.-Ing. Steffen Schön, Prof. Dr.-Ing. habil. Volker Schwieger

Master Theses

Buss, Roman: Weiterentwicklung eines selbstfahrenden Messroboters für die Kontrolle von Spalt und Übergang an Karosserien. (Schwieger, Schröder)

Chatterjee, Trisha: Modules for Simulating & Monitoring Autonomous Cars. (Metzner)

Hesham, Mohamed: Application of Accurate Lane-Level Road Maps in vehicle localization. (Wang)

Harb, Jamal: Rendering of 3D Citymodels at runtime based on map data. (Wachsmuth)

Huber, Christina: Kalman Smoothing für inertial-visuelle Fusion. (Schwieger)

Hu, Wenxuan: Potential analysis of industrial CO2 sources for the provision of synthetic fuels. (Metzner)

Li, Yu: Development of Horizon Provider with a focus on critical areas (Metzner)

Marev, Panayot: Entwicklung eines Verfahrens zur Generierung eines Skyplots mit dynamischen Elevationswinkeln aus Bildern. (Luz)

Pfitzenmaier, Tobias: Strahldivergenz- und Footprintuntersuchung von puls-basierten Laser-scannerstrahlen mittels experimentellen Messungen unter Labor- und Feldbedingungen. (Kerekes)

Preuß, Sabrina: Entwicklung eines Algorithmus zu einem fahrspurgenauen Map-Matching und Aufbau notwendigen Kartenmaterials mit Matlab und ArcGis. (Luz)

Wein, Isabel: Bestimmung einer GNSS Kombinationslösung aus mehreren individuellen GNSS-Messungen für die Überwachung turmförmiger Objekte. (L. Zhang)

Bachelor Theses

Buck, Maximilien: Modellbasierte Leistungserfassung mit Lean Construction gezeigt an einem Praxisbeispiel (Metzner)

Hausmann, Nadine: Untersuchung eines TLS auf Nahbereichskorrektur sowie Einsatzmöglichkeiten bei unterschiedlichen Wetterbedingungen. (Kerekes)

Häusler, Manuel: Evaluierung und Deformationsanalyse des Holzpavillons auf der Bundesgartenschau. (Basalla)

Frolow, Rudolf: Entwicklung einer Applikation zu freien Stationierung mit verdeckten Festpunkten. (Basalla)

Education

SS19 and WS19/20 with Lecture/Exercise/Practical Work/Seminar

Bachelor Geodesy and Geoinformatics (German)

Basic Geodetic Field Work (Wachsmuth, Kanzler)

0/0/5 days/0

Engineering Geodesy I (Schwieger, Kerekes, Balangé)

4/2/0/0

Engineering Geodesy II (Schwieger, Lerke)	1/1/0/0
Geodetic Measurement Techniques I (Metzner, Wachsmuth)	3/1/0/0
Geodetic Measurement Techniques II (Wachsmuth)	0/1/0/0
Integrated Field Work (Kerekes, Metzner)	0/0/10 days/0
Reorganisation of Rural Regions (Helfert)	1/0/0/0
Statistics and Error Theory (Schwieger, Wang)	2/2/0/0

Master Geodesy and Geoinformatics (German)

Causes of Construction Deformations (Lerke, Wang)	1/1/0/0
Deformation Analysis (L. Zhang)	1/1/0/0
Industrial Metrology (Schwieger, Y. Zhang)	1/1/0/0
Land Development (Eisenmann)	1/0/0/0
Monitoring Measurements (L. Zhang, Basalla)	1/1/0/0
Monitoring Project (Lerke)	0/0/2/0
Terrestrial Multisensor Systems (L. Zhang, Lerke, Kerekes)	1/1/0/0
Transport Telematics (L. Zhang, Luz)	2/2/0/0

Master GeoEngine (English)

Integrated Field Work (Kerekes, Metzner)	0/0/10 days/0
Kinematic Measurement Systems (Schwieger, Basalla)	2/2/0/0
Monitoring (L. Zhang, Wang)	1/1/0/0
Thematic Cartography (L. Zhang, Wachsmuth)	1/1/0/0
Transport Telematics (Metzner, Y. Zhang)	2/1/0/0
Terrestrial Multisensor Systems (Lerke, Y. Zhang)	2/1/0/0

Bachelor and Master Aerospace Engineering (German)

Statistics for Aerospace Engineers (L. Zhang, Balangé, Hassan)	1/1/0/0
--	---------

Master Aerospace Engineering (German)

Industrial Metrology (Schwieger, Y. Zhang)	1/1/0/0
Transport Telematics (L. Zhang, Luz)	2/2/0/0

Bachelor Civil Engineering (German)

Geodesy in Civil Engineering (Metzner, Balangé)	2/2/0/0
---	---------

Master Civil Engineering (German)

Geoinformation Systems (Metzner, Hassan)	2/1/0/0
Transport Telematics (L. Zhang, Luz)	2/1/0/0

Bachelor Technique and Economy of Real Estate (German)

Acquisition and Management of Planning Data and Statistics (Metzner, Luz, Kanzler) 2/2/0/0

Bachelor Transport Engineering (German)

Statistics (Metzner, Luz, Kanzler)

0.5/0.5/0/0

Seminar Introduction in Transport Engineering (Basalla)

0/0/0/1

Master Infrastructure Planning (English)

GIS-based Data Acquisition (L. Zhang, Luz)

1/1/0/0



Institute of Geodesy

Geschwister-Scholl-Str. 24D
 D-70174 Stuttgart
 Tel.: +49 711 685 83390
 Fax: +49 711 685 83285
gis@gis.uni-stuttgart.de
<http://www.gis.uni-stuttgart.de>

Head of Institute

Prof. Dr.-Ing. Nico Sneeuw

Emeritus

em. Prof. Dr.-Ing. habil. Dr. tech. h. c. mult. Dr.-Ing. E. h. mult. Erik W. Grafarend

im Ruhestand

Prof. Dr. sc. techn. Wolfgang Keller

Academic Staff

Dr.-Ing. Markus Antoni	Physical Geodesy, Satellite Geodesy
Dr. Karim Douch	Physical Geodesy, Seismology
Dr.-Ing. Omid Elmi	Remote Sensing
PD Dr.-Ing. habil. Johannes Engels	Physical Geodesy, Satellite Geodesy
Dr. Hassan Hashemi Farahani	Physical Geodesy, Satellite Geodesy
Dr.-Ing. Friedrich Krumm (until 31.3)	Adjustment Theory, Mathematical Geodesy
Dr.-Ing. Mohammad Tourian (since 1.8)	Satellite Geodesy, Adjustment Theory

Research Associates

M.Sc. Sajede Behnia	Satellite Altimetry
M.Sc. Dennis Mattes	Satellite Altimetry
Dr.-Ing. Muhammad A. Javaid (until 21.3)	Satellite Geodesy
Dr.-Ing. Wei Liu (until 30.6)	Satellite Geodesy
M.Sc. Saemian Peyman	Satellite Geodesy, Hydrology
M.Sc. Bo Wang (since 27.8)	Satellite Altimetry
PhD Zhi Yin (until 31.1)	Geodynamics, Physical Geodesy

Dr.-Ing. Jinwei Zhang (until 30.4)

Geodetic Data Analysis

Administrative/Technical Staff

Dipl.-Ing. (FH) Thomas Götz

Dipl.-Ing. (FH) Ron Schlesinger

Anita Vollmer

IT System, Controlling

IT System, Technical Support, Gravimetry
Secretary

External Lecturers

Dipl.-Ing. Steffen Bolenz

Dipl.-Ing. Gerhard Grams

Dipl.-Ing. Dieter Heß

Stadtmessungsamt, Stuttgart

Ministerium für Ländlichen Raum und Verbraucherschutz Baden-Württemberg, Stuttgart

Ministerium für Ländlichen Raum und Verbraucherschutz Baden-Württemberg, Stuttgart

Guests

Dr.-Ing Siavash Iran Pour

Prof. Dr. Elsayed Issawy

Assoc. Prof. Yi Lin

PhD student Bingshi Liu

Dr. Huanling Liu

PhD student W. Luan

PhD student Lingdong Meng

Prof. Dr. Alfredo Ribeiro Neto

BSc Yufeng Nie

Prof. Yunzhong Shen

PhD student Ruiqing Song

Prof. Péter Varga

PhD student Xiaohang Wang

Prof. Dr. Hangjiang Wen

Prof. Dr. Caijun Xu

Junior Researcher Yantian Xu

University of Isfahan (3.4–30.9)

National Research Institute of Astronomy and Geophysics Helwan, Egypt (7–24.6)

Tongji University, Shanghai, China (12–27.2 + 1–30.9)

University of Wuhan, Wuhan, China (1.9–31.10)

CASM, Beijing, China (1.8.2019–31.1.2020)

University of Wuhan, Wuhan, China (11.9–19.9)

Tongji University, Shanghai, China (11.9–19.9)

Universidade Federal de Pernambuco, Recife/PE, Brasília (2.9.2019–31.7.2020)

(2.4–30.9)

Tongji University, Shanghai, China (9.9–30.9)

Tongji University, Shanghai, China (11.9–19.9)

Geodetic and Geophysical Research Institute, Sopron, Hungary (4.3–31.5)

University of Wuhan, Wuhan, China (11.9–19.9)

CASM, Beijing, China (1.9–30.9)

University of Wuhan, Wuhan, China (16.8–17.9)

CASM, Beijing, China (11.9.2018–20.9.2019)

Dr.-Ing. ShuangYi
PhD student Tinghui Zhang

China (since 5.1.2019), Humboldt Fellow
Tongji University, Shanghai, China (until 10.9)

Research

Spatial downscaling of GRACE water storage changes data

The satellite missions GRACE and GRACE FO provided a fundamentally new remote sensing tool for a wide spectrum of Earth science applications. They caused a quantum leap both in hydrological understanding of continental scale systems and their interactions as well as for applications. Nevertheless, in hydrology there is a pressing need for more observational evidence, which arises from the limited knowledge of the spatial and temporal dynamics of the surface freshwater variations and discharges. GRACE and GRACE FO are, however, limited in terms of spatio-temporal resolution.

Although the spatio-temporal resolution of GRACE and GRACE FO is limited by the orbit configuration, water storage variation can be downscaled by assimilating the data of different storage compartments with a higher temporal and spatial resolution. To this end, we downscaled the coarse-scale Equivalent Water Height (EWH) of GRACE X_G using fine-scale EWH from WaterGAP Global Hydrology Model WGHM X_W and precipitation data X_P using the copula method. We first obtained uniformly distributed marginals U_G, U_W, U_P by applying probability integral transform into unit cubes from marginal distributions of each data set $F_G(X), F_W(X), F_P(X)$. We then obtained empirical copula of these three data sets. The copula of (X_G, X_W, X_P) is defined as the joint cumulative distribution function of U_G, U_W, U_P

$$C(u_G, u_W, u_P) = \Pr[U_G \leq u_G, U_W \leq u_W, U_P \leq u_P]$$

We then fitted different analytical copulae to the obtained empirical copula and found out that the t-copula fits the best. Using the t-copula, for each month a random field is generated at a fine scale ($0.5^\circ \times 0.5^\circ$), which follows the marginal distribution of coarse-scale GRACE in $5^\circ \times 5^\circ$. The random fields are then turned into GRACE fields by the so-called rank matching approach. Figure 1 shows the result of our downscaling approach for the month April 2004. The downscaled GRACE EWH shows pattern from WGHM and precipitation and GRACE original data itself.

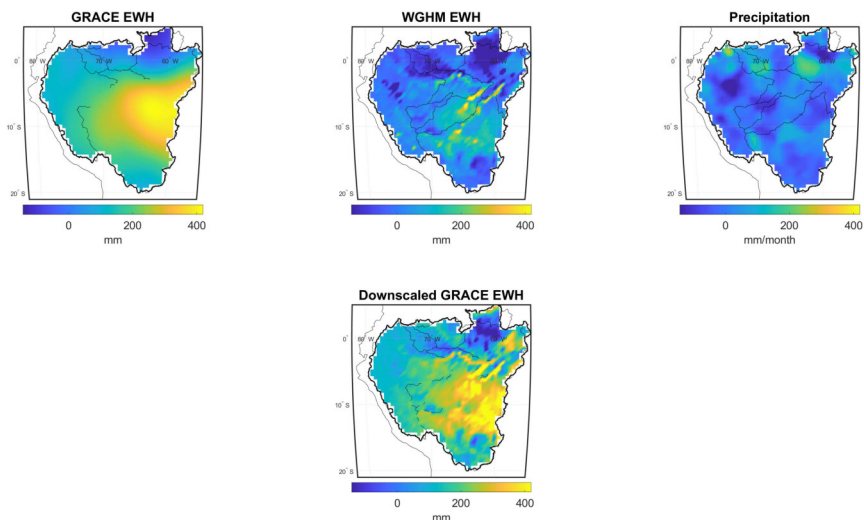


Figure 1: Coarse scale GRACE (top, left) is downscaled to a 0.5×0.5 degree (bottom, center) using fine scale data of WGHM (top, middle) and precipitation data (top, right)

GravSeis: an analysis of the detectability of earthquakes by the Next Generation Gravity Mission

The success of the Gravity Recovery and Climate Experiment (GRACE) mission has established space gravimetry as an irreplaceable means to monitor the Earth's gravity field as well as the mass and distribution within the Earth system at a global scale. Consequently, a follow-on mission has taken over GRACE after more than 15 years of services and the next generation gravity mission (NGGM) is currently under study to ensure a continuation of the observations. The envisioned future mission will consist of 2 pairs of satellites, as opposed to 1 for GRACE and GRACE follow-on. The expected effect is an increase of the spatial and temporal resolution of the recovered gravity fields, thereby widening the scope of utility of the mission. In particular, it has been foreseen that reaching the expected spatio-temporal resolution would enable the observation of the co- and post-seismic gravity signature of a larger number of earthquakes. Evaluating and quantifying to what extent this is possible is the objective of the GravSeis project.

GravSeis is an ESA-funded project gathering researchers from the **Politecnico di Milano**, **Thales Alenia Space Italia** and **GIS**. Our work has consisted in carrying out a closed-loop simulation of an NGGM during its full lifetime in order to evaluate the time series of the realistically degraded, synthetic recovered gravity field. In the forward simulation, a realistic time-variable gravity field is first synthesized, including the signal associated to a variety of earthquakes (different locations, depth, mechanism, orientation etc.), see Figure 2. Then,

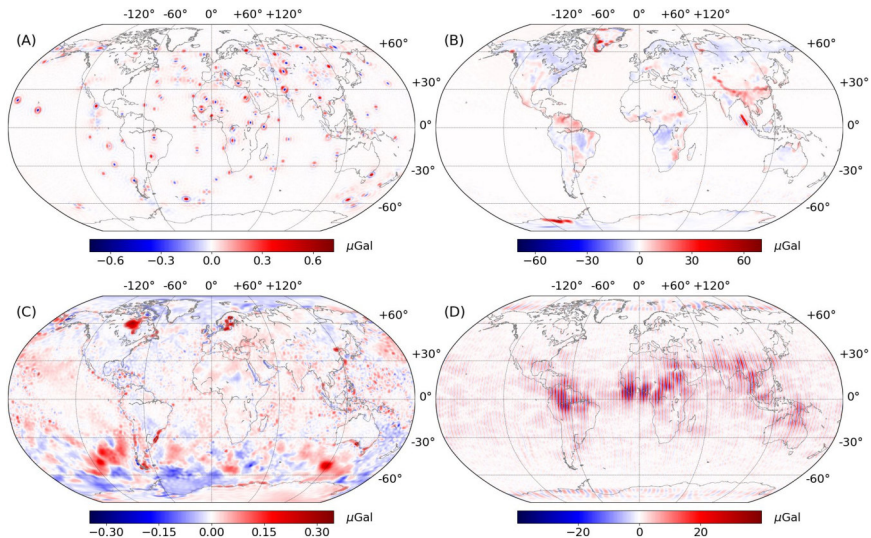


Figure 2: Comparison of the magnitude of the different time-variable gravity signals included in the forward simulation: (A) the gravity signature of the many magnitude $M_W = 7$ earthquakes, (B) the contribution of the atmosphere, ocean, hydrosphere, ice and solid Earth, (C) the modelling error of the high-frequency component of the atmosphere and ocean contribution to the time-variable gravity field and (D) the true error degrading a recovered gravity field model. These plots correspond to the 120-th recovered model.

the measurements made by the orbiting satellites are simulated and degraded with different kinds of modelling errors and additive sensor noise, see Figure 3. In the backward simulation, these measurements are used to recover monthly gravity field models. At the end, a time series of 156 models has been computed, covering a period of more than 11 years during which 291 synthetic earthquakes occurred. Finally, these recovered gravity field models have been analysed to quantify to what extent the gravity signature of earthquakes could be detected and with which accuracy.

Depending on the ability to model correctly the AOHIS background signal, our final results show that it is possible to estimate earthquake's signal amplitude with a relative accuracy lower than 10% in most cases for magnitude $M_W = 7.8$ and larger. In the best case where the AOHIS signal is perfectly modelled, the threshold can be as low as $M_W = 7$. A more detailed investigation shows however that this threshold is likely to change depending on the location. In comparison, the lowest earthquake magnitude threshold that has been detected in GRACE is $M_W = 8.3$. NGGM would therefore bring unprecedented new insights in the monitoring of a larger number of earthquakes, in particular for those occurring offshore.

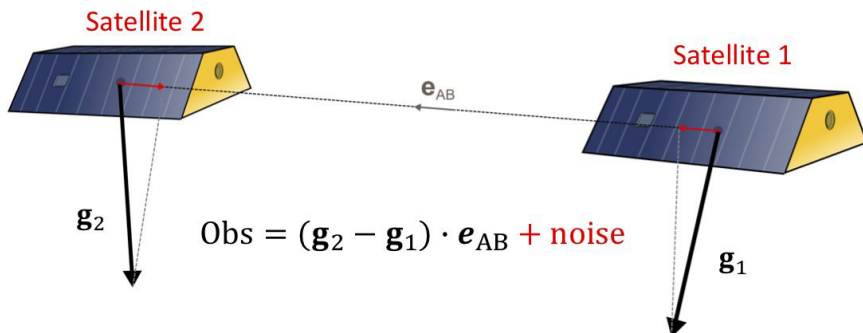


Figure 3: Simplified measurement principle used for the simulation of observables for 1 pair of GRACE-like satellites.

Estimation of river discharge and surface water storage from spaceborne data: full catchment coverage with optimal space and time resolution

A project within the DFG research unit “Global Calibration and Data Assimilation (GlobalCDA)”

Interest in the global freshwater system has been increasing during the last decades, with respect to its role in the Earth system and the sustainable development of water resources. On the one hand, water transport and storage on continents play an important role for atmospheric processes (climate feedback), variability of global and regional sea levels, and global biogeochemical cycles, and have a significant impact on temporal variations of the Earth’s gravity field, deformation of the Earth’s crust, and Earth rotation in space.

Insufficient observational evidence of hydrological parameters at the global scale is a major impediment for progress in hydrological modeling. Although spaceborne sensors offer a synoptic and global view by their very nature, satellite products do have their own limitations in terms of accuracy, temporal resolution and spatial coverage. This project aims to greatly improve the observational database for two key hydrological variables, river discharge and surface water storage, by innovative modeling of results from satellite altimetry (water level) and satellite imagery (surface area). The major research questions that we aim to answer within this project include:

- How can we modify the existing single-stem densification of altimetric measurements and modify it for an entire river basin?

The existing densification method merges water level time series of several virtual stations along the main stem of a river to produce a dense water level time series, i.e. with high temporal resolution. However, the dynamics over the entire basin is not

reflected since the method is only applicable over the main river stem. The modified densification algorithm will ingest all possible altimetric water level time series over an entire river basin to represent the dynamic river system in a river basin.

- How can we methodologically improve the discharge estimation algorithm from multi-mission altimetry and satellite imagery over full catchments?

Typically, multi-mission altimetry for discharge estimation along the main stem is only practiced with three missions, Envisat, Jason-2 and SARAL/AltiKa. However considering the measurements of recently launched missions like Sentinel-3, Jason-3 and CryoSat-2 carry their own challenges in terms of discharge estimation. Moreover, finding an appropriate functional model, that relates directly river discharge to water level and to river width, is still a challenge.

- Can we quantify the amount of surface water storage change within total storage variations?

Surface water storage variations are obtained by combining surface water extent measurements (from satellite imagery) with water level variation (from satellite altimetry). An important issue is how to deal with the inconsistency in temporal sampling between both quantities.

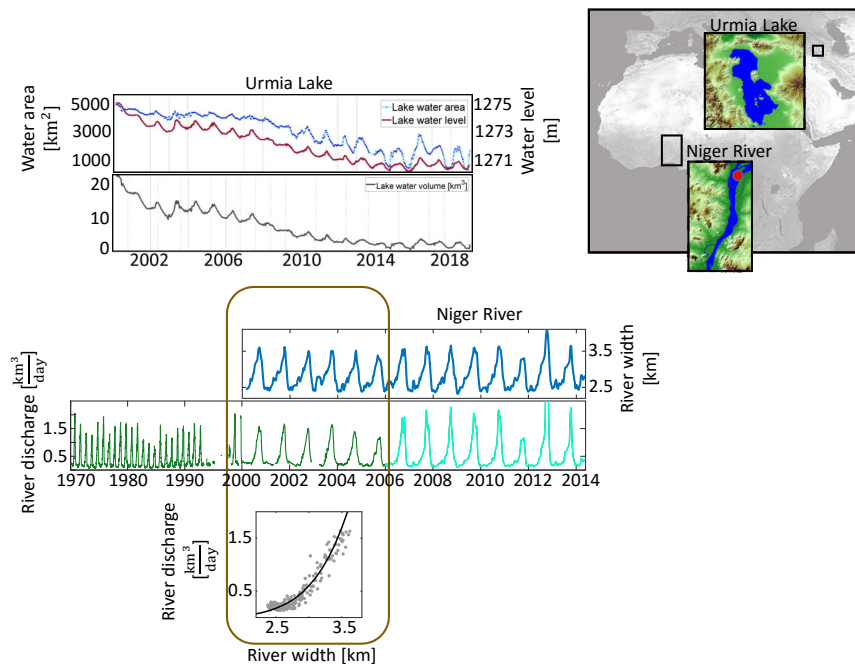


Figure 4: Spaceborne observations can be used to estimate different components of surface water. In the top panel, the time series of lake water area from satellite imagery and water level from satellite altimetry measurements are provided. The lake water volume variations can be calculated by combining lake water area and level measurements. The bottom panel is one example of estimating river discharge using river width measurements from satellite imagery. The gauging station (red dot in the figure) stopped measuring river discharge in the year 2006. On the other hand, river width measurements from the MODIS images are available from 2000. So a rating curve model can be obtained for estimating discharge using the simultaneous measurements between the years 2000 – 2006. As a result, the time series of river discharge can be continued after 2006 by using the width measurements and the developed model.

STREAM: SaTellite Based Runoff Evaluation And Mapping

STREAM is funded by European Space Agency and aims at estimating runoff in river basins from satellite data. It is being executed by Institute for Geo-hydrological Protection- National Research Council (IRPI) and GIS. The project's main objective is to estimate fresh water stored on and below landmasses. To that end, it develops a data-driven approach based on satellite measurements of soil moisture, precipitation, and terrestrial water storage anomalies (TWSA). It focuses on five river basins: Mississippi, Amazon, Murray-Darling, Niger, and Danube. The GIS role is to estimate the baseflow component of runoff using TWSA, observed by Gravity Recovery And Climate Experiment (GRACE), and ground discharge measurements. We obtain TWSA from the NASA's Goddard Space Flight Center (GSFC) global mascon model (Luthcke et al. 2013¹). Figure 5 shows TWSA for two of the basins, Amazon and Mississippi, for Jan. 2003 in terms of equivalent water heights. The mascon geometry is shown there with black boxes. TWSA time series in the entire GRACE span for these basins are shown in Figure 6.

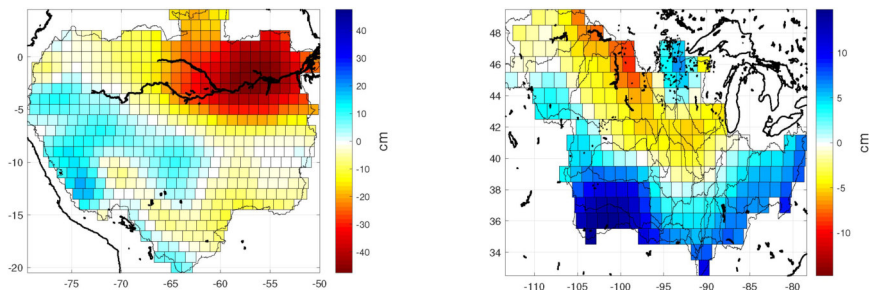


Figure 5: GRACE TWSA for Amazon (left) and Mississippi (right) for Jan. 2003 based on the GSFC global mascon model in terms of equivalent water heights.

To estimate the baseflow runoff, we exploit the runoff-storage (R - S) relationship method (Riegger and Tourian, 2014²; Tourian et al. 2018³). It uses two sets of measurements as input: (i) ground discharge measurements; and (ii) GRACE TWSA time series. The method can be applied if a linear relationship can be established between the baseflow component of ground runoff measurements R_{BS} and TWSA (S)

$$R_{BS}(t) = \frac{1}{\tau} S(t).$$

Herein, τ is an unknown. The storage itself is characterized with an unknown bias (S_0). Furthermore, storage always comes to a runoff with a delay Δt , which causes a phase shift

¹Luthcke SB, Sabaka TJ, Loomis BD, Arendt AA, McCarthy JJ, Camp J (2013) Antarctica, Greenland and Gulf of Alaska land-ice evolution from an iterated GRACE global mascon solution, *Journal of Glaciology*, Vol. 59, No. 216, 2013 doi:10.3189/2013JoG12J147.

²Riegger J, Tourian MJ (2014) Characterization of runoff-storage relationships by satellite gravimetry and remote sensing, *Water Resour Res*, 50: 3444 – 3466, doi: 10.1002/2013WR013847.

³Tourian MJ, Reager JT, Sneeuw N (2018) The total drainable water storage of the Amazon river basin: A first estimate using GRACE, *Water Resour Res*, 54: 3290 – 3312, doi: 10.1029/2017WR021674.

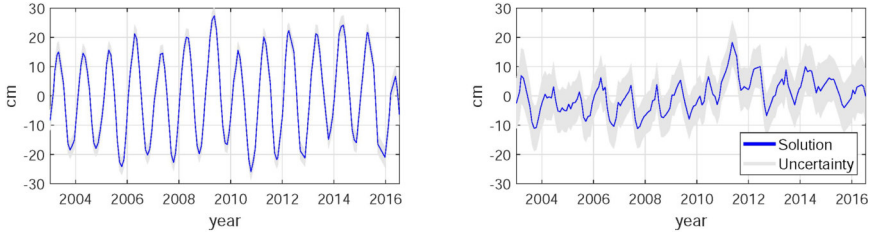


Figure 6: GRACE TWSA time series for Amazon (left) and Mississippi (right) in the time interval 2003 – 2016 based on the GSFC global mascon model in terms of equivalent water heights.

between R_{BS} and S , which is an unknown, too, and is estimated and accounted for with a Hilbert transformation. The final R - S relationship reads as

$$R(t) = \frac{1}{\tau} (S_0 + \Delta S(t + \Delta t)).$$

Estimating the three unknowns yields the function necessary to transform GRACE-observed storage into the baseflow component of runoff. Such a linear relationship can be successfully established in Amazon river basin. This can be identified if monthly pairs of the baseflow runoff and the time-shifted storage are shown in a single picture (Figure 7).

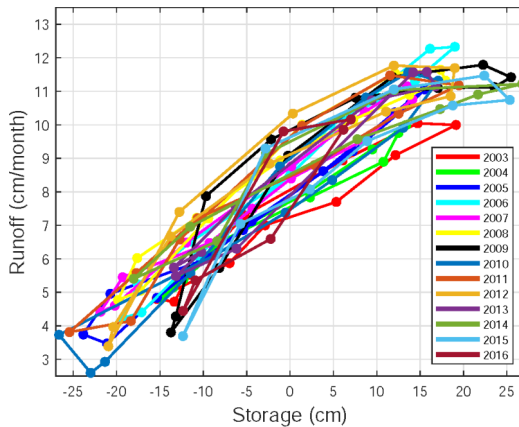


Figure 7: Monthly time series of time-shifted storage for Amazon basin and that of baseflow runoff measurements at the Obidos station.

The shifted storage time series and time series of baseflow runoff are used in a weighted least-squares adjustment in line with Gauß-Helmert model to estimate the remaining unknowns: $\hat{\tau}$ and \hat{S}_0 . Their estimates are used to deliver the baseflow runoff. The results are

summarized in Figure 8, in which estimated baseflow runoff together with total runoff measurements collected at the Obidos station are shown. Uncertainties estimated for the runoff solution are supplied, too.

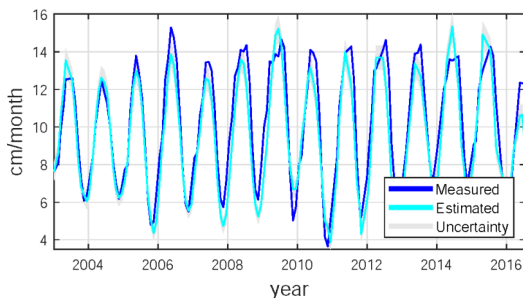


Figure 8: Monthly time series of the estimated baseflow runoff and that of total runoff measurements at the Obidos station.

The RMS differences between the baseflow runoff and total runoff measurements barely reaches one cm/month. The Kling-Gupta Index is 90 percent, which is very high. Furthermore, the baseflow estimate in most cases is lower than the total measurements, as expected. There are a few exceptions, e.g., in 2009, a reason for which is still a topic of active research.

Investigating Granger causality between sea surface temperature and terrestrial water storage change in Europe

Water availability on the continents is vital in many aspects, including human health, economic activity, ecosystem function and geophysical processes. Climate change and unsustainable land management have led to many changes in the water availability of the continents, including Europe, resulting in more extreme events during the past two decades. These events include heat waves, droughts, excessive rain, snowfall, and floods. Terrestrial water storage (TWS) variations represent all available forms of water resource that is the sum of snow, ice, surface water, soil moisture and groundwater and plays a crucial role in the hydrological cycle. Sea surface temperature (SST) has a considerable influence on climate and weather and, as a result, TWS.

In this study, we employ the theoretical framework of Granger causality, which is based on conditional independence, to assess directional dependencies between the leading principal components of SST and the estimation of TWS. More generally, a quantity X is said to Granger-cause Y if an auto-regressive (AR) model of Y has a lower ability to predict the time series of Y than the same AR model augmented with an AR model of X . The Terrestrial Water Storage (TWS) is derived from the Gravity Recovery And Climate Experiment (GRACE) mission products, while the SST principal components are computed from satellite-derived data. The result of this study helps to interpret the influence of climate change on the wa-

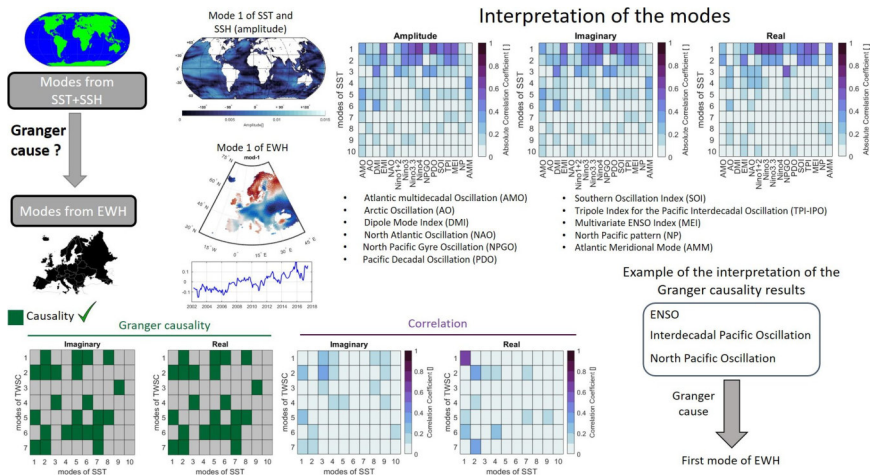


Figure 9: The scheme and summary of the study.

ter storage variability of Europe. Moreover, the investigation of Granger causality of SST on TWS change represents a first step before establishing a prediction scheme. The result of this study was presented in September 2019 at the Intergeo conference in Stuttgart.

Developing an optimum outlier rejection scheme for altimetry processing of inland waters

For a few decades now, access to water monitoring records has become more difficult due to both practical and strategic reasons. Almost in parallel, remote sensing of inland waters has tried to fill in the gap. Among varied satellite based methods, altimetry has proven effective in monitoring water level.

Satellite altimetry was initially designed for oceanographic purposes and, hence, faces multiple challenges when applied over inland waters. This is mainly rooted in disproportionality between the cross-over width and radar footprint size, leading to heterogeneous radar reflections, off-nadir measurements, and less characterized waveforms. Imprecise geophysical corrections even further degrade the accuracy and precision of the derived water heights. Although considerable effort has been made to address every single one of the abovementioned issues, the signal-to-noise ratio of the inland time series are typically far from acceptable. In effect, various sources of error add up and necessitate the so-called outlier rejection.

Outlier rejection can refer to the screening process in two different stages: one, while choosing the representative height for every crossover, and the other, when discarding the erroneous estimates from the time series of heights. So far we have targeted the latter, and tried to find an optimum scheme which is less sensitive towards the seasonality regime of the

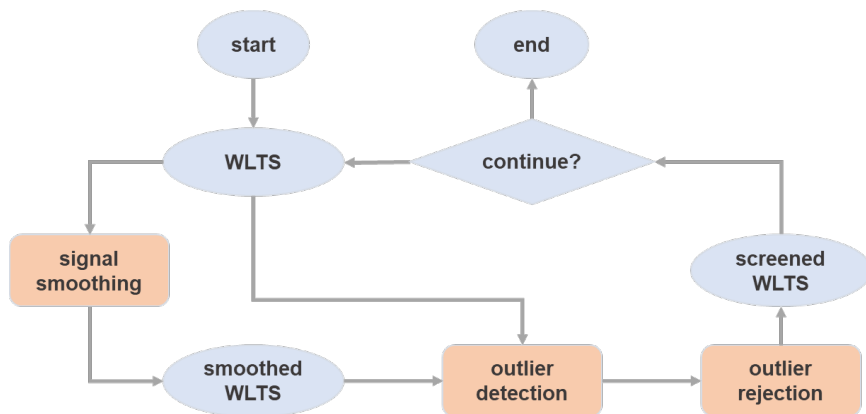


Figure 10: The proposed outlier rejection scheme. WLTS stands for Water Level Time Series.

case study and sampling irregularity of the observations. We have assessed the potential of a couple of methodologies, including Savitzky-Golay filtering and spectral analysis in both Fourier and Least-Squares domains.

Figure 10 shows the overall outlier rejection scheme we utilize. The input samples are first low-pass filtered, and later compared to the original time series. This will allow finding the outlier candidates — the so-called detection or identification step. We will then reject the identified samples in an iterative manner.

Our analysis so far suggests that

- Fourier and Least Squares Spectral Analysis (LSSA) are highly dependent on choice of cut off frequency and the significance level of the constructed spectral domain. Nevertheless, LSSA leads to better results and, taken the irregular sampling of the altimetric time series, is easier to apply. The Savitzky-Golay filter on the other hand outperforms the preceding methods as long as there are not very long periods of no data.
- the statistical criteria by which the outliers are identified, and later on, rejected can make noticeable changes.
- the performance of the suggested methods is also influenced by the nature of the inland water body, meaning that height variation regime of lakes and reservoirs is different from that of a river.

Figure 11 is illustrating the outcome of the proposed methodology over a virtual station in the mountainous basin of Karun, Iran. Taken the long periods of no data, high noise level, and the frequent outlying samples, the results look promising. Our assessment into the topic is still ongoing. We are looking for a robust and versatile approach which would facilitate a semi-automatic generation of water level time series.

case study: Karun basin, Iran
altimetry satellite: Jason-2
crossing width ≈ 320 m
distance along the chainage to the dam ≈ 19.5 km
elevation of the surroundings ≈ 1200 m

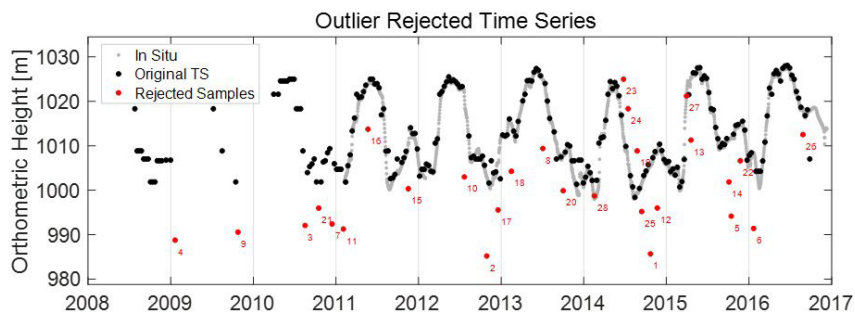


Figure 11: Outlier rejected time series using the smoothing filter Savitzky-Golay and a local rejection approach based on t Location-Scale distribution

Coastal Altimetry using ICESat-2 Photon-Counting Laser Altimeter

Ice, Cloud, and Land Elevation Satellite-2 (ICESat-2), operated by NASA, was launched in September 2018. The Advanced Topographic Laser Altimeter System (ATLAS) on the mission carries six beam laser transmitter with photon counting detectors, which emits 532-nm laser of 10 kHz repetition rate. ATLAS detects individual photons in a 70 cm separation for each shot on the earth's surface in the along-track direction with ~ 17 m diameter footprint. Comparing to radar altimetry, ICESat-2 provides much higher along-track spatial resolution observing global earth surface, including inland water bodies, coasts and open oceans.

For radar altimeters, when the satellite nadir position approaches the coastline, waveform samples become contaminated by land reflections, which causes poor accuracy of water level comparing to open oceans even some retracking methods may fail. Unlike radar altimetry, small footprint (~ 17 m) and dense sampling measurements (0.7 m) of ICESat-2 present an opportunity to measure the water surface directly, and to extract the long wave length from the point cloud.

Measurements of a single track include noise photons which are from solar background radiation, system dark current and speckle effect. For ICESat-2 laser altimeter, it is noticed the ground surface and water surface reflections have a much higher density in the point

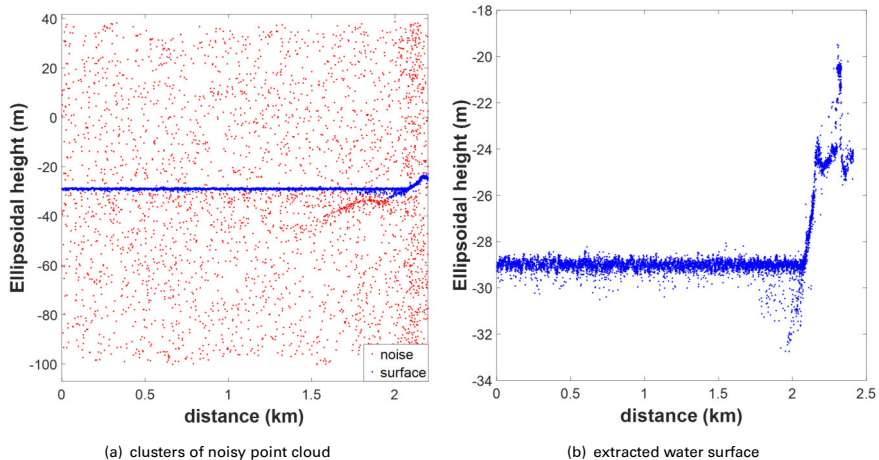


Figure 12: Track 919 over coast of Panama Beach (USA) on 26 Feb 2019

cloud. Therefore, we will lead a density-based algorithm which is called Density-Based Spatial Clustering of Applications with Noise (DBSCAN) (Ester et al., 1996⁴) to eliminate noise points to extract relatively clean water surface. As the data set have the spatial resolution of 0.7 m in the horizontal direction, and the laser pulses penetrate water which reflect under water surface. Before applying DBSCAN algorithm, we need to modify the scale of horizontal direction because the surface reflections have a higher density in the vertical than the horizontal direction.

After applying DBSCAN, the points of blue color are clustered, and the red points are labeled as noise points (Figure 12(a)). The extracted water surface with a part of the land topography is shown in Figure 12(b), but we can use a threshold to reject the part of land topography. We can see the water surface has a thickness of more than 1 m, which is caused by the reflections from the water volume under the surface. The next step is to extract the water surface precisely. For this case we use the method of re-sampling with different quantiles of a size of segment (Mandlbürger et al., 2013⁵) to validate

Table 1: Validate with tide gauge station

	100 m	200 m	300 m
q50	-0.42	-0.42	-0.42
q75	-0.30	-0.29	-0.30
q95	-0.13	-0.12	-0.12
q97	-0.08	-0.08	-0.08
q99	0.02	0.02	0.02
q100	0.17	0.26	0.33

⁴Ester M, Kriegel H-P, Sander J, Xu X, et al. (1996) A density-based algorithm for discovering clusters in large spatial databases with noise, Kdd, Vol. 96, No. 34, pp. 226–231.

⁵Mandlbürger G, Pfennigbauer M and Pfeifer N (2013) Analyzing near water surface penetration in laser bathymetry—A case study at the River Pielach, ISPRS Annals of the Photogrammetry, Remote Sensing and Spatial Information Sciences, Vol. 5.

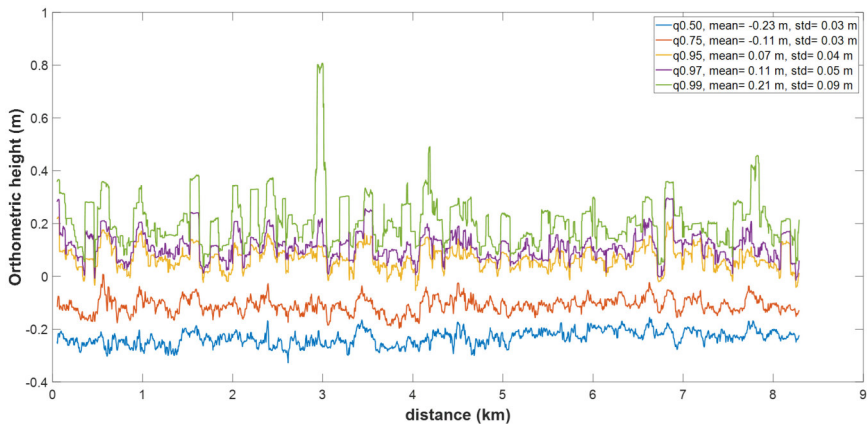


Figure 13: Resampled with resolution of 5 m in 100 m of each segment

with the record of tide gauge station. The design a box with the width of 100/200/300 m moving along the track with a step of 5 m, and in each step different quantiles can be calculated (Figure 13). We found that the result of 99% quantile is the best comparing to the tide gauge station, and segment of 200/300 m shows the similar result of 100 m (Table 1).

RASLyBoCa: Response of Arctic sea level and hydrography to hydrological regime change over boreal catchments

Changes in freshwater influx into the Arctic Ocean are a key driver of regional dynamics and sea level changes in the Arctic waters. Fresh surface waters maintain a strong stratification in the Arctic. This halocline largely shields the cool polar surface water and sea ice from the warmer waters of Atlantic origin below and hence inhibits vertical heat fluxes. Changes in the freshwater content are likely to affect regional steric sea levels, but also the modified ocean dynamics may change the sea level through mass transports within the Arctic. To measure these changes, satellite gravimetry (GRACE) and satellite altimetry open up new avenues of observing the hydrology of large catchments by measuring the water storage over catchments and water level along rivers, which can be transformed into discharge through several methods.

Regarding satellite altimetry, the main problem is the low spatial and temporal resolution, which can be seen in Figure 14. To overcome this problem, we develop a new method to densify altimetry data along the river. Thus, we aim to develop an algorithm which is able to combine the altimetry measurements along the river in time and space, so that it is possible to estimate a water level time series at any desired position along the river. This is done by using the so called Least Squares Collocation (LSC).

The basic idea of this approach is, to separate the measurements y into a trend or seasonal part Ax , a stochastic signal s and noise n :

$$y = Ax + s + n$$

By using this model, one can focus on the signals for the further calculations. Thus, the signals are first estimated by using the covariance information of the measurements. In a second step they are densified to obtain \hat{s}_d . It is then possible to determine the densified water level \hat{y}_d :

$$\hat{y}_d = A_d \hat{x} + \hat{s}_d$$

Until now, the densification was conducted in time along one time series, which is shown in Figure 15. The next step is to establish covariance matrices along the river to conduct the densification in time and space. With this, we will be able to estimate the densified time series at any wanted position on the river.

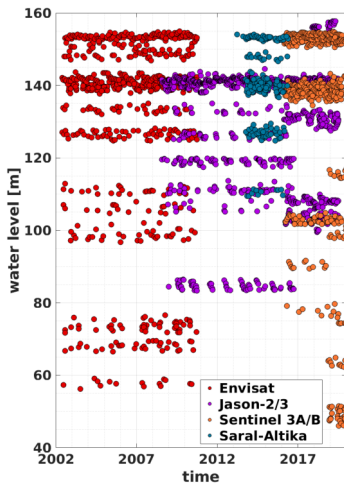


Figure 14: Quite dense altimetry coverage in time and space, but big temporal and spatial gaps in multiple areas of the river.

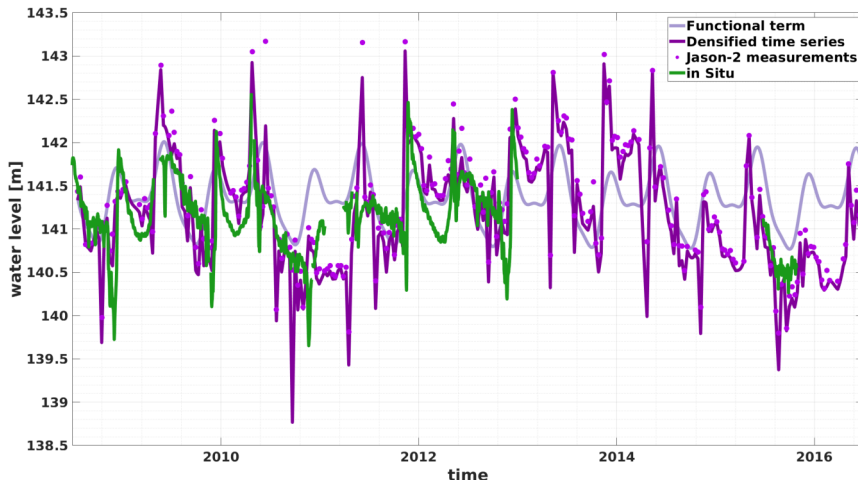


Figure 15: Time series after densification in time with Jason 2 Track 223 compared to in-situ data, the RMSE is 0.49 m. Also the used Jason 2 measurements and the estimated seasonality is shown.

Time Domain Modeling of InSight/SEIS VBB and SP Frequency Calibrations on Earth and on Mars

This activity report is essentially the contents a poster presented at the InSight science team meeting Nr. 15 that took place in Paris from June 17-21.2019, seven months after InSight had landed on Mars and 5 months after the SEIS instrument package had been deployed on the surface of Mars (Fig. 16).

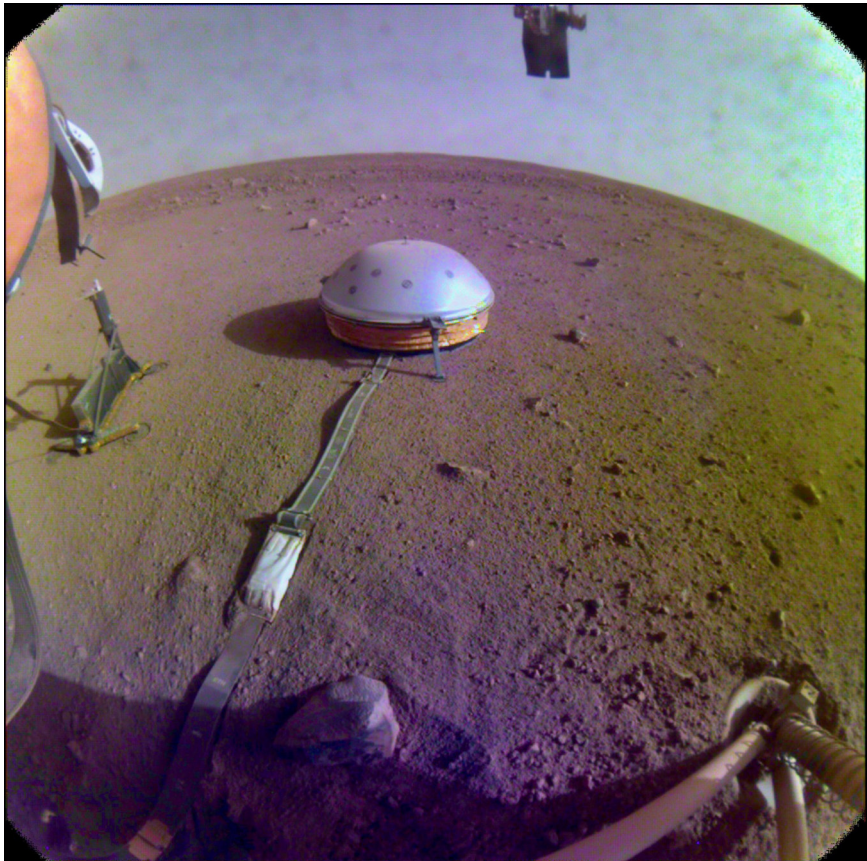


Figure 16: The SEIS instrument package deployed in Elysium Planitia on Mars. The actual seismometer is covered by the wind and thermal shield WTS. On the left the HP³ geothermal heatflow probe of the German Aerospace Agency DLR can be seen. (image:JPL/Caltech/NASA)

InSight is a joint NASA and European mission (Banerdt et al., 2020⁶). It is the first mission to Mars dedicated to the study of the deep interior of our neighboring planet. The primary payload of the mission is the seismometer package SEIS which has been built by a European consortium of universities (IPGP Paris, ETHZ Zürich, Imperial College London) and space agencies (CNES from France, DLR and MPS from Germany). Since it has been deployed and commissioned a variety of seismic signals have been recorded: some originating from the atmosphere, like the passage of dust devils (Banfield et al., 2020⁷), and some from the Martian interior like marsquakes (Giardini et al., 2020⁸). My co-authors for the poster were Erhard Wielandt (Geophysik, Stuttgart), Tanguy Nébut (IPGP Paris) and Nicolas Verdier (CNES, Toulouse) and together we analysed insitu calibrations conducted with SEIS before and after its journey to Mars. For redundancy SEIS contains two 3-component force-feedback seismometers: VBB and SP, a broad-band and a MEMS short-period seismometer, respectively.

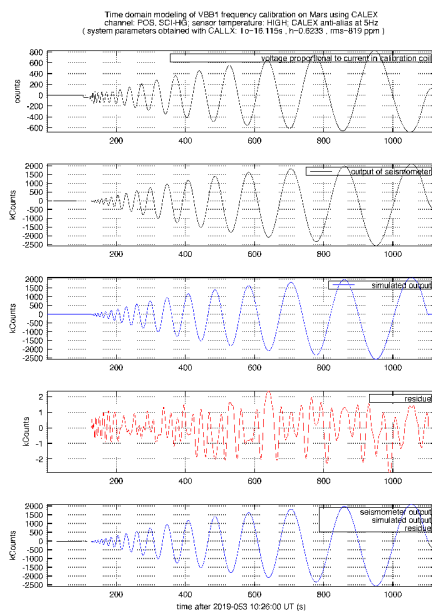


Figure 17: Modeling of a voice coil calibration of sensor VBB1, high-gain channel POS. This calibration experiment was carried out on Mars on Sol 86 of the mission (22.2.2019). The five panels show (top-to-bottom) (1) the input current to the calibration coil, (2) the measured seismometer response, (3) the synthetic response, (4) the residue: difference between traces (2) and (3) and finally (5), a combined plot of the traces from panels 2,3 and 4. The synthetic trace can reproduce the data well: the *rms*-amplitude of the residue is only 0.1% of the total signal. The residue is signal generated and points to imperfections of the linear model.

⁶Banerdt, W.B., Smrekar, S.E., Banfield, D. et al. Initial results from the InSight mission on Mars. *Nat. Geosci.* (2020). <https://doi.org/10.1038/s41561-020-0544-y>

⁷Banfield, D., Spiga, A., Newman, C. et al. The atmosphere of Mars as observed by InSight. *Nat. Geosci.* 13, 190–198 (2020). <https://doi.org/10.1038/s41561-020-0534-0>

⁸Giardini, D., Lognonné, P., Banerdt, W.B. et al. The seismicity of Mars. *Nat. Geosci.* 13, 205–212 (2020). <https://doi.org/10.1038/s41561-020-0539-8>

Inertial seismometers such as the VBB and SP sensors in the InSight/SEIS instrument package (Lognonné et al., 2019⁹) convert ground motion into an electrical voltage. The sensitivity of the seismometers is frequency dependent and in order to estimate this frequency dependence each of the six seismometer components of SEIS is equipped with a calibration coil. An electrical current flowing through the coil exerts a force on the seismometer proof mass mimicking a ground acceleration. A calibration experiment then consists in injecting a known electrical current in the coil (input) and recording the response of the seismometer (output). By modeling the transfer function between input and output the frequency response of the seismometer can be estimated. The advantage of performing the modeling in the time-domain over spectral division in the frequency domain is that non-linear distortions can be more easily identified.

Ideally a seismometer behave as a linear system. However real-life mechanical and electrical components exhibit also a small non-linear response. On this poster we evaluate the linear part of the VBB and SP instrument response and inspect the residues for evidence of a non-linear component to the response.

The VBB calibration signal (Fig. 17) consists of a down-sweep from 5 Hz to 5 mHz and thus only allows a characterization of the VBBs in this band. Furthermore the time-domain amplitude of the initial, high frequency response is small such that this part of the transfer function will be ill constrained if estimated with a least-squares procedure. On this poster we ignore the high frequency roll-off and model only the response in the pass-band and the low-frequency corner. We use impulse-invariant recursive Schüssler-filters for the modeling in the time domain (Wielandt, 2009¹⁰). The POS channel is analyzed in figures 17 and 18. Its transfer function is proportional to acceleration from 16s period to DC: thus it has the characteristics of a gravimeter.

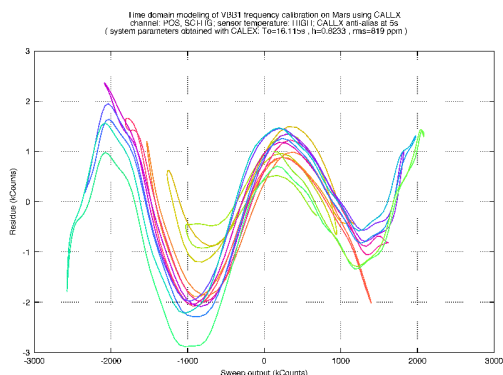


Figure 18: Analysis of residue from Fig. 17: the residue is plotted against the output signal. Progression in time is color coded. A polynomial up to order five with dominant odd order terms is needed to model this non-linear behaviour.

⁹Lognonné, Ph. et al., SEIS: InSight's Seismic Experiment for Internal Structure of Mars. Space Sci. Rev. (2019). DOI: <https://doi.org/10.1007/s11214-018-0574-6>.

¹⁰Wielandt, E. CALLEX software package. <http://www.software-for-seismometry.de/software/calex/>

Conclusions

We have evaluated all calibrations of the SP and VBB seismometers (both VEL and POS channels). Both VBB and SP sensor calibrations can be modeled with a simple second order system with only three free parameters: gain, A , corner period, T_o , and fraction of critical damping, h . VBB calibrations conducted at -54°C , -45°C and -35°C reveal no temperature dependence of the (linear part of the) transfer function.

The residues obtained in modeling the sweep calibrations conducted on Mars are large compared to the seismic background noise and are correlated with the input signal. This indicates that a linear model is insufficient to fully describe the seismometer response.

All three VBBs show a small non-linear distortion with odd symmetry. This is true both for the VEL and POS channels. Frequency calibrations of the SEIS flight unit conducted in 2017 at CNES in Toulouse (not shown) did not reveal any non-linear response presumably because the CNES vault is too contaminated by antropogenic noise.

For the SP1 seismometer (not shown) the residue is dominated by a signal approx. 90° out of phase with the linear model prediction: an as yet unidentified inductance or capacitance could be generating such a residue.

At this time we are unable to identify the culprit of the VBB non-linearities: both mechanical and electronic components may be responsible. Since the calibration current has not been measured and we only know the digital input to the D/A-converter, the non-linearity may also originate from the D/A-converter. Detailed experiments with the flight spare conducted in a seismically quiet vault may lead to a better understanding and eventually to a fully non-linear description of the VBB transfer function.

Acknowledgements

RWS would like to thank the Max Plank Institute for Solarsystem Research, MPS (Göttingen) for financial support and the opportunity to work for 8 weeks at the NASA Jet Propulsion Laboratory (JPL) in Pasadena during the commissioning and deployment phase of InSight/SEIS.

Publications

(<https://www.gis.uni-stuttgart.de/en/research/publications/index.html>)

Refereed Journal Publications

Abou Zaki, N., A. Torabi Haghghi, P. M. Rossi, M. J. Tourian, and B. Kløve (2019): Monitoring Groundwater Storage Depletion Using Gravity Recovery and Climate Experiment (GRACE) Data in Bakhtegan Catchment, Iran. In: *Water* 11.7. DOI: 10.3390/w11071456.

Arabsahebi, R., B. Voosoghi, and M. J. Tourian (2019): A denoising–classification–retracking method to improve spaceborne estimates of the water level–surface–volume relation over the Urmia Lake in Iran. In: *International Journal of Remote Sensing*. DOI: 10.1080/01431161.2019.1643938.

- Ashraf, S., A. AghaKouchak, A. Nazemi, A. Mirchi, M. Sadegh, H. R. Moftakhari, E. Hassan-zadeh, C. Y. Miao, K. Madani, M. Mousavi Baygi, H. Anjileli, D. R. Arab, H. Norouzi, O. Mazdiyasn, M. Azarderakhsh, A. Alborzi, M. J. Tourian, A. Mehran, A. Farahmand, and I. Mallakpour (2019): Compounding effects of human activities and climatic changes on surface water availability in Iran. In: *Climatic Change* 152.3-4. DOI: 10.1007/s10584-018-2336-6.
- Babadi, M., M. Sattari, and S. Iran Pour (2019): Exploring the potential of full waveform airborne LiDAR features and its fusion with RGB image in classification of a sparsely forested area. In: *ISPRS - International Archives of the Photogrammetry, Remote Sensing and Spatial Information Sciences XLII-4/W18*. DOI: 10.5194/isprs-archives-XLII-4-W18-147-2019.
- Ghobadi-Far, K., S.-C. Han, J. Sauber, F. Lemoine, S. Behzadpour, T. Mayer-Gürr, N. Sneeuw, and E. Okal (2019): Gravitational Changes of the Earth's Free Oscillation From Earthquakes: Theory and Feasibility Study Using GRACE Inter-satellite Tracking. In: *Journal of Geophysical Research: Solid Earth*. DOI: 10.1029/2019JB017530.
- Hosseini-Moghari, S. M., S. Araghinejad, K. Ebrahimi, and M. J. Tourian (2019): Introducing modified total storage deficit index (MTSDI) for drought monitoring using GRACE observations. In: *Ecological Indicators* 101. DOI: 10.1016/j.ecolind.2019.01.002.
- Lognonné, P., SEIS-team, and R. Widmer-Schnidrig (2019): SEIS: Insight's Seismic Experiment for Internal Structure of Mars. In: *Space Sci Rev* 215.12. DOI: 10.1007/s11214-018-0574-6.
- Ringler, A., J. Steim, D. Wilson, R. Widmer-Schnidrig, and R. Anthony (2019): Improvements in seismic resolution and current limitations in the Global Seismographic Network. In: *Geophysical Journal International* 220.1. DOI: 10.1093/gji/ggz473.
- Sabzehee, F., V. Nafisi, S. Iran Pour, and B. D. Vishwakarma (2019a): Analysis of the precipitation climate signal using empirical mode decomposition (EMD) over the Caspian catchment area. In: *ISPRS - International Archives of the Photogrammetry, Remote Sensing and Spatial Information Sciences XLII-4/W18*. DOI: 10.5194/isprs-archives-XLII-4-W18-923-2019.
- Sabzehee, F., V. Nafisi, S. Iran Pour, and B. D. Vishwakarma (2019b): Investigation of the correlation between GRACETWS and soil moisture in Sarakhs catchment. In: *ISPRS - International Archives of the Photogrammetry, Remote Sensing and Spatial Information Sciences XLII-4/W18*. DOI: 10.5194/isprs-archives-XLII-4-W18-931-2019.
- Wang, S., W. Xu, C. Xu, Z. Yin, R. Bürgmann, L. Liu, and G. Jiang (2019): Changes in Groundwater Level Possibly Encourage Shallow Earthquakes in Central Australia: The 2016 Petermann Ranges Earthquake. In: *Geophysical Research Letters* 46.6. DOI: 10.1029/2018GL080510.

Xu, G., C. Xu, Y. Wen, and Z. Yin (2019): Coseismic and Postseismic Deformation of the 2016 MW 6.2 Lampa Earthquake, Southern Peru, Constrained by Interferometric Synthetic Aperture Radar. In: *Journal of Geophysical Research: Solid Earth* 0.0. DOI: 10.1029/2018JB016572.

Books & Miscellaneous

Antoni, M. (2019): *Calculus with Curvilinear Coordinates – Problems and Solutions*. Springer International Publishing. ISBN: 978-3-030-00415-6. DOI: 10.1007/978-3-030-00416-3.

Iran Pour, S., N. Sneeuw, M. Weigelt, and A. Amiri-Simkooei (2019): “Orbit Optimization for Future Satellite Gravity Field Missions: Influence of the Time Variable Gravity Field Models in a Genetic Algorithm Approach”. In: *International Association of Geodesy Symposia*. Springer Berlin Heidelberg. DOI: 10.1007/1345_2019_79.

Yi, S. (2019): *Application of Satellite Gravimetry to Mass Transports on a Global Scale and the Tibetan Plateau*. Springer Singapore. DOI: 10.1007/978-981-13-7353-4.

Conference Presentations

Behnia, S. and N. Sneeuw (2019): In search for an optimum outlier rejection scheme: application to altimetric time series. FroGS 2019, Stuttgart, Germany, 17–19 September 2019.

Cai, J., K. Qian, N. Sneeuw, Y. Lin, and W. Li (2019): A-optimal design Regularization and its Applications in Extreme Learning Machine for Regression Analysis and Multi-class Classification. IUGG, Montréal, Canada, 8–18 July 2019.

Camici, S., L. Brocca, C. Massari, C. G. Giuliani, N. Sneeuw, H. Hashemi Farahani, M. Restano, and J. Benveniste (2019a): A satellite-based approach for total runoff estimation: stream project. AGU Fall Meeting 2019, San Francisco, USA, 9–13 December 2019.

Camici, S., L. Brocca, C. Massari, C. G. Giuliani, N. Sneeuw, H. Hashemi Farahani, M. Restano, and J. Benveniste (2019b): Total runoff estimation from satellite data: STREAM project. FroGS 2019, Stuttgart, Germany, 17–19 September 2019.

Camici, S., L. Brocca, C. Massari, G. Giuliani, N. Sneeuw, H. Hashemi Farahani, and J. Benveniste (2019c): Total runoff estimation through the exploitation of multiple satellite data: STREAM project. Satellite inspired hydrology in an uncertain future: an H SAF and HEPEX workshop, Reading, Great Britain, 25–28 November 2019.

Devaraju, B., V. Sharma, V. Kumar, M. Weigelt, and N. Sneeuw (2019): Analysing the lower degree harmonics of time-variable gravity field via the polar-form of spherical harmonics. IUGG, Montréal, Canada, 8–18 July 2019.

Elmi, O. and N. Sneeuw (2019a): A Graph-Based Image Segmentation Algorithm for Extracting Dynamic River Masks. IUGG, Montréal, Canada, 8–18 July 2019.

- Elmi, O. and N. Sneeuw (2019b): Estimation of River Discharge using Non-Parametric Machine Learning Techniques. IUGG, Montréal, Canada, 8–18 July 2019.
- Elmi, O., M. J. Tourian, and N. Sneeuw (2019a): A Graph-Based Image Segmentation Algorithm for Extracting Dynamic River Masks. ESA Living Planet Symposium, Milano, Italy, 13–17 May 2019.
- Elmi, O., M. J. Tourian, and N. Sneeuw (2019b): Estimation of River Discharge using Non-Parametric Techniques. FroGS 2019, Stuttgart, Germany, 17–19 September 2019.
- Feng, W., C. Wang, M. Zhong, C. Shum, H. Hsu, N. Sneeuw, K. Douch, Q. Chen, and H. Yeh (2019): Potential hydrological and seismological applications of the next-generation gravity field missions based on multi-pair constellations and joint sino-European numerical simulations. IUGG, Montréal, Canada, 8–18 July 2019.
- Gao, Y., J. Cai, and N. Sneeuw (2019): Applying directional statistics to GNSS carrier phase observations and to spherical harmonic phase spectra. FroGS 2019, Stuttgart, Germany, 17–19 September 2019.
- Ghobadi Far, K., S. Han, J. Sauber, F. Lemoine, S. Behzadpour, T. Mayer-Gürr, and N. Sneeuw (2019): A Feasibility Study of Detection of Earth's Free Oscillations Excited by the 2004 Sumatra Earthquake Using GRACE Inter-Satellite Tracking Data. IUGG, Montréal, Canada, 8-18 July 2019.
- Lin, Y., X. Li, T. Zhang, W. Li, J. Yu, N. Sneeuw, and J. Cai (2019): Estimation of water volume variations for large-scale lake based on multi-source satellite data. IUGG, Montreal, Canada, 8–18 July 2019.
- Mattes, D., H. Hashemi Farahani, and N. Sneeuw (2019): Densifying radar altimetry-derived water level time series along rivers by least squares collocation. FroGS 2019, Stuttgart, Germany, 17–19 September 2019.
- Nie, Y., Y. Shen, Q. Chen, J. Cai, and N. Sneeuw (2019): Synergistic Observation Analysis of GRACE Follow-On and Chinese Future TianQin-II Mission. FroGS 2019, Stuttgart, Germany, 17–19 September 2019.
- Peyman, S., K. Douch, and N. Sneeuw (2019): Investigating Granger causality between sea surface temperature and terrestrial water storage change in Europe. FroGS 2019, Stuttgart, Germany, 17–19 September 2019.
- Purkhauser, A., R. Pail, M. Hauk, P. Visser, N. Sneeuw, P. Saemian, W. Liu, J. Engels, Q. Chen, C. Siemes, R. Haagmans, and L. Massotti (2019): Comprehensive analysis of the influence of different parameters on the achievable gravity fields of NGGM: Results of the ESA-ADDCON project. IUGG, Montréal, Canada, 8–18 July 2019.
- Saemian, P., H. Hashemi Farahani, and N. Sneeuw (2019): A comprehensive assessment of GRACE decorrelating filters for hydrological applications. EGU, Wien, 7–12 April 2019.

Tourian, M. J. and N. Sneeuw (2019): Spatio-temporal downscaling in Geodesy: A call to action. FroGS 2019, Stuttgart, Germany, 17–19 September 2019.

Yi, S., K. Heki, C. Song, S. Kang, Q. Wang, and L. Chang (2019): Substantial meltwater contribution to the Brahmaputra revealed by satellite gravimetry. Asia Oceania Geosciences Society 2019, Singapore.

Yi, S., Y. Pan, and N. Sneeuw (2019): Contemporary evolution of the Island of Hawaii observed by spaceborne gravimetry. FroGS 2019, Stuttgart, Germany, 17–19 September 2019.

Zhang, T., Y. Lin, J. Cai, and N. Sneeuw (2019): Accuracy evaluation and comparison of an optimized learning method on remote sensing imagery classification. FroGS 2019, Stuttgart, Germany, 17–19 September 2019.

Poster Presentations

Behnia, S., M. J. Tourian, A. Ribeiro Neto, and N. Sneeuw (2019): São Francisco as monitored by Radar Altimetry Satellites. South America Water from Space II, Manaus, Brazil, 4–7 November 2019.

Chang, L., H. Tang, S. Yi, and W. Sun (2019): The Trend and Seasonal Change of Sediment in the East China Sea Detected by GRACE. EGU, Wien, 7–12 April 2019.

Chen, Q., J. Engels, N. Sneeuw, and T. van Dam (2019): Feasibility study of the Next Generation Gravity Mission (NGGM) for atmosphere. ESA Living Planet Symposium, Milano, Italy, 13–17 May 2019.

Douch, K., G. Cambiotti, N. Sneeuw, A. Anselmi, A. Marotta, and R. Sabadini (2019): On the Possibility to monitor the Co- and Post-seismic Signal with the Next Generation Gravity Mission. IUGG, Montréal, Canada, 8–18 July 2019.

Douch, K., A. Knabe, and J. Müller (2019): Satellite gradiometry as concept for recovery of the time-variable gravity field. IUGG, Montréal, Canada, 8–18 July 2019.

Issawy, E., N. Sneeuw, O. Elmi, M. J. Tourian, S. Roohi, M. Javaid, and H. Mohamed (2019): In-land Water Monitoring Using Spaceborne Geodetic Sensors. EGU, Wien, 7–12 April 2019.

Javaid, M. and W. Keller (2019): Data mining of spherical harmonic (SH) coefficients using artificial neural networks (ANN). EGU, Wien, 7–12 April 2019.

Shrestha, P., L. Samaniego, S. Thober, R. Kumar, S. Behnia, and O. Rakovec (2019): Towards scale independent lake-hydrology modeling in semi-arid regions: mHM lake module (mLM) development. EGU, Wien, 7–12 April 2019.

Sneeuw, N. and P. Saemian (2019): Next-Generation Gravity Missions for Drought Monitoring. ESA Living Planet Symposium, Milano, Italy, 13–17 May 2019.

Vishwakarma, B., P. Bates, N. Sneeuw, and J. Bamber (2019): Mapping global water stress from GRACE satellite data. EGU, Wien, 7–12 April 2019.

Wang, B. and N. Sneeuw (2019): Monitoring inland surface water level using Sentinel-3 data. FroGS 2019, Stuttgart, Germany, 17–19 September 2019.

Widmer-Schnidrig, R., E. Wielandt, N. Verdier, P. Lognonné, T. Pike, and SEIS-team (2019): Time Domain Modeling of InSight/SEIS VBB and SP Frequency Calibrations on Earth and on Mars. InSight Science Team Meeting No.15, Paris, 17–21. June 2019.

Yi, S. and K. Heki (2019): Heterogeneous oceanic mass distribution in GRACE observations and its leakage effect. EGU, Wien, 7–12 April 2019.

Zhang, J. and N. Sneeuw (2019): An empirical spatial downscaling of GRACE by statistical assimilation of multiple hydrological variables. EGU, Wien, 7–12 April 2019.

Theses

(<https://www.gis.uni-stuttgart.de/forschung/dissertationen/>)

Muhammad Athar Javaid: Data mining in GRACE monthly solutions

Elmi Omid: Dynamic water masks from optical satellite imagery

Liu Wei: Understanding ocean tide aliasing in satellite gravimetry

Zhang Jinwei: Assessing the statistical relations of terrestrial water mass change with hydrological variables and climate variability

Master Theses

(<https://www.gis.uni-stuttgart.de/lehre/abschlussarbeiten/>)

Dalu Dong: Converted Total Least Squares method and Gauss-Helmert model with applications to transformation among ITRF realizations

Dennis Mattes: Analysis of waveforms in the satellite altimetry by using neural networks

Bo Wang: Monitoring inland surface water level from Sentinel-3 data

Tianshu Wang: Performance of CryoSat-2 altimetry over Salar de Uyuni

Chunqin Xu: Analysis of River Regime Change in Arctic Basins

Bachelor Theses

(<https://www.gis.uni-stuttgart.de/lehre/abschlussarbeiten/>)

Lun Yan: Water level analysis in Tibet using CryoSat-2

Guest Lectures and Lectures on special occasions

Awange, J (Curtin University of Technology, Perth, Australia): Environmental Geoinformatics: Extreme Hydro-Climatic and Food Security Challenges - Exploiting the Big Data (26.7.)

Chen, Q (Tongji University, Shanghai): Modelling Temporal Variations of Accelerometer Calibration Parameters (4.7.)

Activities in National and International Organizations

Grafarend E.

Professor h.c., University of Navarra, Pamplona, Spain

Professor h.c., University of Tehran, Iran

Professor h.c., Wuhan University, China

Fellow International Association of Geodesy (IAG)

Elected Member of the Finnish Academy of Sciences and Letters, Finland

Elected Member of the Hungarian Academy of Sciences, Hungary

Member Royal Astronomical Society, Great Britain

Corresponding Member Österreichische Geodätische Kommission (ÖGK)

Emeritus Member German Geodetic Commission (DGK)

Gauss Society, Göttingen

Member of the "Leibniz Gesellschaft der Wissenschaften", Berlin

Member Flat Earth Society

Elected Member Leibniz-Sozietät, Berlin

Keller W.

Doctorate honoris causa, Wrocław University of Environmental and Life Sciences, Wrocław, Poland

Sneeuw N.

Distinguished Professor, Land Satellite Remote Sensing Application Center (LASAC), China

Professor h.c. (Luoji chair), Wuhan University, China

Adjunct Professor of the College of Engineering, University of Tehran, since 2015

Fellow International Association of Geodesy (IAG)

Search Committee Politecnico Milano, Italy

Full Member Deutsche Geodätische Kommission (DGK)

Chair, Assessment Panel Space Research, NWO, Netherlands

Member of GGOS working group Committee on Satellite Missions

Member of Gauss-Gesellschaft e.V., since 2018

Member of the editorial board of Surveys in Geophysics

Member of the editorial board of Studia Geophysica et Geodaetica

Member Eötvös Honory Board (Eötvös 100), 2019

Courses – Lecture/Lab/Seminar

Bachelor Geodesy and Geoinformatics (German):

Amtliches Vermessungswesen und Liegenschaftskataster (Grams)	2/0/0/0
Ausgleichsrechnung I, II (Krumm, Douch, Elmi)	3/1/0/0
Einführung Geodäsie und Geoinformatik (Sneeuw)	2/2/0/0
Integriertes Praktikum/Integrated Field Work (Sneeuw)	10 days
Landesvermessung (Antoni)	2/2/0/0
Physikalische Geodäsie (Sneeuw, Hashemi Farahani)	2/2/0/0
Referenzsysteme (Sneeuw, Douch)	2/2/0/0
Satellitengeodäsie (Sneeuw, Douch)	1/1/0/0
Wertermittlung I (Bolenz)	2/0/0/0

Master Geodesy and Geoinformatics (German):

Aktuelle Geodätische Satellitenmissionen (Sneeuw)	2/2/0/0
Amtliche Geoinformation (Heß)	2/0/0/0
Ausgewählte Kapitel der Parameterschätzung (Krumm, Engels)	2/2/0/0
Erderkundung (Sneeuw)	2/0/0/0
Geodynamische Modelle (Engels, Douch)	2/2/0/0
Grundstücksbewertung II (Bolenz)	2/0/0/0
Koordinaten- und Zeitsysteme in der Geodäsie (Sneeuw)	2/0/0/0
Physikalische Geodäsie (Engels, Hashemi Farahani)	2/2/0/0
Satellitengeodäsie (Sneeuw, Hashemi Farahani, Antoni)	2/1/0/0

Master GeoEngine (English):

Advanced Mathematics (Antoni, Mattes)	3/2/0/0
Foundations of Satellite Geodesy (Sneeuw, Douch)	2/1/0/0
Integriertes Praktikum/Integrated Field Work (Sneeuw)	10 days
Map Projections and Geodetic Coordinate Systems (Antoni)	2/1/0/0
Physical Geodesy (Sneeuw, Hashemi Farahani)	2/1/0/0
Satellite Geodesy Observation Techniques (Tourian, Douch)	2/1/0/0
Statistical Inference (Tourian, Douch)	2/1/0/0

Institute of Navigation



Breitscheidstraße 2
 D-70174 Stuttgart
 Tel.: +49 711 685 83400
 Fax: +49 711 685 82755
ins@nav.uni-stuttgart.de
<http://www.nav.uni-stuttgart.de>

Head of Institute

Prof. Dr.techn. Thomas Hobiger

Deputy: Dr.-Ing. Aloysius Wehr
 Secretary: Helga Mehrbrodt
 Retired Professor: Prof.i.R. Dr.-Ing. Alfred Kleusberg

Staff

Dipl.-Ing. Doris Becker	Navigation Systems
Dipl.-Geogr. Thomas Gauger	GIS Modelling and Mapping
Dr. Tomasz Hadas (since 9/2019)	GNSS troposphere
M.Sc. Tomke Jantje Lambertus	Parameter Estimation in Dynamic Systems
M.Sc. Clemens Sonnleitner	Autonomous flight, ADS-B
M.Sc. Rui Wang (since 11/2019)	GNSS, RTK, integrity
Dipl.-Ing. (FH) Martin Thomas	Laser Systems, Digital Electronics and Hardware Programming
M.Sc. Arunprasad Vijayaraghavan	Hardware and FPGA programming
Dr.-Ing. Aloysius Wehr	Laser Systems, Optical and Wireless Communication

IT

Regine Schlothan

Electronic Lab and Precision Mechanical Workshop (ZLW)

Dr.-Ing. Aloysius Wehr (Head of ZLW)
 Sebastian Schneider (Electrician)
 Michael Pfeiffer (Mechanician Master)

External teaching staff

Hon. Prof. Dr.-Ing. Hans Martin Braun - RST Raumfahrt Systemtechnik AG, St.Gallen
 Dr. Werner Enderle - ESA/ESOC

Preface

The scientific and teaching activities of the Institute of Navigation (INS) in the year 2019 have followed national and international trends, with a strong focus on navigation solutions for autonomous systems. Driven by the chance to contribute to the efforts of establishing a test site for energy efficient and autonomous flying, the INS has set a focus on autonomous flying and topics related to the safe integration of unmanned aerial vehicles in existing and future airspaces. Based on this topical orientation of the institute a new logo (cf. Fig.1) was designed and shall be used for all internal and external communication of the INS.



Figure 1: New logo of the Institute of Navigation.

Research Projects

Project - Sensors for an alarm system against drowning in a bathtub

This project was initiated by the company Horcher and has been supported by Central Innovation Programme for small and medium-sized enterprises (SMEs). The project's objective is the development of a system preventing people from drowning in a bathtub in e.g. nursing homes for the elderly. Project partners are company Horcher, Institute of Navigation (INS) and German Institutes of Textile and Fiber Research (DITF). INS was assigned the task to develop and realize the sensor system, which comprises MEMS-Inertial Measurement Units (MEMS-IMUs), air pressure sensors, humidity sensors and an Indoor Microwave Positioning and Data Transmission System (IMPDS). The sensors and the transmitters of IMPDS are mounted on the patient's body. Therefore, the electrical items are developed in close cooperation with DITF regarding the requirements of so called wearable electronics.

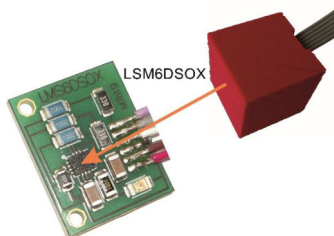


Figure 2: IMU LSM6DSOX from STMicroelectronics.

First MEMS-IMUs were studied regarding the objectives of the alarm system. The empirical studies underlined the fact, that MEMS sensors exhibits large drifts and are not suited for long term positioning tasks with hardly any movement, which is the case when taking a bath. However, the sensor LSM6DSOX from STMicroelectronics (s. Fig. 3) has got a machine learning core. Using this feature, it becomes possible to discern different movements. Therefore, a precise positioning of the body is not required anymore. If movements are recognized, which may cause a drowning situation an alarm is triggered. Up to now, 13 postures can be detected: sitting straight, bending right, left, forward and backward by discerning three bending intensities each. To improve the system robustness, low cost air pressure sensors were studied empirically (s. Fig 3). Fig. 4 depicts that measurement noise is a concern. The ultra small waterproof pressure sensor DPS 368 of the company Infineon is selected for our application. It works underwater and this case can be well detected (s. Fig. 5).

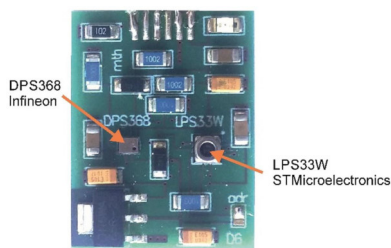


Figure 3: Test-PCB with pressure sensors.

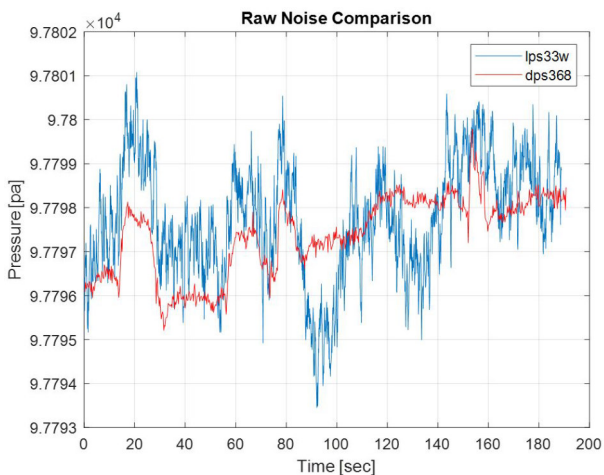


Figure 4: Signal noise comparison of two pressure sensors.

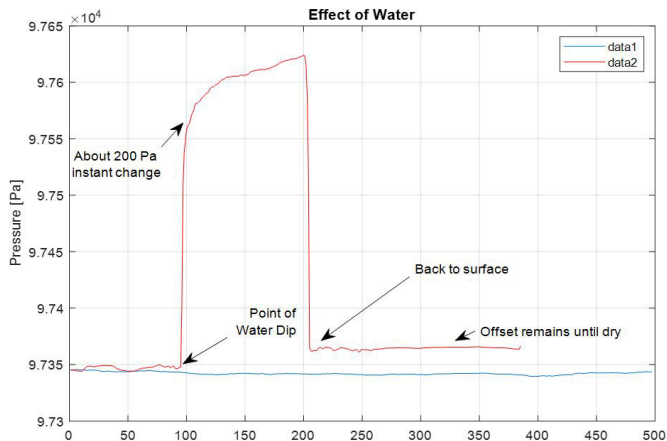


Figure 5: Dipping the pressure sensor into water.

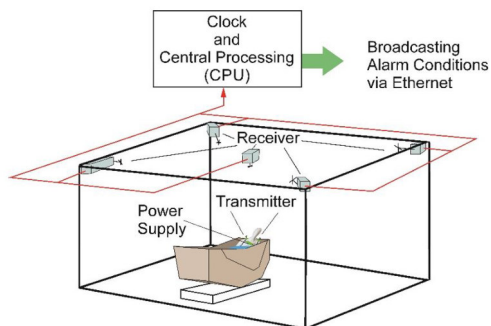


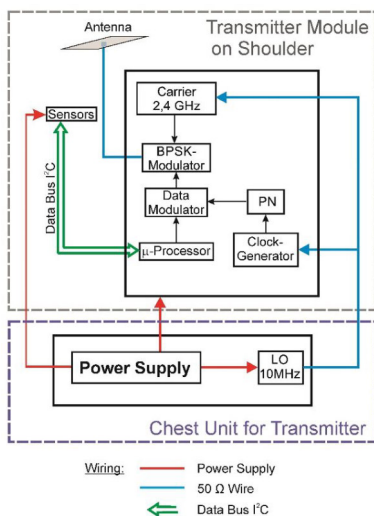
Figure 6: Concept of IMPDS.

The most challenging part of the project is the development of IMPDS. The concept shows Fig. 6. Two Microwave transmitters (2.4 GHz) are mounted on the right and left shoulder and fixed on an elastic belting around the chest and shoulder of a person. They send signals coded by pseudo noise codes (PN codes) for ranging and data transmission to the five receivers. The slant ranges derived from code and phase measurements of the five receivers and the data of e.g. air pressure sensor, IMU and humidity sensors are linked to the central processing unit (CPU). This unit estimates the positions of the two transmitters on the base of the slant ranges, evaluates the sensor data and determines the alarm condition. The projected system data is compiled in Table 1.

Table 1: Projected System data of IMPDS.

Number of Receivers	5
Transmitter on Body	2
Range	10 m
Carrier Frequency	2.4 GHz
Coding	PN
Positioning Accuracy	1 cm ³
Ranging Accuracy	1 mm
Measurement Rate	10 Hz

Fig. 7 shows the block diagram of the transmitter with separate power supply and clock. Power supply and clock is needed only once, whereas the transmitter module is required twice. The receiver concept is depicted in Fig. 8. The 2.4 GHz carrier signal is mixed down to an intermediate frequency of 10 MHz and is sampled by 8 bit analog to digital converters (ADC). These 8 bit complex values (I and Q) are processed in a FPGA applying software defined radio (SDR) algorithms. The FPGA outputs a serial data stream comprising sensor data (e.g. IMU, air pressure and humidity), timing data, carrier and code phase \emptyset determined by DLL. The Microprocessor performs decoding and relaying of data to the central processing unit. Fig. 9 shows receiver breadboards without the microprocessor. Presently the SDR-software for the FPGA and the software for positioning and decoding are under development and test.

**Figure 7:** Transmitter.

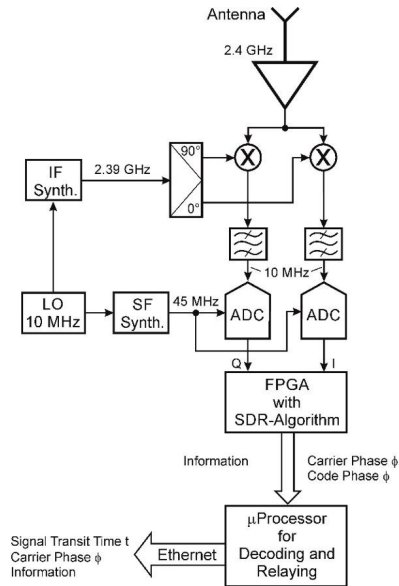


Figure 8: Receiver.

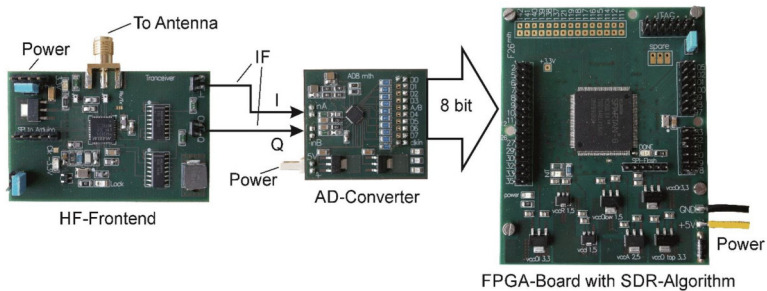


Figure 9: Components of the receiver breadboard.

Acknowledgements

This Project is supported by Central Innovation Programme for small and medium-sized enterprises (SMEs) funded by the Federal Ministry for Economic Affairs and Energy.

Project - Test site for electric, energy-efficient and autonomous flight

The INS is one of the institutes of the University of Stuttgart that is part of a consortium with partners of industry establishing two test sites for electric, energy-efficient and autonomous flight. The project is financed by Baden-Württemberg's Ministry of Economic Affairs, Labour and Housing. Its goal is to enable research facilities and industry to verify and demonstrate overall manned and unmanned flight systems under realistic conditions.

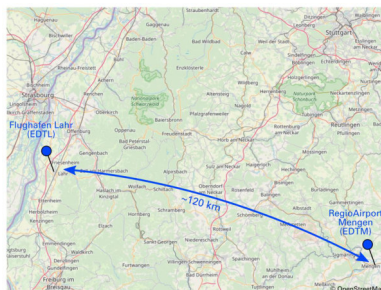


Figure 10: Locations of the two test sites for electric, energy-efficient autonomous flight.

In 2019 the consortium selected two airports in Baden-Württemberg which conform best to the very opposing requirements for either urban or autonomous flight. The locations of the two test sites are shown in Figure 10. The test site dedicated to the topic of autonomous flight is the RegioAirport Mengen (ICAO: EDTM) due to low population density. Dedicated to urban flight is the Flughafen Lahr (ICAO: EDTL) because of its vicinity to the city and critical infrastructure. At the test sites experimental aircrafts with Permit To Fly (PTF) as well as Urban Air Mobility (UAM) vehicles of all sizes, manned or unmanned can be tested concerning reliability, controllability (also beyond visual line of sight), management of approach and landing phases as well as the behavior of the aircraft in conflict situations.

At the airport, official approvals are provided in order to facilitate the project development. It is possible to store equipment in a hangar at the test site. Moreover, existing ground infrastructure is immediately available. During the project additional equipment for navigation purposes, positioning and air space surveillance is set up there. An overview of planned infrastructure available at the test site close to Mengen can be seen in Figure 11. The organization and coordination of the installations of the different ground base infrastructures for navigation, positioning and air space surveillance from the different partners is done by the INS. The institute also acquired a GNSS reference receiver for high precision RTK landing approaches, which will be placed at the RegioAirport Mengen in 2020.

In 2019 a general ruling for aircrafts with a maximum take off weight (MTOW) below 10kg has been acquired and first test flights with drones have been carried out by the Institute of Flight Mechanics and Controls at the Airport Mengen and one of the partners carried out test flights at the Flughafen Lahr.

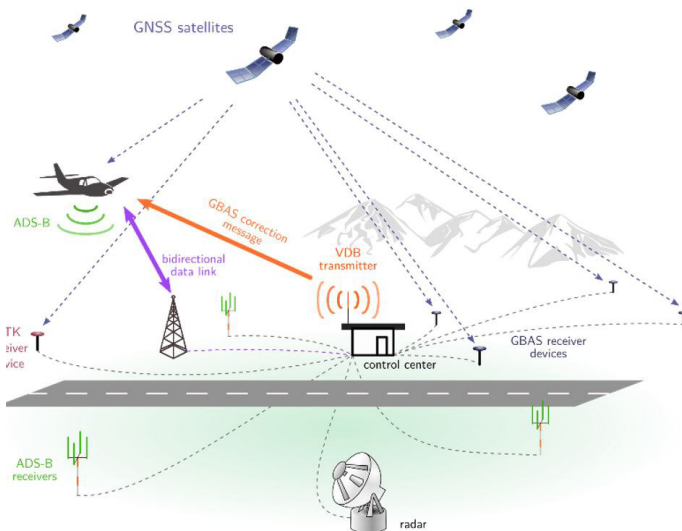


Figure 11: Overview of the provided ground base infrastructure at the RegioAirport Mengen (EDTM).

PyGACT - a Python toolkit for determination of relative GNSS antenna phase center variations

Evolvements of GNSS technology require that instrumental error sources are well understood and can be corrected in analysis. In particular, the phase center offset (PCO) and phase center variations (PCV) are available with high accuracy. While absolute calibrations are available for high-end geodetic antenna, most of the low-cost mass-market antenna remain uncalibrated. Thus, we have developed a Python toolbox called PyGACT, which allows to estimate relative PCO as well as PCV maps and analyze C/N0 and multipath characteristics, so that it is feasible to use consumer-grade antennas for precise GNSS positioning. Instead of using spherical harmonic (SH) coefficients with global support, we add the option to estimate PCV maps in the form of 2D B-splines. This allows to better adapt to the local satellite visibility conditions. Moreover, the antenna characteristics are not only obtained for GPS and GLONASS, but also include Galileo and Beidou frequencies.

The following Figures (12-14) show the results for target antenna ANN-MS.

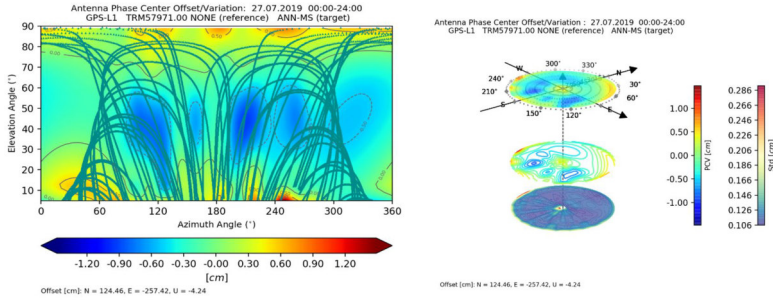


Figure 12: PCV map with the B-spline model for GPS-L1.

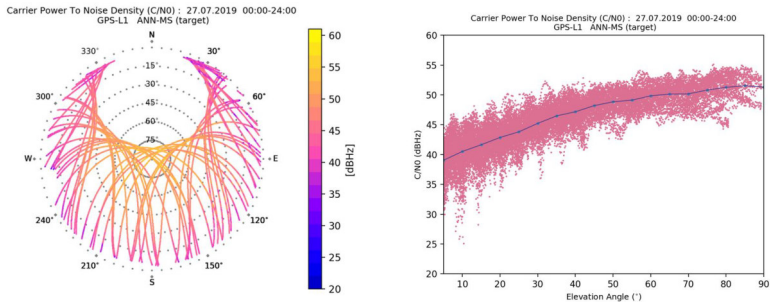


Figure 13: C/N0 Fig. 2: C/N0 and C/N0- elevation for GPS-L1.

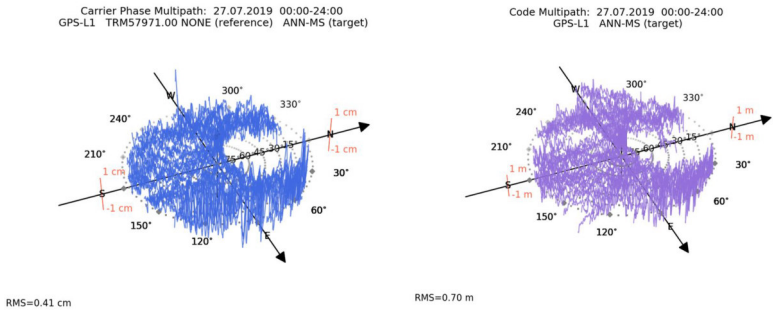


Figure 14: Carrier-phase and code multipath skyplots for GPS-L1.

Project: Dynamic non-linear parameter estimation by means of particle filtering on the GPU

As one of its research foci the INS has identified the topic of modern dynamic non-linear parameter estimation methods for autonomous navigation applications. Significant improvements in positioning, navigation and timing (PNT) concerning precision, accuracy, integrity and availability over the last century have enabled a manifold of applications which are part of our daily life. In recent years the requirements of autonomous navigation have led to several challenges that need to be addressed in order to realize such ground-breaking concepts for aircraft, ship and land vehicle navigation. Most classical estimators rely on the idea that observations errors are following Gaussian normal distributions and third and higher order moments of the probability distributions are zero. However, as this might not be totally correct for real-world sensors, one faces the challenge to determine the “most likely” state of a navigation system under the consideration of the real stochastic properties. Moreover, the solution space could be bounded or limited to given sets within the mathematical spaces of real or natural numbers. In most standard navigation applications, the extended Kalman filter (EKF) is used as it is simple to implement and yields acceptable results. Nevertheless, the EKF relies on a Gaussian white noise distribution in the prediction and update steps which would ensure that the Kalman filter yields an (near-) optimal solution. Furthermore, the dynamic state-space model has to be well known and its stochastic properties and their time evolution needs to be well understood. In reality, navigation applications are more complex and will typically include non-linear systems and measurements which do not necessarily follow a Gaussian normal distribution. The EKF uses a linearization around the mean of the current state, and hence, the original problem is transformed into an approximative problem and solved such that it does not have to be the optimal solution of the original problem. The linearization can deteriorate the accuracy of the obtained solution or even lead to the divergence of the solution.

In our research project we focus on particle filters which can be considered as an alternative approach when reflecting on the aforementioned issues. The particle filter belongs to the group of Bayesian filtering techniques and it does not necessarily require the knowledge of the stochastic properties in advance. Hence, it is also suitable for nonlinear problems having measurements with non-Gaussian distributions, because it preserves the nonlinear structure of the problem.

The basic idea of this filter is to create a set of particles where each particle represents a possible realization of the state vector which is assigned a weight. In each epoch the states of particles are predicted based on their process model. If measurements are available, the weight of each particle is recomputed, leading to an update of the PDF based on the residuals between observed and computed measurements.

Fig. 15 shows an example of particle filtering during a test drive when using GNSS code phase observations only. The particle cloud and the positional deviations with respect to the reference positions is dispersed. This is due to the fact that the vehicle had just passed a sharp

curve in an area, where the GNSS observations were strongly deteriorated by multipath and signal blockage. Hence, the particle cloud does not follow a Gaussian normal distribution.

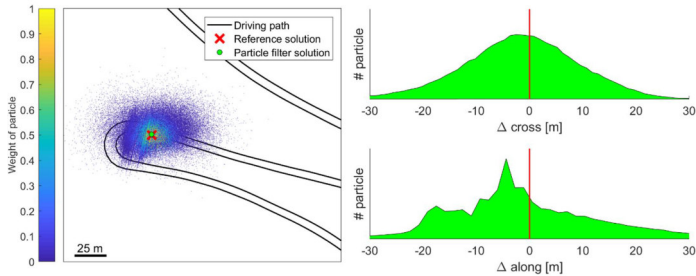


Figure 15: Snapshot of the particle filter solution based on GNSS code-phase data at a location where reduced satellite visibility led to noisy and biased observations.

A major drawback of the particle filter is its computational cost which makes it difficult to process a large particle cloud. However, the particle cloud processing is well suited for parallelization. To speed up the processing we use a graphics processing unit (GPU) to run the particle filter algorithms on a commercial of-the-shelf computing platform. The implementation of the algorithm is outlined in Fig. 16. At every epoch, observational data are obtained and pre-processed on the CPU. Such data are then sent to the GPU where the main steps of the particle filter are performed using multiple threads. After each step, the main information, i.e. the estimated mean state and its stochastic properties are returned to the CPU. In 2019 the INS started to set up a GNSS software for parallel particle filtering and general GNSS data processing. The software is implemented in C++ and the previous described filtering process was tested using GNSS data from different test drives.

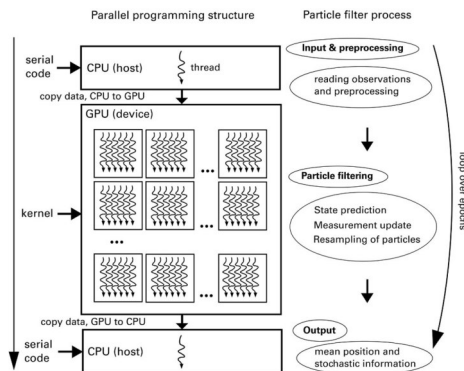


Figure 16: Parallel processing in particle filtering using a graphics processing unit.

Modelling and Mapping Air Concentration and Atmospheric Deposition of Reactive Nitrogen Species in Baden-Württemberg for 2012 to 2016 - Main Results

Main results of the research project “Nitrogen background air concentration and atmospheric deposition Baden-Württemberg 2020 - Part 1: Regional scale modelling”, funded by the State Agency for Environment, Baden-Württemberg (LUBW) are achieved in 2019. Maps of wet and dry deposition of reactive nitrogen N_r compounds are generated on a hectare raster for Baden-Württemberg, Germany. An integrative modelling approach is applied, combining interpolation methods for wet deposition, emission maps and statistical dispersion models for ammonia as well as results from atmospheric transport models (Figure 17). The results are useful input for tasks such as evaluating threats to terrestrial ecosystems by excess atmospheric N concentration (critical level exceedance), N deposition (critical load exceedance), or establishing N balances for valuating excess nutrient loads on agricultural land (critical surplus exceedance).

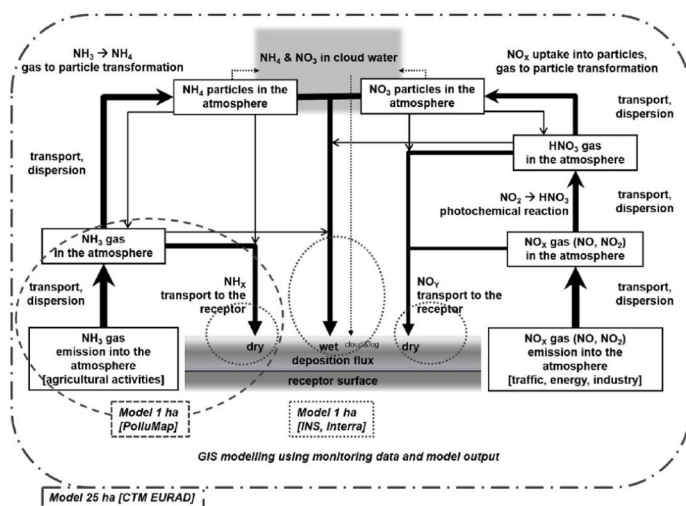


Figure 17: Outline of the integrated modelling approach [adopted from Hertel (2009); modified].

Air concentration and deposition fluxes of reactive nitrogen (N_r) in Baden-Württemberg are modelled using the chemical transport model (CTM) EURAD providing a 25 ha grid resolution output, the inferential model PolluMap, GIS based geostatistical modelling, and regression modelling, respectively. Hence different modelling approaches are combined in order to derive 1 ha grid maps of air concentration and atmospheric deposition of N_r species.

The outline of the model combination is presented in Figure 17. Oxidised nitrogen (NO_x , NO_y) and reduced nitrogen (NH_y , NH_x) are modelled separately, due to different emission sources, lifetime, in-atmosphere reactions including production of secondary N_f species and specific deposition velocities.

All atmospheric pathways of N_f from emission over transport, in-air physico-chemical reaction, air concentration and wet and dry deposition fluxes are modelled in hourly time steps using the CTM EURAD.

The ecosystem level model output resolution (1 ha) for concentration and deposition fluxes of N_f species is achieved by GIS implemented modelling. Where ever possible measurement data are integrated into the modelling approach, minimising deviations between reliable monitoring data and modelling results.

PolluMap (Meteotest) is used for modelling ammonia concentration and dry deposition using 1 ha local emission and land use data along with regional CTM EURAD output air concentration data and monitoring data of ammonia on an annual base.

Wet deposition and dry deposition into forests is calculated using GIS procedures (geostatistical modelling) carried out by INS based on annual forest monitoring data (open field, throughfall and canopy budget model data, respectively), 1 ha precipitation fields, and land cover data.

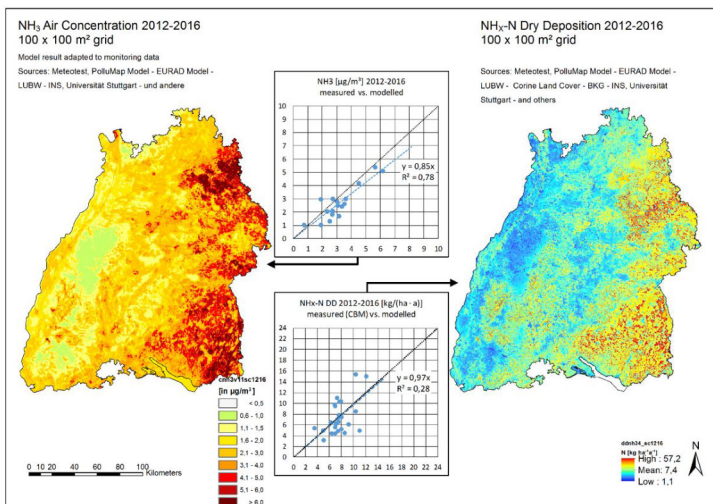


Figure 18: Modelling and mapping results of air concentration of ammonia (NH_3) adjusted to measurement data and dry deposition of reduced nitrogen ($\text{NH}_x\text{-N}$) in Baden-Württemberg averaged for 2012-2016 (1ha grid resolution each) - graphs are showing the comparison with respective monitoring data at measurement sites.

GIS based regression modelling is applied in order to derive high resolution precipitation data, and N_r wet and dry deposition estimates from monitoring results for forest areas (Interra).

Main model outcome of the project are 5-year average air concentration and deposition maps (Figure 18, and 19). Since the model combination applied where ever possible is based on measured data, or at least includes a fitting to data derived from annual measurements, the result compares quite well with ground truth monitoring (graphs in Figure 18 and 19).

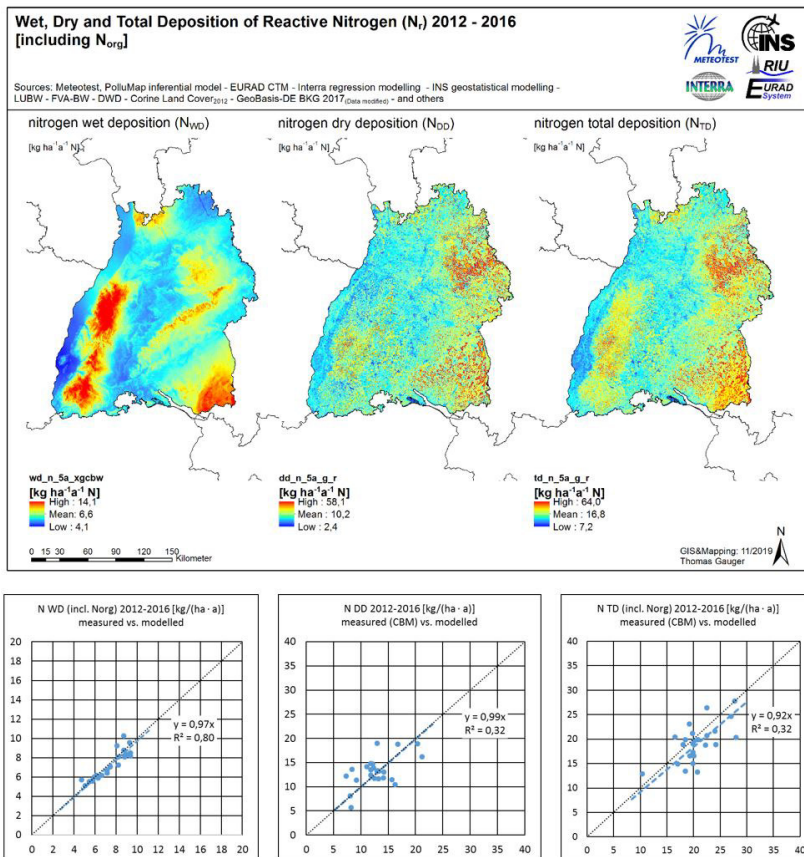


Figure 19: Maps of wet, dry and total deposition of total reactive nitrogen in Baden-Württemberg averaged for the years 2012-2016 - graphs are showing the comparison with respective monitoring data at forest measurement sites.

The Ministry of the Environment, Climate Protection and the Energy Sector Baden-Württemberg and the State Agency for Environment (LUBW) financially supports this scientific

project. It is part of StickstoffBW, an initiative of the federate state of Baden-Württemberg, elaborating basic information and data for regional politics and administrative execution with respect of ecological relevant nitrogen input. Project results are supporting EU and national regulations on air pollution control and emission abatement (EU NEC directive, BImSchG, TA-Luft), which are to be implemented on the sub-national level of the federate states of Germany. Moreover, scientific interest is supported by the project results, e.g. for studies of ecosystem flux assessment, ecological impact assessment, biodiversity, and nature protection. Administrative applications aiming at emission control and abatement of air pollutants are using reactive nitrogen data with reference to permission of projected animal husbandry, road construction, industrial settlements, and power plants, respectively. Results of the project are designated for public use and accessible via <https://www.lubw.badenwuerttemberg.de/medienuebergreifende-umweltbeobachtung/stickstoffbw>.

Publications and Presentations

- Gauger, T. (2019): Forschungsarbeiten im Rahmen der StickstoffBW AG1 Deposition-Modellierung der Stickstoff Hintergrunddeposition und Konzentrationen in Baden-Württemberg 2018. Thünen-Institut, Braunschweig, Institutsseminar des Institutes für Agrarklimaschutz (TI-AK), 15.01.2019 [oral presentation]
<https://www.thuenen.de/de/ak/aktuelles-und-service/veranstaltungen/archiv/>
- Gauger, T. (2019): Modellierung und Kartierung von reaktivem Stickstoff in Baden-Württemberg: Modellkombination, atmosphärische Konzentration und Deposition. 17. NH₃-Workshop 2019. Gewerbeaufsichtsamt Hildesheim 5.-6.11.2019. [oral presentation]
<https://www.luen-ni.de/NH3>
- Hadas, T., Hobiger, T. (2019a): GNSS Meteorology: State of the Art, Challenges and Perspectives. Presented at the Second Summer School of DAAD Thematic Network, University of Stuttgart, Stuttgart, Germany.
- Hadas, T., Hobiger, T. (2019b): Real-Time GNSS Meteorology: State of the Art and Challenges. Presented at the EMS Annual Meeting 2019, Technical University of Denmark (DTU).
<https://meetingorganizer.copernicus.org/EMS2019/EMS2019-902.pdf>
- Klopotek, G., Hobiger, T., Haas, R., Jaron, F., La Porta, L., Nothnagel, A., Plötz, C. (2019): Position Determination of the Chang'e 3 Lander With Geodetic VLBI. *Earth, Planets and Space*, 71(1), 23.
<https://doi.org/10.1186/s40623-019-1001-2>
- Lambertus, T., Hobiger, T. (2019): Ein GPU basierter Partikelfilter für GNSS Codephasen-Positionierung in Echtzeit. Presented at the InterGEO 2019, Frontiers of Geodetic Science, Stuttgart, Germany.

- Lambertus, T., Hobiger, T. (2019): Single Point Positioning by Means of Particle Filtering on the GPU. In 2019 European Navigation Conference (ENC). Presented at the European Navigation Conference (ENC), Warsaw, Poland.
<https://doi.org/10.1109/EURONAV.2019.8714148>
- Lambertus, T., Reinking, J. (2019): An Outlier Detection Approach for GNSS-SNR Analysis. GNSS+R 2019, IEEE Specialist Meeting on Reflectometry Using GNSS and Other Signals of Opportunity. Presented at the GNSS+R 2019, IEEE Specialist Meeting on Reflectometry using GNSS and other Signals of Opportunity, Benevento, Italy.
- Roggenbuck, O., Reinking, J., Lambertus, T. (2019): Determination of Significant Wave Heights Using Damping Coefficients of Attenuated GNSS SNR Data From Static and Kinematic Observations. Remote Sensing, 11(409).
<https://doi.org/10.3390/rs11040409>
- Strandberg, J., Hobiger, T., Haas, R. (2019): Real-Time Sea-Level Monitoring Using Kalman Filtering of GNSS-R Data. GPS Solutions, 23(3), 61.
<https://doi.org/10.1007/s10291-019-0851-1>
- Vijayaraghavan, A., Wehr, A., Hobiger, T. (2019): Development of an Indoor Microwave Positioning and Data Transmission System. InterGEO 2019.
http://www.nav.uni-stuttgart.de/dokumente/forschung_publication/2019/Vijayaraghavan-indoor_mikrowave_pos_6.pdf

Bachelor Thesis

- Genauigkeitsuntersuchung von Trajektorien eines integrierten Navigationssystems (Becker)
- Entwicklung eines modularen C++-Programms auf dem Raspberry Pi zur Positionsbestimmung mit einem ublox-Empfänger (Wehr)
- Evaluiierung von Smartphone GNSS Rohdaten (Becker)

Master Thesis

- Influence of the Choice of GNSS Reference Station concept on Kinematic Positioning (Becker)
- Collision Detection Algorithm for Protecting Vulnerable Road Users (Wehr)
- Kalman Filtering of Aircraft Positions Based on ADS-B Real-Time Data (Lambertus)
- Design and Implementation of a Python Module for Quaternions (Hobiger)
- Development of a Python-Toolkit for GNSS antenna phase characteristics (Hobiger)
- Loosely Coupled GNSS/IMU Integration by means of Ensemble Kalman Filtering (Sonnleiter)

Activities in National and International Organizations

Thomas Hobiger

Editorial board member "Journal of Geodesy"
 Editorial board member "Earth, Planets and Space"
 Editorial board member "Acta Geodaetica et Geophysica"
 Co-chair of IAG working group 4.3.9 "GNSS-R"
 Member of the Global Geodetic Observing System (GGOS) consortium
 Corresponding member of the Austrian Geodetic Commission
 Fellow of the International Association of the Geodesy
 Member of the Institute of Navigation (U.S.)
 Member of the Royal Institute of Navigation
 Member of the German Institute of Navigation

Alfred Kleusberg

Fellow of the International Association of the Geodesy
 Member of the Institute of Navigation (U.S.)
 Member of the Royal Institute of Navigation
 Member of the German Institute of Navigation

Thomas Gauger

Member of VDI/DIN KRdL working group on Deposition parameters [NA 134-02-01-08 UA]
 Member of ICP Forests
 Member / Guest scientist of Bund-Länder-Fachgespräch Stickstoffdeposition (FGN)
 Member of StickstoffBW, AG1 Deposition

Education (Lecture / Practice / Training / Seminar)

Introduction of Geodesy and Geoinformatic (BSc) (Hobiger, Becker)	2/2/0/0
Electronics and Electrical Engineering (Wehr)	2/1/0/0
Satellite Measurement Engineering (Wehr)	2/1/0/0
Measurement Techniques in Navigation (Wehr)	1/3/0/0
Parameter Estimation in Dynamic Systems (Hobiger, Lambertus)	2/1/0/0
Adjustment Theory (Hobiger, Lambertus)	2/1/0/0
Navigation I (Becker)	2/2/0/0
Inertial Navigation (Hobiger, Sonnleitner)	2/2/0/0
Radar Measurement Methods I (Braun)	2/0/0/0
Radar Measurement Methods II (Braun)	2/1/0/0
Dynamic System Estimation (Becker)	2/1/0/0
Integrated Positioning and Navigation (Becker)	2/1/0/0
Satellite Navigation (Hobiger, Becker)	2/1/0/0
Interplanetary Trajectories (Becker)	1/1/0/0
Integrated Fieldwork (Becker, Lambertus)	(SS 2019)

Institute for Photogrammetry



Geschwister-Scholl-Str. 24D

D-70174 Stuttgart

Tel.: +49 711 685 83336

Fax: +49 711 685 83297

info@ifp.uni-stuttgart.de

<http://www.ifp.uni-stuttgart.de>

Head of Institute

Prof. Dr.-Ing. Uwe Sörgel

Deputy:

apl. Prof. Dr.-Ing. Norbert Haala

Personal Assistant:

Martina Kroma (until 9/2019)

Ute Schinzel (from 10/2019)

Emeritus Professors:

Prof. Dr.-Ing. Dr. hc. mult. Fritz Ackermann

Prof. Dr.-Ing. Dieter Fritsch

Academic Staff

M.Sc. Tobias Bolz (since 2/2019)

Dr.-Ing. Michael Cramer

Dipl.-Ing.(FH) Markus Englich

apl. Prof. Dr.-Ing. Norbert Haala

M.Sc. Lena Joachim (since 11/2019)

M.Sc. Michael Kölle

M.Sc. Dominik Laupheimer

Dr. techn. Gottfried Mandlbürger

M.Sc. Stefan Schmohl

M.Sc. Philipp Schneider

Dipl.-Ing. Patrick Tutzauer (until 5/2019)

Dr.-Ing. Volker Walter

Object Reconstruction from SAR Images

Photogrammetric Systems

Laboratory, Computing Facilities

Photogrammetric Computer Vision

Integrative Computational Design

Crowd-based Data Collection

Classification in Remote Sensing

Laser Bathymetry

Deep Learning in 3D Remote Sensing

SAR Interferometry

Facade Interpretation

Geoinformatics

Stipendiaries and external PhD Students

M.Sc. Hasan Almassri	Localization and mapping (SLAM)
M.Sc. Stefan Cavegn	Image-based Mobile Mapping
M.Sc. Ke Gong	3D Reconstruction
M.Sc. Rami Khamis	3D Building Modelling
Dipl.-Phys. Hendrik Schilling	Classification of Hyperspectral Data
M.Sc. Mehrdad Nekouei Shahraki	Photogrammetric Image Processing
M.Sc. Shuhang Zhang	UAV Data Collection

Guests

Dr. Quanye Du (until 2/2019)	Image Orientation
Dr. Edyta Hadas (from 11/2019)	Tree detection from Laser Scanning
M.Sc. Cesar de Paula (until 10/2019)	Laser-Bathymetrie

External Teaching Staff

Dipl.-Ing. Stefan Dvorak, Amt für Stadtentwicklung und Vermessung, Reutlingen

Research Activities in ifp organized in four thematic Groups

Geoinformatics	Dr.-Ing. Volker Walter
Photogrammetric Computer Vision	apl. Prof. Dr.-Ing. Norbert Haala
Photogrammetric Systems	Dr.-Ing. Michael Cramer
Remote Sensing	Prof. Dr.-Ing. Uwe Sörgel

Research Projects

Crowdsourcing the Collection of High-Quality Training Data for Machine Learning

Machine learning techniques, such as Convolutional Neural Networks, have become state-of-the-art for the automatic interpretation and annotation of various data. However, these methods require huge amounts of labeled data (ground truth). Commonly, such labels are collected by experts, but since the labeling process is very time-consuming, this approach causes large costs and might not be feasible. The focus of this research lies in outsourcing this tedious and costly task to the crowd (crowdsourcing). However, the crowd is composed of people with very different cultural backgrounds and abilities. Therefore, we must expect very inhomogeneous quality. Hence, quality control and improvement methods are crucial when using crowdsourced data as training data for machine learning algorithms.

As already demonstrated in various studies, one method for quality improvement is the so-called "Wisdom of the Crowd", which means, that large groups of people are smarter and can solve complicated problems even better than specialists can. This approach leads to high-quality results by collecting data not only once but multiple by different crowdworkers. One goal of our research is to determine the optimal amount of multiple data collections, whereas the other goal is to minimize the labelling costs (see Figure ??).

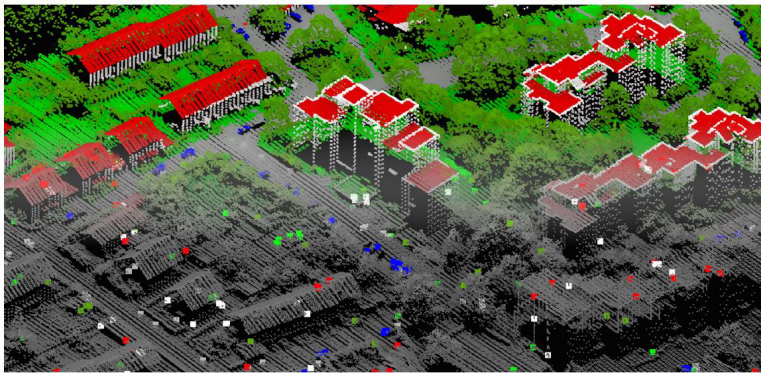


Figure 1: By combination of Active Learning and Crowdsourcing, a completely labeled training dataset provided by an expert (upper half of figure) can be replaced by a sparse training dataset generated by crowdworkers (bottom half of figure).

For this purpose we combine machine learning techniques and human perception. In this context, Active Learning (AL) strategies can be applied, where the machine queries for most informative instances, so that human labeling effort can be minimized by focusing on these samples.

In order to reach a large pool of potential workers that collect labels, web-based tools are developed for the crowd-based collection of data. While it is our goal to collect labels for different data representations by the crowd such as imagery, 3D point clouds and 3D meshes, we are further investigating which representation is best suited for this process.

Joint Semantics for Meshed Models and 3D Point Clouds in Urban Scenes

The past decade has shown that 3D data collection and data processing has increasingly become feasible and important in the domain of photogrammetry and remote sensing. Common representations for 3D data are point clouds, volumetric representations, projected views (i.e. RGB-D images or renderings), and meshes. Amongst them, 3D point cloud processing may currently be the most popular topic - in particular concerning semantic segmentation. However, textured meshes as generated from LiDAR point clouds and imagery have some favorable characteristics.

Whereas point clouds are an unordered set of points, meshes are graphs consisting of vertices, edges, and faces that provide explicit adjacency information. Intrinsically, meshes facilitate data fusion by utilizing LiDAR points and multi-view stereo points for the geometric reconstruction while leveraging high-resolution imagery for texturing (hybrid data storage). Nowadays, joint photogrammetric and LiDAR collection is state of the art for airborne systems (hybrid acquisition). Recently, the joint orientation of LiDAR data and aerial imagery became feasible (hybrid adjustment). Concerning the recent hybridization trend, from our point of view, enhancing the core 3D point clouds to textured meshes may replace unstructured point clouds as default representation for urban scenes in the future. Notwithstanding, textured meshes are a mostly overlooked topic in the domain of photogrammetry and remote sensing despite their advantageous characteristics. For these reasons, we investigate the semantic segmentation of textured meshes in urban areas as generated from LiDAR data and oblique imagery.

We propose a novel association mechanism that enables information transfer between point clouds and meshes. The association mechanism can be used in a two-fold manner: (i) feature transfer to stabilize semantic segmentation of one representation with features from the other representation and (ii) label transfer to achieve the semantic annotation of both representations. The association mechanism takes care of discrepancies between the two 3D representations. Discrepancies may exist due to geometric simplifications during the meshing and georeferencing issues of LiDAR data and imagery. Besides, meshes are surface descriptions that cannot handle multi-target capability like LiDAR point clouds. Naturally, the point density of the LiDAR cloud is higher than the face density. That is why the association assigns many LiDAR points to each face (many-to-one relationship).

We establish a feature-based pipeline for semantic mesh segmentation. As a result, we can utilize any arbitrary feature-based approach that allows a simple extension of the feature vector. Utilizing our mechanism, we enhance per-face feature vectors with available LiDAR features. By these means, we leverage inherent features from both data representations (multi-modality). Due to the many-to-one relationship, we calculate the per-face median for LiDAR features and the texture. Figure ?? depicts a subset of the mesh with its faces colored by associated median intensity (LiDAR feature) and median RGB (radiometric feature).

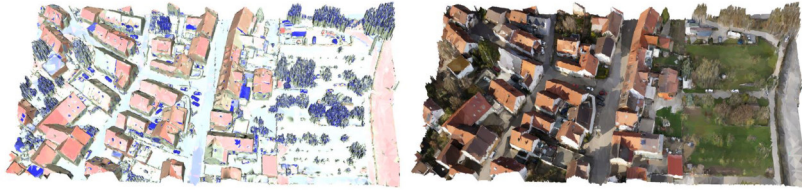


Figure 2: Per-face features. Left: median intensity, where blue indicates low values and red high values. Right: median RGB.

After the semantic mesh segmentation, we transfer predicted mesh labels to the LiDAR point cloud at a stroke by leveraging our association mechanism. Hence, we end up with a labeled mesh and a labeled point cloud by using available information from both data representations. Figure ?? shows the prediction result for the semantic mesh segmentation supported by LiDAR features (left) and its transferred prediction to the LiDAR point cloud (right).

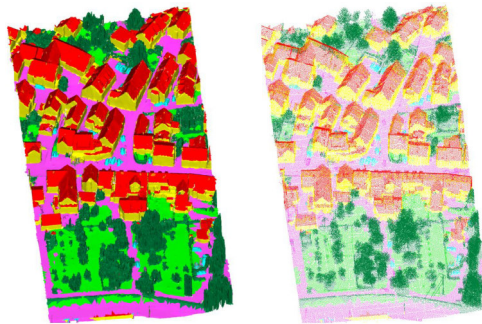


Figure 3: Predicted semantic mesh segmentation utilizing mesh-inherent and LiDAR-inherent features (left) along with its transferred labels to the dense LiDAR point cloud (right, sub-sampled by factor 20 for visualization). Class color code: building mass/facade (yellow), roof (red), impervious surface (magenta), green space (light green), mid and high vegetation (dark green), vehicle (cyan), chimney/antenna (orange) and clutter (gray).

Virtual Reality for Photogrammetric Data

Although VR has been around for some years now, there seems to be relatively little usage in the photogrammetric community. When building virtual environments out of data acquired by photogrammetry or LiDAR, a considerable amount of manually editing the textured mesh is often employed to create a truly immersive experience. This is partly due to the massive number of triangles in automatically generated meshes, which often requires simplification for a more manageable number of faces. This manual, and to a certain extent artistic, labor limits such an approach to smaller scale areas or single monuments and requires relatively high effort and thus results in high cost. In contrast, we want to keep manual post-processing in this study to a minimum in order to keep costs down and thereby practicability and scalability high.

We implemented our application using the Unity game engine. Additional frameworks, namely the unity packages SteamVR and version 3 of VRTK assisted in making it suitable for VR. Regarding hardware, the final program runs on a mid-range gaming laptop. Connected to the laptop is a HTC Vive VR system, including a head mounted display and two handheld controllers. The application contains one or more scenes displaying geospatial data, allowing the user to move around and, to a certain degree, interact with the objects in it.

We investigated the usage of such a VR framework to visualize textured 2.5D and 3D meshes, generated from airborne imagery by photogrammetry. The goal is to present such data to the general public more relatable than with simpler 3D viewers. This shall demonstrate the capabilities of photogrammetry and may help to win new students to the field. We could show that creating such an application is possible without much expert knowledge in game development or manual post-processing and therefore represents a feasible option for photogrammetric practitioners.



Figure 4: In-game screenshot.



Figure 5: In-game screenshot.



Figure 6: Impressions of our application at public relations events.

Hybrid Processing of Ultra-high Resolution UAV LiDAR and Image Point Clouds for Monitoring Applications

The quality of 3D point clouds captured by aerial and mobile mapping platforms still experiences a considerable boost due to the ongoing advancements in LiDAR technology and Multi-View-Stereo-Matching (MVS). One main advantage of MVS is that the resulting geometric accuracy directly corresponds to the Ground Sampling Distance (GSD) and thus the scale of the evaluated imagery. In contrast, the potential to measure multiple responses of the reflected signal using LiDAR sensors is advantageous, especially to collect data both on and below vegetation using airborne data acquisition. Airborne LiDAR and MVS were originally developed as competing approaches. Meanwhile considerable research efforts focus on systems for joint collection and evaluation of LiDAR and image data to further improve the accuracy, density and reliability of the generated point clouds. Furthermore, full use of the geometric information provided from these data sources additionally requires a semantic analysis of the respective point clouds.

Within our work on combining LiDAR and image processing at different steps of the photogrammetric processing chain we aim at the generation of ultra-high accurate 3D point clouds using an UAV platform. One main purpose of this research is deformation monitoring of a ship lock and its surrounding area. In that test area subsidence of about 1-10 mm/a relative to the stable surroundings have been observed over the past few years. For area-covering monitoring of such changes, 3D point clouds at mm-accuracy have to be provided twice a year. Up to now, such accuracy demands presume terrestrial data collection using geodetic instruments, such as level instruments, total stations and differential GNSS. However, these engineering geodesy techniques are limited to build structures and natural objects due to economic reasons. In contrast, area-covering 3D measurement opts for the use of airborne platforms. Photogrammetric data collection at a mm-scale requires image acquisition at a similar resolution, which typically presumes the use of UAVs. If (signalized) ground control points are available with sufficient accuracy and distribution, in principle integrated georeferencing and subsequent dense image matching can provide 3D point clouds in the accuracy of some millimeters. However, our project aims on the measurement of subsidence of terrain surfaces, which are covered to a considerable part by vegetation like trees, bushes and shrubs. This opts for the use of LiDAR, due to its ability to penetrate such vegetation, especially if multiple returns are measured and analysed, e.g. using full waveform recording. While originally, UAVs were limited to camera-based systems, meanwhile the use of even high-end LiDAR became state-of-the-art. Thus, subsidence measurement can be realized by collecting LiDAR as well as image data from a UAV platform at different epochs.

Highly accurate georeferencing of the captured data is the most important prerequisite while aiming at the monitoring of subsidence. In a nutshell, the flight trajectory of the LiDAR platform is required with sufficient accuracy to compute the respective 3D points from LiDAR range measurement. Therefore, IMU and GNSS measurements provide the required position and attitude of the platform, which allows 3D point accuracies of some centimeters, especially if a suitable calibration of the sensor system is guaranteed. However, since our application aims at sub-centimeter accuracies, further improvement is required. We apply a hybrid orientation of airborne LiDAR point clouds and aerial images. This hybrid georeferencing is an extension of the traditional LiDAR strip adjustment with additional observations from the bundle adjustment of image blocks. It improves the overall stability of the block regarding the risk of a global deformation, thus sub-centimeter accuracies could be verified.

This integration of aerial imagery not only increases the resulting accuracy of the LiDAR points during georeferencing, it also provides a precise co-registration of both data sources. This allows accurate alignment of LiDAR points to 3D points from dense image matching. By these means, further processing can benefit from the complimentary properties of LiDAR and MVS point clouds.

Figure ?? and Figure ?? demonstrate the complimentary characteristics of LiDAR and MVS on a sample from our test area. Figure ?? depicts the RGB coloured points generated by MVS. While MVS directly provides the respective RGB colour values for the visualization of these points, the overlaid LiDAR data is colour coded according to the respective elevation.



Figure 7: Comparison of 3D points from MVS (RGB) and LiDAR measurement (height coded). Yellow line defines profile depicted in Figure ??.

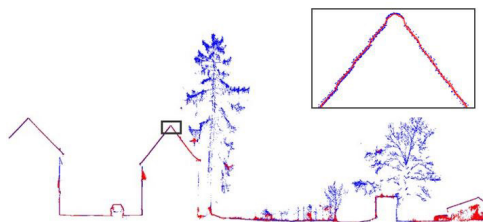


Figure 8: Extracted profile with 3D points from LiDAR (blue) and MVS (red).

Finally, the yellow line represents the profile used to extract the points depicted in Figure ?. The discrepancies between the point clouds from MVS (red) and LiDAR (blue) are especially evident at trees. In general, the polar measurement principle of LiDAR allows the detection of one or multiple returns along a single laser ray path. At twigs and branches, but also at power lines, multiple returns are captured for a single laser pulse since the laser beam cone hits targets smaller than the laser footprint in different distances along the ray path. MVS point cloud generation presumes that the same surface patch is seen from at least two camera positions. This can result into problems especially if the object appearance changes rapidly when seen from different positions. This holds true for semi-transparent objects like trees and bushes. Problems can also occur for objects in motion like vehicles, pedestrians, etc., or in very narrow urban canyons due to occlusions. Differences between LiDAR and MVS also occur at grass, which is penetrated by the laser signal to a certain extent. Thus, these heights are measured somewhere between the top surface and the ground depending on the vegetation density, while multi-view stereo matching, in turn, always returns the topmost surface and does not penetrate the vegetation layer. While in the past, LiDAR and image matching were considered as competing techniques, the closer integration of both techniques is the logical next step we are currently working on.

Integrated Georeferencing of Mobile Mapping Image Sequences without using any Ground Control Points

Determination of 3D ground control point coordinates is a time-consuming task that is frequently performed by a surveying team on site. Moreover, surveying work is often conducted in dangerous road environments. Hence, we showed the feasibility of image orientation computation by using no ground control points. However, our integrated georeferencing approach, that is based on the structure-from-motion tool COLMAP, exploits initial exterior orientation parameters from direct georeferencing as well as pre-calibrated relative orientation parameters among cameras.

Our relatively small but demanding study area depicted in Figure ?? is located at a very busy junction of five roads in the city center of Basel, Switzerland. It includes large multi-story buildings that create a very challenging environment for GNSS positioning. We mapped three street sections of this study area twice, with a time difference of ca. 16 minutes. The vehicle-based mobile mapping research platform featured three forward looking pinhole cameras as well as two multi-head panoramic cameras equipped with fisheye optics tilted forward and backward by 90° each (see Figure ??). Furthermore, a NovAtel SPAN inertial navigation system served for direct georeferencing of the imagery acquired at typically 5 fps. This navigation system consists of a tactical grade inertial measurement unit and a L1/L2 GNSS kinematic antenna. In case of good GNSS coverage, these sensors provide an accuracy of horizontally 10 mm and vertically 15 mm during post-processing.

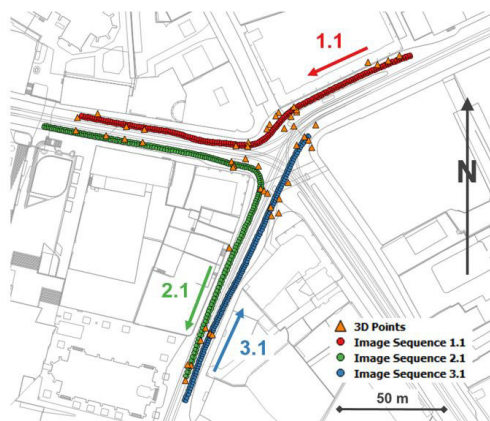


Figure 9: Base map of the study area with overlaid 3D reference points and projection centers of selected image sequences (Source of base map: Geodaten Kanton Basel-Stadt).

We performed integrated georeferencing without using any ground control points employing both three and twelve cameras, i.e. stereo forward imagery as well as five images per panorama camera. Our minimal configuration consisting of a forward pointing stereo camera



Figure 10: Multi-view multi-sensor configuration of the mobile mapping system of the Institute of Geomatics (IGEO), University of Applied Sciences and Arts Northwestern Switzerland (FHNW), which was used for capturing a dataset in Basel in August 2015.

system and a backward facing camera head delivered slightly poorer results. However, the need for only processing 25% of the total amount of images denotes a significant efficiency increase. Thus, check point investigations using three cameras are depicted in Table ?? . While mapping 1 (left) shows a small horizontal improvement from 135 mm to 109 mm, the 2D RMSE value reduces significantly from 509 mm to 337 mm for mapping 2 (right). The height RMSE value of mapping 1 lowers from 228 mm to 139 mm, mainly caused by sequence 2.1. In contrast, induced by sequence 3.2, there is a small degradation from 463 mm to 495 mm for mapping 2. Even though 3D RMSE values for all but for 3.1 were improved, there are still mean values of 177 mm and 601 mm for mapping 1 and 2, respectively. However, integrated georeferencing values of sequences from the same mapping are more homogeneous compared to direct georeferencing. In summary, horizontal components can rather be improved than height values, especially if all height residuals point to the same direction and amount to several decimeters. Nonetheless, exploiting at least one reference height allows for mitigation of this issue.

[mm]	Seq.	ΔH	$\Delta 2D$	$\Delta 3D$	Seq.	ΔH	$\Delta 2D$	$\Delta 3D$
DG	1.1	138	95	168	1.2	605	466	764
	2.1	500	266	567	2.2	633	515	816
	3.1	46	44	64	3.2	150	548	568
	Mean x.1	228	135	266	Mean x.2	463	509	716
	1.1	116	102	155	1.2	563	340	658
IG	2.1	178	121	215	2.2	518	304	601
	3.1	121	104	160	3.2	403	367	545
	Mean x.1	139	109	177	Mean x.2	495	337	601

Table 1: RMSE values in mm for check point residuals between direct (DG) as well as integrated georeferencing (IG) and tachymetry. Either 10 or 11 check points per sequence were utilized. Three cameras of the multi-view mobile mapping configuration were used, i.e. two cameras pointing forward and one directed backward.

IntCDC: Environment Monitoring for a Cyber-Physical Construction Platform

The Cluster of Excellence IntCDC (Integrative Computational Design and Construction for Architecture) of the University of Stuttgart aims to rethink design, fabrication and construction in order to tackle the current challenges of the building industry, such as the lack of sustainability and productivity. IntCDC is funded by the German Research Foundation (DFG).

One of the research activities within this interdisciplinary project is the development of a cyber-physical construction platform for automated on-site assembly of prefabricated building elements. Figure ?? shows how an automated tower crane will work collaboratively with a robotic partner system in order to perform the on-site assembly.

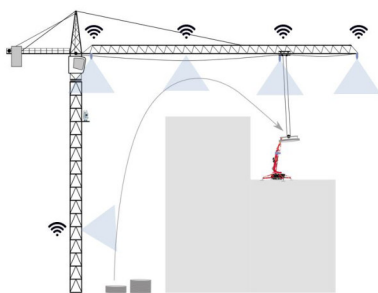


Figure 11: Cyber-physical construction platform with monitoring system.

In cooperation with the Institute for System Dynamics, the control for the automated tower crane and the corresponding monitoring system will be developed and tested on a crane at our test site. The goal is to develop a fully automated load handling including the pick and place processes and the transportation in between. Therefore, task scheduling, path planning and an online feedback for collision avoidance during transportation is needed. Monitoring the construction site at different scales is essential for all these tasks. That is why we will develop methods to monitor the complex, unstructured environment of construction sites with cameras and laser scanners with focus on load monitoring, workspace monitoring for path planning and progress monitoring for task scheduling.

While the first two tasks are mainly focused on deriving 3D geometry, the last task requires the semantic interpretation of the data. The goal is to obtain a semantically segmented 3D model of the whole construction site to be able to compare it with planning data. Thus, information about the construction progress can be derived. Therefore, we will develop methods for the semantic segmentation of highly complex, unstructured environments.

Three-dimensional Path Planning of UAVs Imaging for Complete Photogrammetric Reconstruction

With the availability of lightweight unmanned aerial vehicles (UAVs) and compact imaging sensors, UAVs are being widely used in remote sensing and photogrammetry. High-quality 3D models are of great use in the field of cultural heritage documentation and structural inspection. However, complex structures are often concave and have the nature of self-occlusion. Mapping them normally with nadir images often results in incompleteness and the precision loses additionally. Therefore, considering the specification of the UAV platform, planning viewpoints in three-dimensional space would be the best solution for lightweight UAVs mapping complex structures.

In this study, we introduce the photogrammetric constraints into the framework of model-based view planning, to plan a path for multicopter UAVs imaging for complete photogrammetric 3D reconstruction. The completeness and precision of the coarse input model are firstly analyzed and additional viewpoints are then planned to increase the quality of the 3D model. Camera geometry constraints like baseline and observe angle are considered while the error ellipsoid of each observed point guides the view planning as well.

The proposed method is inspired by the framework of model-based view planning, but with a two-phase's viewpoint addition (see Figure ??). The input of the methodology is a dense image matching (DIM) point cloud, reconstructed triangulated mesh and corresponding camera network from a prior flight. We firstly analyze the completeness of the point cloud. To analyze the completeness of the DIM point cloud, it should be compared with a "complete" object. The triangulated mesh is reconstructed considering the visibility and with small gaps or holes completed. The incomplete part is marked out by point cloud index calculation and filtering. Then we do a two-phase camera addition. The first phase is adding cameras to make the point cloud complete, which results in a "strengthen camera network". After that, the theoretical precision of each point is estimated, and the second phase is to increase the photogrammetric precision and an "optimized camera network" is finally acquired.

In order to evaluate the proposed 3D path planning method in the matter of accuracy, precision, and completeness, we compare the result of the reconstructed DIM point cloud from different modes of flight planning, including nadir flight and its combination with 3D path from the proposed method and Agisoft Metashape. Table ?? shows the quantitative comparison of the DIM point cloud. The precision quantifies how many reconstructed points are close to a ground truth point. The recall quantifies how many ground truth points are close to a reconstructed point, which can be recognized as completeness. Moreover, the incomplete area coverage and the precision in the incomplete area were evaluated as well to test the performance of two 3D planning methods specifically for incomplete area. As can be seen from Table ??, the DIM point cloud precision of all 3D methods was significantly higher than the nadir flight. The 3D configuration of the flight paths may reduce noisy DIM points. The recall of 3D planning methods was higher as well, as adding more oblique images covered more structures. Compared with the MS path, the 3D path had a 2.6% higher recall but

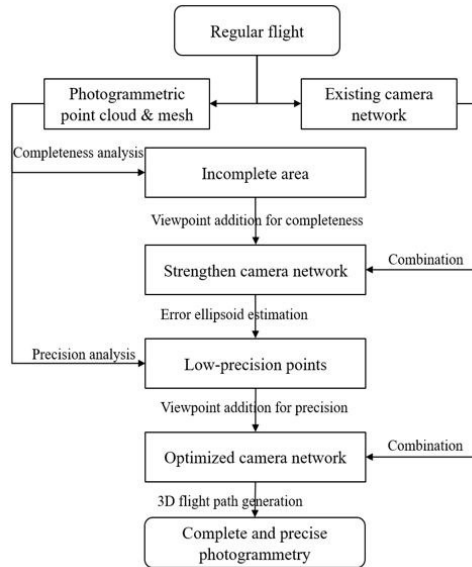


Figure 12: Flowchart of the proposed path planning method.

doubled coverage of the incomplete area. Its precision in the incomplete area was higher than MS as well.

Figure ?? shows the overview and zoomed snapshot of DIM point clouds from all paths. The first row is the overview, in which yellow rectangles represent zoom-in areas in the following rows. In zoom level 1, the facade of the center ship lock building was well-reconstructed in the flight 3D, however, the result from flight MS was as incomplete as the nadir one. Zoom level 2 was a small building on the ship lock. The result from nadir and MS were barely the same while there were some points on the facade in our result. In zoom level 3, the result from nadir and MS had lack of information underneath the road, while our method successfully captured the data there.

Flight path	Precision	Recall	Incomplete area coverage	Precision in incomplete area
Nadir	66.0%	40.0%	0%	-
3D	75.2%	60.1%	37.7%	53.6%
MS	76.0%	57.5%	16.1%	48.0%

Table 2: Quantitative comparison of the DIM cloud from all flight paths.

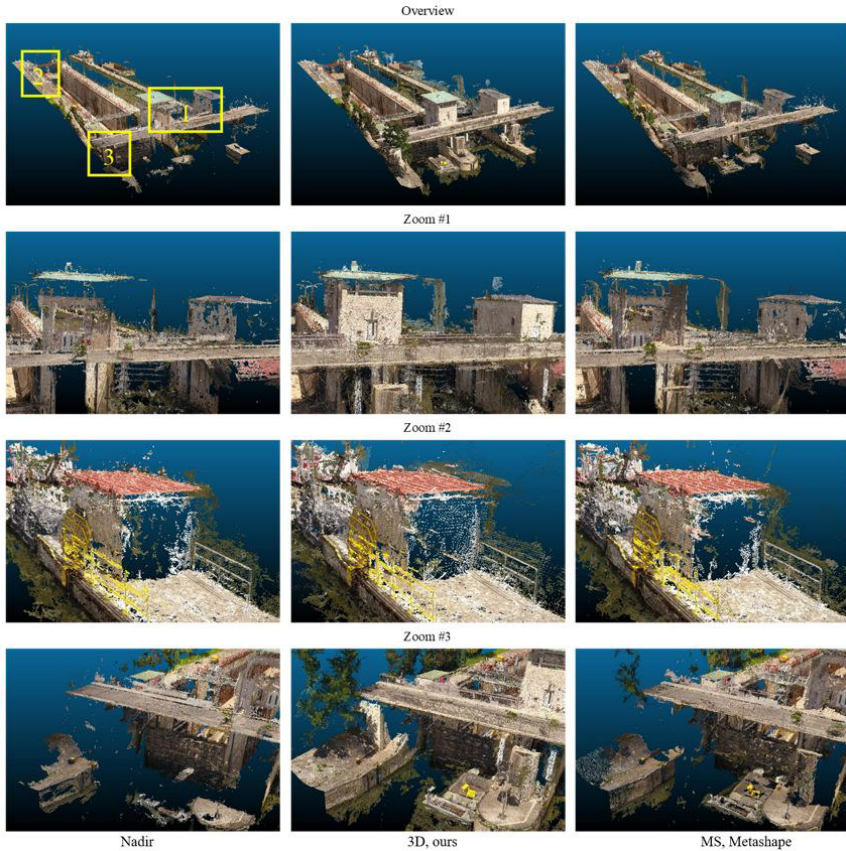


Figure 13: Overview and detailed comparison of DIM point cloud from different flights.

Mesh Refinement with Multi-view Stereo Satellite Images

The 3D reconstruction of surface models from optical imagery is a long-standing problem in photogrammetry and computer vision. In recent years, satellite sensors have stepped into a new era, which makes the reconstruction with satellite images competitive to traditional airborne imagery and very promising. Nowadays, multi-view stereo (MVS) satellite imagery is available and the ground sample distance (GSD) can reach 30cm (for example WorldView-3). There are also some well-organized MVS satellite benchmarks, which were established in the last five years. Many researches have a focus on point cloud or DSM generation from the satellite MVS imagery. The standard pipeline of 3D reconstruction from satellite images is based on a strategy that matches each stereo pair individually and then fuses them all. The Semi-Global Matching (SGM) algorithm is the most popular choice for the matching process.

The SGM algorithm provides high quality results and tolerable computing time, but it suffers from the fronto-parallel bias and a preference for areas of constant disparity. Moreover, most state-of-the-art algorithms only produce a 2.5D representation of the surface and do not attempt to reconstruct detailed 3D structures.

In order to circumvent this limitations, we propose a novel mesh refinement method for satellite MVS reconstruction. As same as the standard mesh refinement, our method starts from an initial mesh model. We generate a fused Digital Surface Model (DSM) by following a standard MVS satellite 3D reconstruction pipeline. We then produce the mesh model from the DSM by Poisson Reconstruction. The initial mesh is coarse but has correct topology. The vertices of the initial mesh are adjusted iteratively in the direction that can reduce the photo discrepancy of all image views. To represent the photo discrepancy and take account the regularization, we established an energy function by applying the Rational Polynomial Coefficients (RPC) model. Differ from the traditional pinhole cameras, the satellite sensors provide the RPCs instead of in- and exterior parameters. That also makes none of the algorithm for pinhole camera can be applied directly to satellite images. The inconsistency of the textures in different views causes an higher gradient of the vertices. The energy function is minimized by gradient descent, which yields a refined mesh with minimal photometric re-projection error and maximal similarity between correspondences.

We implemented our algorithm with C++ and tested it on a public MVS satellite benchmark called "Creation of Operationally Realistic 3D Environment" (CORE3D) program. The benchmark is founded by the "Intelligence Advanced Research Projects Activity" (IARPA). We selected the data covering the downtown of Jacksonville, Florida, USA as our test site. The test site has in total 26 Worldview-3 images (30cm GSD), which are collected between October 2014 and February 2016. The size of the test data is ca. 750m*750m. A 2.5D LiDAR DSM with 50cm GSD is provided along the satellite images as ground truth. Currently, there is no access to 3D ground truth to evaluate the 3D elements quantitatively. Instead, we evaluate the 3D structures qualitatively and then evaluate the height difference with the 2.5D reference DSM. According to the intersection angle and the illumination condition of the images, we selected 80 suitable stereo pairs to conduct our mesh refinement.

Two examples of the mesh model generated from the SGM based pipeline and our refined mesh are shown in Figure ?? and Figure ?. We additionally show the related area in Google Earth as a reference.

The first example shows the Bank of America Tower. According to Figure ??(a) and (b), the pyramid-like top has a sharper top in the refined result. The stair structures on the top are more significant. The facade of the building is reconstructed after the mesh refinement process. The concave parts of the tower is reconstructed successfully, which never exist in the 2.5D mesh model but only in true 3D mesh model. As shown in Figure ??, the city hall of Jacksonville is selected as another example and it is reconstructed from MVS satellite imagery and refined. Comparing the SGM-based mesh and the refined mesh models, we find our refinement pipeline reconstructs the small details on the edge of the building successfully. For example, the rectangular structure locates in the middle bottom is getting explicit after the refinement.

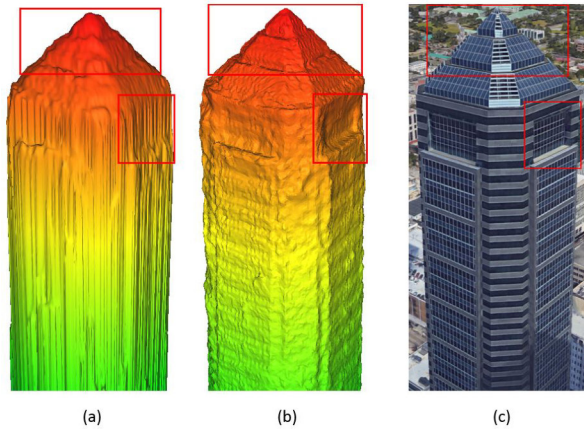


Figure 14: Reconstruction of the Bank of American Tower: (a) SGM-based mesh model (b) Refined mesh model (c) Google Earth reference.

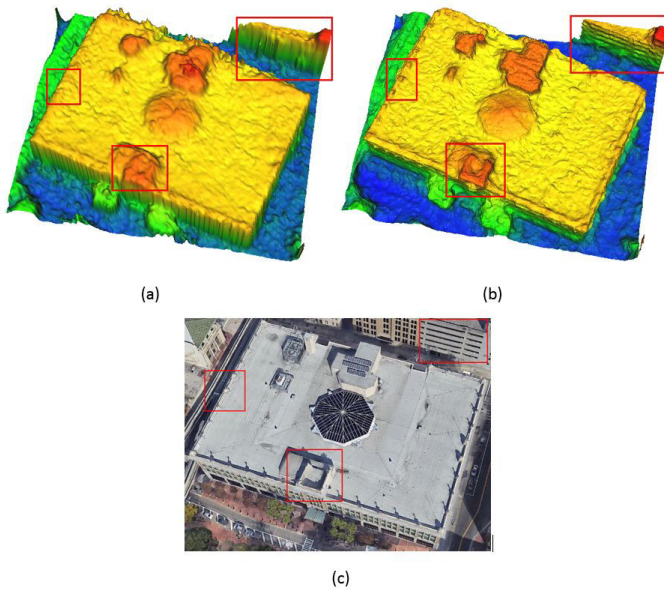


Figure 15: Reconstruction of the Jacksonville city hall: (a) SGM-based mesh model (b) Refined mesh model (c) Google Earth reference.

	Completeness @3m (%)	RMSE @3m (m)	NMAD (m)	68% quantile (m)
SGM based Reconstruction	82.090	1.017	0.774	1.351
Mesh Refinement	82.746	0.957	0.607	1.205

Table 3: Evaluation result of Jacksonville test sit.

To evaluate the accuracy, we estimate the Root-Mean-Squared Error (RMSE) of the height difference from mesh model to reference DSM. Here we treat the errors larger than 3m (10 times of GSD) as outliers. Then we calculate the percentage of the points with error less than 3m as the completeness of the model. For robustness evaluation, the Normalized Median Absolute Deviation (NMAD) and the 68% quantile of the error distribution are employed. The evaluation results are demonstrated in Table ???. After the refinement, the completeness is increased by 0.7%, the RMSE is reduced by 6cm, the NMAD is decreased by 17cm and the 68% quantile error is decreased by 15cm. Therefore, compared to the SGM-based reconstruction algorithm, our mesh refinement method maintains completeness at similar level, improves the accuracy and the robustness.

According to our research, for the first time, the reconstruction of full-3D surface structures with MVS satellite imagery is achieved by our mesh refinement algorithm. The refinement also tends to improve the accuracy of the 2.5D elevation values.

Using DInSAR for Monitoring of Mining Tailing Dams

The European satellite mission Sentinel-1 was the launched in 2014. It acquires synthetic aperture radar (SAR) images globally. The weather independency of this active remote sensing technique allows this system to sample the whole earth every 12 (6 for Europe) days. Due to the COPERNICUS open data policy, all images can be used free of charge.

Because of the coherent nature of the SAR sensor, pairs of images can be analyzed interferometrically. The phase difference in the received signal allows a deduction about a change in the surface. Advanced differential interferometric SAR (DInSAR) analyses like small baseline subset (SBAS) and persistent scatterer interferometry (PSI) are examining dozens of consequential SAR images. They take in account complex atmosphere correction, and deformation models to achieve an estimation of deformation velocities better 1cm/year.

In an EIT research project, we are investigating the possibilities of DInSAR for cost efficient monitoring of tailing dams around the world. A tailing dam is typically an earth-fill embankment dam used to store byproducts of mining operations after separating the ore from the gangue. The sudden failures of such dams in 2015 and 2019 in Brazil and Myanmar have shown the necessity of new strategies to monitor critical dams globally.

Because all Sentinel-1 images since 2014 are available in the archive, we can analyze the behavior of the collapsed dams, to compare them with stable ones and derive spatial and temporal patterns of critical deformation.

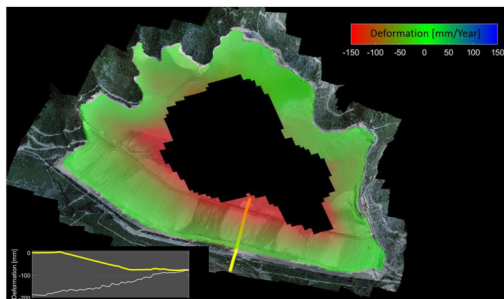


Figure 16: Deformation velocities on a tailing dam over one year. The deformation profile (bottom left) indicates a displacement of up to 200mm in this timespan. The data has been derived using small baseline subset (SBAS) analysis of 31 Sentinel-1 SAR images.

Airborne (PolIn)SAR for Coastal Protection

Large areas of the German North Sea lie in the Wadden Sea and are exposed to the influence of tides and storm surges. To ensure the safety of seafaring traffic and the protection of the coastal areas among other things, up to date high-resolution geodata is required. This data includes digital surface and terrain models, digital imagery and a variety of 3D line geometry such as water-land-boundaries or 3D structural lines.

Due to the changing water levels and weather conditions, the time window for data acquisition is extremely shallow. The use of airborne SAR (Synthetic Aperture Radar) makes it possible to stretch this window, as it is possible to acquire data even with closed cloud coverage and it is able to cover a up to five times bigger area then state of the art ALS scanners.

As part of the GeoWAM project (www.geowam.net), we try to develop a new solution to harness the advantages of SAR imaging. Project partners include:

- German Federal Institute for Hydrology (BfG)
- Lower Saxony State Agency for Water Management, Coastal and Nature Conservation
- German Aerospace Center (DLR)
- Karlsruhe Institute for Technology
- Disy Informationssysteme GmbH

The Institute for Photogrammetry focuses on the analysis of the image data provided by the DLR to extract 3D structures for different purposes:

- Monitoring of coastal protection buildings like dikes, reclamation areas and groy nes (see Figure ??)
- Monitoring of movement within the mudflat (see Figure ??)

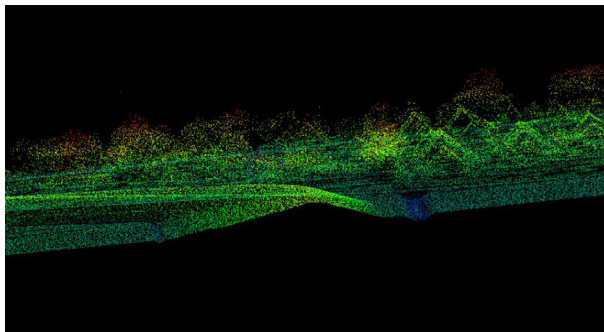


Figure 17: View of the digital surface model with land reclamation area on the left, the dike in the middle and the drainage channel.

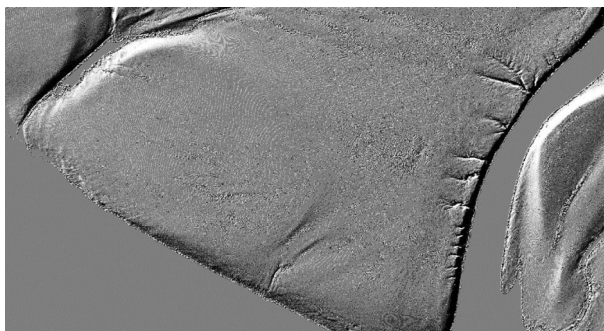


Figure 18: Shading of the mudflat.

Bathymetry by Fusion of Airborne Laser Scanning and multi-spectral Aerial Imagery

In the third, and last year of the DFG research project "Bathymetry by fusion of airborne laser scanning and multi-spectral aerial imagery" research work was concentrated on:

- Deriving bathymetry from multispectral images via Convolutional Neural Networks
- Dissemination of the achieved research results

Deriving bathymetry from multispectral images via Convolutional Neural Networks

Following the general aim of the DFG research project of combining concurrently captured data from active and passive sensors for deriving bathymetry, an approach of using active laser bathymetry data for providing ground truth for spectrally based depth estimation via deep learning was pursued. The basic idea is that the relation between multi-spectral information of the aerial images and water depth is established via a Convolutional Neural Network (CNN). In contrast to the standard use of CNNs for segmentation and classification, the network acts as a depth predictor, in this case featuring per-pixel depth estimation capabilities.

In contrast to conventional approaches for deriving depth from multi-spectral images based on orthophotos, the approach aims at (i) dealing with raw aerial images and (ii) strict consideration of ray bending due to refraction at the air-water-interface. The radiometric information captured in a single image pixel does not directly relate to water depth but rather to the slanted distance within the water column (see Figure ??a). Thus, the CNN is setup in a way to predict these slanted underwater distances using reference data from the concurrently acquired LiDAR point cloud (cf. Figure ??c+d). The framework comprises the following steps:

- Derivation of digital models of the water surface (Water Surface Model, WSM) and the water bottom (Digital Terrain Model, DTM) from the bathymetric LiDAR data.
- Orientation of the concurrently acquired multi-spectral images via direct georeferencing based on GNSS and IMU observations or by conducting a bundle block adjustment.
- Ray tracing of each image ray hitting the water body and (i) intersecting the ray with the WSM, (ii) applying the refraction correction, and (iii) intersecting the bended ray with the DTM. The slanted distances between the two intersection points serve as reference data for the CNN.
- Setup, training, testing, and validation of a CNN in U-Net architecture. For each pixel of the wetted perimeter the networks predicts the slanted underwater distance.
- Calculation of a 3D point cloud per image by multiplying the vector unit of the bended underwater image ray with the CNN-predicted distance.

Figure ?? shows the general concept of image ray tracing (a), the study area Autobahnsee, Augsburg, Germany (b), the LiDAR derived reference underwater distances for a single image (c), and the predicted underwater distances for the same image (d). Compared to the LiDAR measurements as reference, the CNN-derived water depths show a bias of -15 cm and a standard deviation of 35 cm. Shadows from overhanging vegetation and occasional sun glint effects are responsible for the systematic offset. Improvements of the approach with respect to automatic classification of land, water, underwater vegetation, and sun glint together with water depth estimation are currently work in progress.

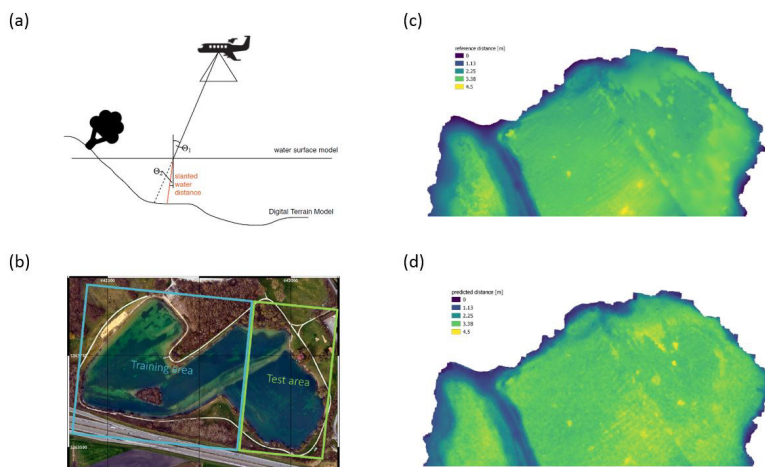


Figure 19: CNN-based estimation depth estimation from multispectral images, (a) principle sketch of image ray tracing based on LiDAR derived water surface and terrain models, (b) study area Autobahnsee, Augsburg, Germany, divided into training and test area, (c) ground truth: LiDAR derived underwater distances, (d) CNN-predicted underwater distances

Dissemination

In 2019, the research results achieved within the DFG project “Bathymetry by fusion of airborne laser scanning and multi-spectral aerial imagery” were published in conference proceedings (DGPF annual conference) and peer-reviewed journal papers (PE&RS, ISPRS Journal of Geo-Information). In addition to scientific articles, Gottfried Mandlbürger, delivered a series of (invited) talks at international workshops (ISPRS, EuroSDR, Photogrammetric Week) and university courses (University of Innsbruck).

The project officially ended at December 31, 2019.

References 2019

- Cramer, M., Mandlbürger, G., Laupheimer, D., Haala, N., Havel, P.: Potenzial ultrahoch-auflösender und -genauer UAV-basierter 3D-Datenerfassung. Dreiländertagung der DGPF, der OVG und der SGPF in Wien, Österreich - Publikationen der DGPF, Band 28, 2019, 472-482.
- Farghaly, D., Urban, B., Sörgel, U., Elb, E.: Differentiating forest types using TerraSAR-X spotlight images based on inferential statistics and multivariate analysis. Remote Sensing Applications: Society and Environment.

- Gross, W., Tuia, D., Sörgel, U., Middelmann, W.: Nonlinear Feature Normalization for Hyperspectral Domain Adaptation and Mitigation of Nonlinear Effects. *IEEE Transactions on Geoscience and Remote Sensing*, 57(8), 5975-5990.
- Haala, N., Mandlbürger, G., Cramer, M., Laupheimer, D., Kölle, M.: Kombinierte Analyse hochpräziser Punktwolken aus UAV -Photogrammetrie und Laserscanning im Hinblick auf Setzungsmessungen. 20. Internationale Geodätische Woche Oberurgul 2019, 10 p.
- Innerhofer, D., Mandlbürger, G., Steinbacher, F., Aufleger, M.: Vermessung hochalpiner Seen mittels moderner Technologien. Dreiländertagung der DGPF, der OVG und der SGPF in Wien, Österreich - Publikationen der DGPF, Band 28, 347-362.
- Kölle, M., Laupheimer, D., Haala, N.: Klassifikation hochaufgelöster LiDAR- und MVS-Punktwolken zu Monitoringzwecken. Dreiländertagung der DGPF, der OVG und der SGPF in Wien, Österreich - Publikationen der DGPF, Band 28, 692-701.
- Mandlbürger, G.: Through-Water Dense Image Matching for Shallow Water Bathymetry. *Photogrammetric Engineering, Remote Sensing*, 85(6), 445-455.
- Mandlbürger, G., Jutzi, B.: On the Feasibility of Water Surface Mapping with Single Photon LiDAR. *ISPRS Int. J. Geo-Inf.* 2019, 8(4), 188.
- Mandlbürger, G., Lehner, H.: Single Photon LiDAR - Grundlagen und erste Evaluierungsergebnisse. Dreiländertagung der DGPF, der OVG und der SGPF in Wien, Österreich - Publikationen der DGPF, Band 28, 443-457.
- Mandlbürger, G., Lehner, H., Pfeifer, N.: A Comparison of Single Photon and Full Waveform LiDAR. *ISPRS Ann. Photogramm. Remote Sens. Spatial Inf. Sci.*, IV-2/W5, 397-404.
- Mulsow, C., Mandlbürger, G., Ressler, C., Maas, H.G.: Vergleich von Bathymetriedaten aus luftgestützter Laserscanner- und Kameraerfassung. Dreiländertagung der DGPF, der OVG und der SGPF in Wien, Österreich - Publikationen der DGPF, Band 28, 318-333.
- Schmohl, S., Sörgel, U.: Submanifold Sparse Convolutional Networks for Semantic Segmentation of Large-Scale ALS Point Clouds. *Ann. Photogramm. Remote Sens. Spatial Inf. Sci.*, IV-2/W5, 77-84.
- Schmohl, S., Sörgel, U.: ALS Klassifizierung mit Submanifold Sparse Convolutional Networks. Dreiländertagung der DGPF, der OVG und der SGPF in Wien, Österreich - Publikationen der DGPF, Band 28, 111-122.
- Tutzauer, P., Laupheimer, D., Haala, N.: Semantic Urban Mesh Enhancement Utilizing a Hybrid Model. *ISPRS Ann. Photogramm. Remote Sens. Spatial Inf. Sci.*, IV-2/W7, 175-182.
- Winiwarter, L., Mandlbürger, G.: Classification of 3D Point Clouds using Deep Neural Networks. Dreiländertagung der DGPF, der OVG und der SGPF in Wien, Österreich - Publikationen der DGPF, Band 28, 663-674.

Winiwarter, L., Mandlbürger, G., Schmohl, S., Pfeifer, N.: Classification of ALS Point Clouds Using End-to-End Deep Learning. PFG - Journal of Photogrammetry, Remote Sensing and Geoinformation Science, Aug 2019, 1-16.

Yang, C. H., Sörgel, U.: Evaluation of a PSI-based Change Detection Regarding Simulation, Comparison, and Application. Int. Arch. Photogramm. Remote Sens. Spatial Inf. Sci., XLII-2/W13, 1959-1965.

Yang, C. H., Mütterthies, A., Sörgel, U.: Workable Monitoring System Based on Spaceborne SAR Images for Mining Areas - Stings Development Project. Int. Arch. Photogramm. Remote Sens. Spatial Inf. Sci., XLII-2/W13, 1951-1957.

Doctoral Theses

Groß, W.: Merkmalstransfer in Hyperspektraldaten durch nichtlineare Merkmalsnormierung. Supervisor: Sörgel, U.

Schmid, S.: Semi-Dense Filter-Based Visual Odometry for Automotive Augmented Reality Applications. Supervisor: Fritsch, D.

Yang, C.H.: Spatiotemporal Change Detection Based on Persistent Scatterer Interferometry - A Case Study of Monitoring Urban Area. Supervisor: Sörgel, U.

Master Theses

Abramow, A.: Entwickeln und Evaluieren neuartiger retro-reflektierender Referenzelemente für den industriellen Einsatz. Supervisors: Heidemann, R. (Faro Europe GmbH & Co. KG), Haala, N.

Akeredolu, O.G.: Evaluation of Sentinel-1/-2 data for classification tasks. Supervisor: Cramer, M.

Batbayar, J.: Integration of multiple collected polygons with a raster-based approach. Supervisor: Walter, V.

Budde, L.E.: Unsicherheitsauswertung von semantischer Segmentierung mittels Neuronaler Netze. Supervisors: Schmohl, S., Sörgel, U.

Chen, C.C.: Multi-Modal Object Pose Estimation with a Graph-Based System for Gangway Operation. Supervisor: Haala, N.

Chen, D.: Fast Automatic 3D Reconstruction for Household Objects using Consumer RGB-D Cameras. Supervisors: Lindermayr, J. (Fraunhofer IPA), Haala, N.

Chen, Y.: Road Inventory Mapping with Street-Level Imagery from iPhone - A Combination of Structure from Motion and Deep Learning. Supervisor: Cramer, M.

- Dai, S.: Shading of Elevation Model from Laser Scan Data. Supervisors: Haala, N., Steffen, R. (PointCab), Graner, M. (PointCab).
- Ding, C.: Using Satellite and StreetView Images For Identifying the Living Quality of Residential Area in ShangHai. Supervisors: Sörgel, U., Zhu, X. (TUM).
- Du, Y.: Towards Combining Volunteered Geographical Information and Remote Sensing. Supervisor: Walter, V.
- Hirt, P.R.: Automatisierte Fusion von 2D- und 3D-Sensordaten zur zuverlässigen Detektion von Strukturmerkmalen. Supervisors: Frey, C. (Fraunhofer-IPM), Haala, N.
- Hoppe, K.: Fusion of point clouds from Photogrammetry and LiDAR with point-wise quality values. Supervisors: Wenzel, K. (nFrames), Hauck, M.A. (nFrames), Haala, N.
- Joachim, L.: Wolkenerkennung in Satellitenaufnahmen des sichtbaren Spektralbereichs bei Nacht. Supervisors: Storch, T. (DLR), Haala, N.
- Jose, N.: Integration and Quality Evaluation of Building Groundplans collected by the Crowd. Supervisor: Walter, V.
- Koutnik, M.: Abbiegeassistent für VANs - Konzepterstellung, technische Analyse und Erstellung eines Testaufbaus. Supervisors: Puchinger, W. (Daimler AG), Haala, N.
- Li, B.: Multi-Feature Based Localization System Using Graph Optimization for Autonomous Driving. Supervisors: Sörgel, U., Maile, F. (ZF).
- Liu, M.: HDR Image Improvement of Terrestrial Laser Scanning. Supervisors: Haala, N., Steffen, R. (PointCab), Graner, M. (PointCab).
- Schmidt, J.: Georeferenzierung von simultan aufgenommenen UAS-Bild- und Laserdaten. Supervisors: Mandlbürger, G., Cramer, M.
- Shams, H.: Semantic Mesh Segmentation Using PointNet++. Supervisors: Laupheimer, D., Haala, N.
- Shamshirbandi, N.: Creating a 3D virtual city with CityGML data by LOD1 and LOD2 of Schleswig-Holstein. Supervisor: Walter, V.
- Shu, F.: Implicit Joint Semantic Segmentation of Images and Point Clouds. Supervisors: Laupheimer, D., Haala, N.
- Straub, J.: Optimierung eines Sensorsystems für die Erfassung und semantische Interpretation von Punktwolken im Agrarbereich. Supervisors: Cramer, M., Kölle, M., Reiser, D. (Uni Hohenheim).
- Usche, T.: Klassifikation der Landbedeckung in Luft- und Satellitenbildern unter Ableitung von Ground Truth aus dem amtlichen Datenbestand. Supervisors: Kölle, M., Wampach, M. (LGL), Wild-Pfeiffer, F. (LGL).
- Wang, Y.: A low cost demonstrator for autonomous driving. Supervisor: Cramer, M.

Wang, Y.: Adversarial Networks in Domain Adaption for Remote Sensing Image Classification. Supervisors: Sörgel, U., Zhu, X.

Xia, Z.: Stereo Reconstruction of Human Faces with Deep Learning. Supervisors: Ulrich, J. (Carl Zeiss AG), Haala, N.

Bachelor Theses

Li, B.: Automatic 3D Reconstruction from Multi-Date Satellite Images. Supervisors: Gong, K., Haala, N.

Peshkova, P.: 3D-Rekonstruktion von sakralen Kunstwerken mit Bild- und Laserdaten. Supervisor: Cramer, M.

Roth, M.: Empirische Genauigkeitsuntersuchung einer metrischen UAV-Kamera. Supervisor: Cramer, M.

Wu, Y.: Land cover classification using Sentinel-2 images by pattern recognition network. Supervisor: Sörgel, U.

Yin, Y.: Entwicklung und Evaluierung eines Web-Tools zur crowd-basierten Erfassung von Bäumen aus 3D Punktwolken. Supervisors: Kölle, M., Walter, V.

Awards

Mandlbürger, G.: U.V. Helava Best Paper Award: Mandlbürger, G., Pfennigbauer, M., Pfeifer, N.: Design and evaluation of a full-wave surface and bottom-detection algorithm for LiDAR bathymetry of very shallow waters. ISPRS Journal of Photogrammetry and Remote Sensing 150, 1-10.

Activities in National and International Organizations

Cramer, M.:

Co-Chair ISPRS WG I/9: Integrated Sensor Orientation, Calibration, Navigation and Mapping

Mitglied im DIN Normungsausschuss NA 005-03-02 AA "Photogrammetrie und Fernerkundung"

Englich, M.:

Webmaster ISPRS

Haala, N.:

Chair ISPRS WG II/2: Point Cloud Generation

Chair EuroSDR Commission II: Modelling and Processing

Vorsitz DGPF Arbeitskreis Sensorik und Plattformen

Sörgel, U.:

Vice President German Society for Photogrammetry, Remote Sensing and Geoinformation (DGPF)

Chair ISPRS WG III/3: SAR-Based Surface Generation and Deformation Monitoring

Walter, V.:

National Correspondent of the ISPRS Commission IV

Education - Lectures/Exercises/Training/Seminars

Bachelor "Geodäsie und Geoinformatik"

Geoinformatics I (Walter)	2/2/0/0
Geoinformatics II (Walter)	1/1/0/0
Image Processing (Haala)	2/1/0/0
Integrated Fieldworks (Haala, Hobiger, Sneeuw)	0/0/4/0
Introduction into Geodesy and Geoinformatics (Cramer, Hobiger, Sneeuw, Sörgel)	4/2/0/0
Photogrammetry (Cramer)	2/1/0/0
Remote Sensing (Sörgel)	2/1/0/0
Signal Processing (Sörgel)	2/1/0/0
Urban Planning (Dvorak)	2/0/0/0

Master Course "Geodäsie und Geoinformatik"

Aerotriangulation (Cramer)	1/1/0/0
Computational Geometry (Walter)	1/1/0/0
Computer Vision for Image-based Acquisition of Geodata (Haala)	1/1/0/0
Databases and Geographical Information Systems (Walter)	1/1/0/0
Digital Terrain Models (Haala)	1/1/0/0
Fundamentals in Urban Planning (Dvorak)	2/0/0/0
Georeferencing of photogrammetric Systems (Cramer)	1/1/0/0
Modelling and Visualisation (Haala)	1/1/0/0
Pattern Recognition and Image Understanding (Haala)	1/1/0/0
Remote Sensing (Sörgel)	1/1/0/0
Scientific Presentation Seminar (Haala)	0/0/0/2
Web-based GIS (Walter)	1/1/0/0

Master Course GEOENGINE

Airborne Data Acquisition (Cramer)	2/1/0/0
Computer Vision (Haala)	2/1/0/0
Geoinformatics (Walter)	2/2/0/0
Signal Processing (Sörgel)	2/1/0/0
Integrated Fieldworks (Haala, Hobiger, Sneeuw)	0/0/4/0

Pattern Recognition (Sörgel)	2/1/0/0
Remote Sensing (Sörgel)	2/1/0/0

Master Course “Infrastructure Planning”

Introduction to GIS (Walter)	2/0/0/0
------------------------------	---------

Master Course “Aerospace Engineering”

Image Processing (Haala)	2/1/0/0
Introduction into projective Geometry (Cramer)	2/0/0/0